

JSCSEN 72(10)921–1037(2007)

UDC 54:66

ISSN 0352–5139

Journal of the Serbian Chemical Society 72, No. 10, 921–1037 (2007)

Journal of the Serbian Chemical Society

VOLUME 72

NO 10

BELGRADE 2007

CONTENTS

Organic Chemistry and Biochemistry

- D. Malešev and V. Kuntić*: Investigation of metal–flavonoid chelates and the determination of flavonoids via metal–flavonoid complexing reactions 921
- R. Ozen and N. S. Kus*: A mild and effective method for the conversion of alkenes into alcohols in subcritical water (Short communication) 941
- A. Nićiforović, M. Adžić, S. D. Spasić and M. B. Radojičić*: Do altered activities of superoxide dismutases and the level of NF- κ B modulate the effects of gamma radiation in HeLaS3 cells?.... 945
- S. Kevrešan, B. Kovačević, V. Ćirin–Novta, K. Kuhajda, J. Kandrač, K. Pavlović and Lj. Grbović*: Biochemical changes in cuttings of *Robinia pseudoacacia* after treatment with naphthenate ... 953
- C. Capetanos, V. Saroglou, P. D. Marin, A. Simić and H. D. Skaltsa*: Essential oil analysis of two endemic *Eryngium* species from Serbia 961

Theoretical Chemistry

- I. Gutman*: The McClelland approximation and the distribution of π -electron molecular orbital energy levels 967

Inorganic Chemistry

- S. S. Konstantinović, B. C. Radovanović, Z. B. Todorović and S. B. Ilić*: Spectrophotometric study of Co(II), Ni(II), Cu(II), Zn(II), Pd(II) and Hg(II) complexes with isatin- β -thiosemicarbazone..... 975
- N. Raman and S. Johnson Raja*: DNA cleavage, structural elucidation and anti-microbial studies of three novel mixed ligand Schiff base complexes of copper(II)..... 983

Electrochemistry

- R. E. Sabzi, A. Hasanzadeh, K. Ghasemlu and P. Heravi*: Preparation and characterization of carbon paste electrode modified with tin and hexacyanoferrate ions 993
- E. Biçer and E. Coşkun*: Voltammetric study of the interaction between oxacillin sodium and cysteine in the presence and absence of Mn(II) ions in neutral buffer solution..... 1003

Chemical Engineering

- E. Djordjević, S. Kabelac and S. Šerbanović*: Pressure drop during evaporation of 1,1,1,2-tetrafluoroethane (R-134a) in a plate heat exchanger..... 1015

Materials

- J. Dostanić, G. Ušćumlić, T. Volkov–Husović, R. Jančić–Heinemann and D. Mijin*: The use of image analysis for the study of interfacial bonding in solid composite propellant..... 1023

Environmental Chemistry

- V. Püschmann, Z. Koblíha, E. Halánek and I. Tušarová*: A simple *in situ* visual and tristimulus colorimetric method for the determination of diphosgene in air..... 1031

REVIEW

Investigation of metal–flavonoid chelates and the determination of flavonoids *via* metal–flavonoid complexing reactions*

DUŠAN MALEŠEV and VESNA KUNTIĆ**

*Institute of Physical Chemistry, Faculty of Pharmacy, University of Belgrade,
Vojvode Stepe 450, 11000 Belgrade, Serbia*

(Received 2 June 2006, revised 4 April 2007)

Abstract: Flavonoids constitute a large group of polyphenolic phytochemicals with antioxidant properties which are overwhelmingly exerted through direct free radical scavenging. Flavonoids also exhibit antioxidant properties through chelating with transition metals, primarily Fe(II), Fe(III) and Cu(II), which participate in reactions generating free radicals. Metal–flavonoid chelates are considerably more potent free radical scavengers than the parent flavonoids and play a prominent role in protecting from oxidative stress. To unravel the origin of their potent biological action extensive physico–chemical studies were undertaken to reveal the chemical structure, chelation sites, assess the impact of the metal/ligand ratio on the structure of the complexes and the capacity of flavonoids to bind metal ions. In spite of such extensive efforts, data on the composition, structure and complex-formation properties are incomplete and sometimes even contradictory. The aim of this paper is to give a personal account on the development of the field through a retrospective evaluation of our own research which covers approximately 40 complexes of flavonoids from different flavonoids subclasses (rutin, quercetin, 3-hydroxyflavone, morin and hesperidin) with several metal ions or groups and suggest directions for future research. Special emphasis will be given to the site of the central ion, the composition of the complexes, the role of pH in complex formation, the stability of metal–flavonoid complexes and their potential application for analytical purposes.

Keywords: flavonoids, chelates, free radical scavengers, stability constants, quantitative analysis.

FLAVONOIDS

The Hungarian Nobel laureate Albert Szent-Györgyi discovered flavonoid compounds in 1936.¹ Using evidence from his own experiments, he hypothesized that a new vitamin – vitamin P works synergistically with vitamin C in citrus extracts to strengthen capillaries.² Although the description of flavonoids as vitamins was eventually found to be inaccurate, research into their beneficial potentials continued and has increased dramatically over the past two decades.^{3–6}

* On the occasion of author's retirement (D. Malešev).

** Corresponding author. E-mail: vkvesa@yahoo.com

doi: 10.2298/JSC0710921M

Flavonoids (*flavus* – yellow), or bioflavonoids, are a ubiquitous group of polyphenolic substances which are present in most plants, concentrated in the seeds, fruit skin or peel, bark and flowers.³ More than 4000 different flavonoids have been identified to date, making them the largest group of plant chemicals. Many fruits and vegetables, especially buckwheat, apple and onion, are some of these sources. Beverages prepared from plant extracts (beer, tea, wine, fruit juice) are the principal source of dietary flavonoid intake.^{7–16}

Health benefits of flavonoids

Scientific studies conducted in the last few years generated a growing interest in the potentially important role of flavonoids in maintaining human health. A considerable number of plant medicines contain flavonoids, which have been reported by many authors as having anti-bacterial, anti-inflammatory, anti-allergic, anti-mutagenic, anti-viral, anti-neoplastic, anti-thrombotic, and vasodilatory actions.^{17–31} Overwhelmingly, the pharmacological effects are related to the anti-oxidant activity of flavonoids, arising through their ability to scavenge free radicals. When generated in excess, free radicals can damage biomolecules, and are therefore implicated in the etiology of several diseases and ageing.³² Radical scavenging by flavonoids occurs *via* electron donation from the free hydroxyls on the flavonoid nucleus with the formation of a less reactive flavonoid aroxyl radical, which is stabilized by resonance and therefore plays only a moderate role in the propagation of radical-induced damage in biological systems. The anti-oxidant activity of flavonoids correlates well with their physiological function *in vivo*, because oxidative stress is known to participate in the initial process of atherosclerosis leading to coronary heart disease and other patho-physiological events. A number of studies have revealed that flavonoids act as anti-oxidants by scavenging reactive oxygen species.^{33–42}

Specifically, flavonoids reduce the risk of stroke and heart disease (the so-called French paradox, the lack of a positive correlation between a high intake of saturated fat and the occurrence of coronary heart disease is related at least partly to the consumption of red wine,⁴³ which is rich in flavonoids), protect against age-related vision disorders, relieve hay fever, sinusitis, asthma symptoms, alleviate inflammatory skin conditions, reduce inflammation in joints and muscles, common to rheumatoid arthritis, minimize menopausal hot flushes, shrink hemorrhoids, reduce varicose veins and battle viral infections.^{17–31,44}

A considerable number of pharmaceutical preparations containing flavonoids as active substance are commercially available today. For example, *Ginkgo biloba* leaf extract,⁴⁵ used in the treatment of symptoms in the early stages of Alzheimer's disease, vascular dementia and memory impairment,⁴⁶ is the most widely sold phytomedicine in Europe. Some of the commercial pharmaceutical preparations which include the flavonoid rutin are widely used for curing veins diseases. Quercetin, the most biologically active and common dietary flavonoid, is generally used as a dietary supplement.

Structure and spectral characteristics of flavonoids

The carbon atoms in flavonoid molecules are assembled in two aromatic rings, commonly denoted as A and B, which are connected by a three-carbon “bridge”: C₆–C₃–C₆, thus forming a diphenyl-propane structure with the central unit being a benzo- γ -pyrone (chromone). Multiple hydroxyl groups, sugar, oxygen, or methyl groups are attached to this core structure. Depending on the oxidation state of the heterocyclic ring, flavonoids are classified as flavones, flavanols, flavanones, flavonols, flavanones or isoflavones (Fig. 1).³

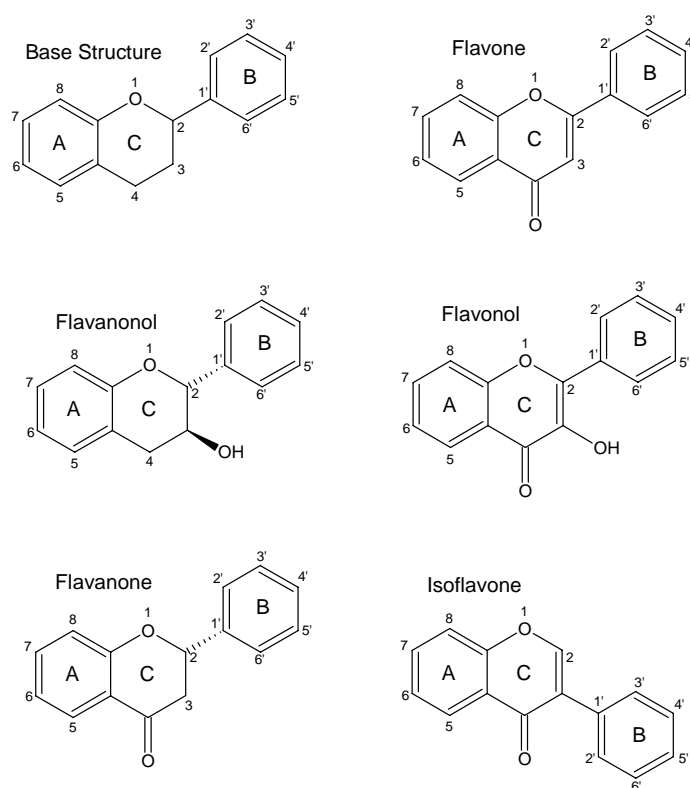


Fig. 1. The flavonoid nucleus consists of benzo- γ -pyrone (ring A and ring C) and benzene (ring B). The major classes of flavonoids are flavone, flavanone, flavonol, flavanone and isoflavone.

Being pigments responsible for the color of leaves, herbs and petals, flavonoids strongly absorb ultraviolet (UV) radiation. Therefore UV-Vis spectroscopy remains the main tool for structural analysis of flavonoids. Typically, two major absorption maxima are observed in the UV-Vis spectrum of flavonoids. The absorption maximum observed in the range 240–285 nm is referred to as band II and the one between 300–400 nm as band I. In general terms, absorption band II may be considered as originating from $\pi \rightarrow \pi^*$ transitions in the A ring, a ben-

zene system, whereas the absorption band I is attributed to transitions in the B ring, a cinnamoyl system. The position of band I in flavones is between 304–350 nm, while flavonols absorb in the range 352–385 nm. Highly oxygenated flavones and flavonols tend to absorb at longer wavelengths than those with fewer oxygen substituents. Methylation or glycosylation of the hydroxyl groups on the flavonoid nucleus usually results in hypsochromic shifts, predominantly of band I. The book by Marby⁵ provides a detailed catalogue of UV spectra of 175 flavonoids.

METAL–FLAVONOID CHELATES

Due to their specific chemical structure, flavonoids easily chelate metal ions and create complex compounds.

Biological activity of metal–flavonoids complexes: chelates as free radical scavengers

In addition to direct free radical scavenging, flavonoids exert anti-oxidant activity through interactions with the reduced form of transition metals, primarily Fe(II), Fe(III) and Cu(I), which participate in reactions generating free radicals.⁴⁷ Flavonoids may sequester metal ions by chelating and preventing metal-mediated generation of free radicals and, accordingly, may protect the potential biological targets from oxidative stress. Thus, the overall anti-oxidant action of flavonoids appears to be a combination of a direct reaction with free radicals and chelating the metal ions responsible for the production of reactive oxygen species.

It was confirmed in numerous studies that flavonoids function as anti-oxidants mainly by chelating metal ions.^{48–60} Moreover, experimental data have shown that the chelates are considerably more effective free radical scavengers than the free flavonoids. Kostyuk *et al.*⁵⁶ found that complexes of rutin, dihydroquercetin or epicatechin with Fe(II), Fe(III), Cu(II) or Zn(II) are more effective radical scavengers than the free flavonoids, due to the acquisition of additional superoxide dismutating centers. These complexes show elevated efficiency in protecting red blood cells against asbestos-induced oxidative injury *in vitro*. According to the same authors, the Cu–rutin complex was found to be the most effective anti-oxidant against asbestos-induced lipid peroxidation in pulmonary tissue *in vivo*.⁵⁶ Moridani *et al.*⁵⁷ found that the Fe(III) complexes of flavonoids were much more effective than the free flavonoids in protecting isolated rat hepatocytes against hypoxia–reoxygenation injury. By using the 1,1-diphenyl-2-picrylhydrazyl radical scavenging method, de Souza and de Giovani⁵⁸ found antioxidant activities of the quercetin, rutin, galangin, and catechin complexes more effective than free flavonoids. Afanas'ev *et al.*⁵⁹ found that Fe(II)– and Cu(II)–rutin complexes were more efficient free radical scavengers *in vitro* and *ex vivo*. These complexes decreased the production of oxygen radicals by xanthine oxidase, rat liver microsomes and the rat peritoneal macrophages, as well as the generation of oxygen radicals by bronchioalveolar cell from bleomycin-treated rats by 2–30 times compared to the parent rutin.⁵⁹ The anti-oxidative activities of morin and its

Pd(II)- and Pt(II)-complexes were also investigated.⁶⁰ The anti-oxidative effects (scavenging superoxide radicals) of the complexes were greater than that of morin itself, while the Pt(II)-complex exhibited stronger scavenging efficacy than the Pd(II)-complex. Both the Pd(II)- and Pt(II)-complexes showed an inhibitory effect on lipid peroxides which was greater than that of free morin.⁶⁰ Due to anti-oxidative mechanisms, morin complexes with La(III), Gd(III) and Lu(III) ions against three bacterial strains, *i.e.*, *Escherichia coli*, *Klebsiella pneumoniae* and *Staphylococcus aureus* showed inhibitory action.⁶¹ Rare earth metal(III) complexes with quercetin can bind to DNA thereby changing its transcription and repressing the growth of tumor cells.⁶²

Complexes of flavonoids play an important role in limiting metal bioavailability and suppressing metal toxicity. For example, aluminum has been implicated in neurological and bone disorder. The complexation of Al(III) by quercetin reduces aluminum overload in the diet.⁶³ By forming complexes, flavonoids appear to be a suitable antidote for heavy metal poisoning *in vivo*.⁶⁴ Quercetin, as an active biological ligand, might be an appropriate Mo(VI) chelator in the case of molybdenum deficiency caused by irradiation, since the use of molybdenum salts is undesirable because of their high toxicity.⁶⁵

Physico-chemical features of metal-flavonoid complexes

Understanding the mechanisms of chelation of flavonoids by metal ions permits a better understanding of their complex anti-oxidant properties. Therefore, many metal-flavonoid complexes have been synthesized and characterized in the past several years.⁶⁶⁻⁷⁴ Elemental and thermal analyses, conductivity and cyclic voltammetry, as well as IR, Raman, ¹H-NMR, ¹³C-NMR, UV-Vis and fluorescence spectroscopy have been used to assess relevant interactions of flavonoids and metal ions, the chelation sites, the dependence of the complex structure on the metal/ligand ratio, the capability of flavonoids in binding metal ions, *etc.* However, data on the composition, structure and complex-formation features are sometimes incomplete and contradictory. The outcome largely depends on the experimental condition and the type of assay employed.

Metal-flavonoid complex compounds are the subject of our longtime research during which their properties, composition, complex formation features, stability constants, as well as analytical appraisal were investigated.⁷⁵⁻¹¹¹ Starting in the early 1980's until now, approximately 40 complexes of flavonoids from different flavonoids subclasses (rutin, quercetin, 3-hydroxyflavone, morin and hesperidin, Fig. 2) with a number of metal ions or metal groups have been investigated. Considering the importance of metal chelation for the understanding of the anti-oxidant behavior of flavonoids, our aim is to give a personal account on the development of the field through a retrospective of our own research. In addition, analytical methods suitable for routine analysis involving the spectrophotometric determination of flavonoids *via* complexing reactions are also reported.

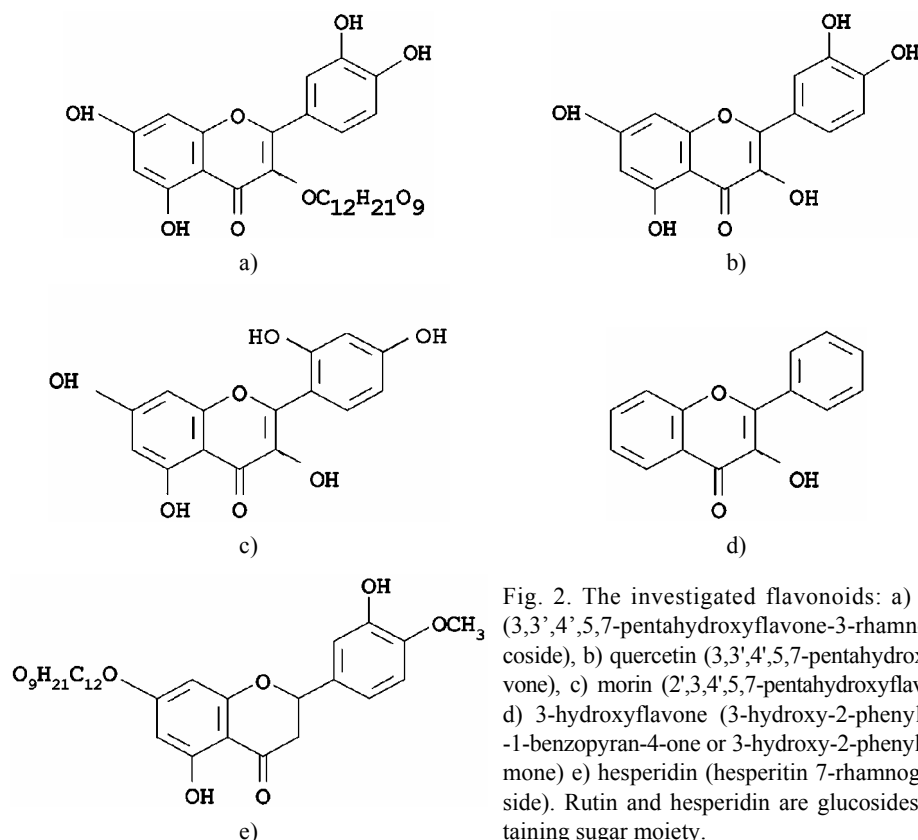


Fig. 2. The investigated flavonoids: a) rutin (3,3',4',5,7-pentahydroxyflavone-3-rhamnoglucoside), b) quercetin (3,3',4',5,7-pentahydroxyflavone), c) morin (2',3,4',5,7-pentahydroxyflavone), d) 3-hydroxyflavone (3-hydroxy-2-phenyl-4*H*-1-benzopyran-4-one or 3-hydroxy-2-phenylchromone) e) hesperidin (hesperitin 7-rhamnoglucoside). Rutin and hesperidin are glucosides containing sugar moiety.

UV-Vis spectra

Metal-flavonoid chelates are usually colored. In the presence of metal ions, a bathochromic shift is typically observed in the absorption spectra of flavonoids. The reaction with AlCl_3 , described for the first time in 1962,³ is actually the earliest presented complexing reaction of flavonoids with aluminum as the central ion and flavone as the ligand. Already then it was observed that complex formation causes a bathochromic shift in both absorption bands, I and II, and that the shift is reversed by increasing the acidity of the medium. A similar behavior is observed for all flavonoid subclasses possessing 5-hydroxy-4-keto, 3-hydroxy-4-keto and/or *o*-dihydroxy groups, suggesting that these moieties are important for chelation. This red shift is caused by the increased conjugative effect when the complexes are formed to give a new ring (Fig. 3).

The site of the central ion

In each flavonoid molecule, there are three domains that can likely interact with metal ions, *i.e.*, the 3',4'-dihydroxy group located on the B ring, the 3-hydroxy or 5-hydroxy and the 4-carbonyl groups in the C ring. Generally, the chela-

ting properties of flavonoids toward metal ions have been attributed to the presence of the 3- or 5-hydroxypyran-4-one, rather than the *ortho*-hydroxyl groups in the B ring.¹¹² Our own IR spectroscopic results the Pd(II)-quercetin¹⁰² (Fig. 4) and UO₂(II)-rutin¹⁰¹ (Fig. 5) complexes also confirm that the benzoyl moiety is the major site for metal chelation. There are, however, studies proposing the catechol moiety as the major site for metal chelating.^{54,66} The results of Bodini *et al.*¹¹³ indicate that coordination to the catechol group of quercetin is the strongest for iron, even in acidic media. Cornard and Merlin⁷⁰ assert the opposite, that in acidic media the *ortho*-dihydroxyl groups of quercetin are never involved in complexation with Al(III). The same authors found two binding sites in the Al(III)-quercetin complex; the first one involved in complex formation is the 3-hydroxychromone and the second one is the *ortho*-hydroxy groups, which are strongly dependent on the medium and pH. Depending on the experimental conditions, as well as with an excess of the metal ion, Torreggiani *et al.*⁷² also found that two chelating processes occurred consecutively, implicating two binding sites in the Cu(II)-quercetin complex. Based on ¹H-NMR, DTA curves and fluorescence spectroscopy, Tang *et al.*⁶⁰ proposed the site of metal ion in chelation given in Fig. 6.

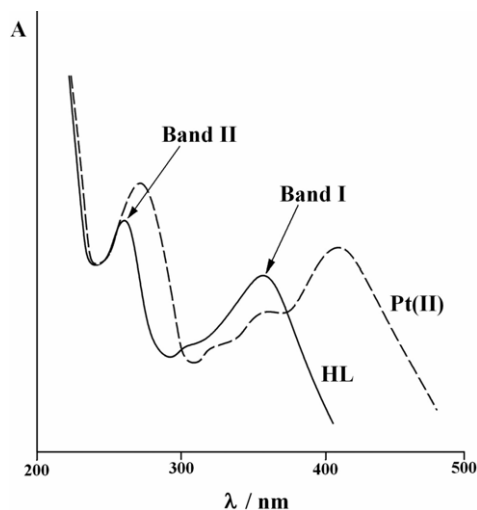


Fig. 3. The red shift of band I and band II in morin (HL) after reaction with Pt(II).⁶⁰

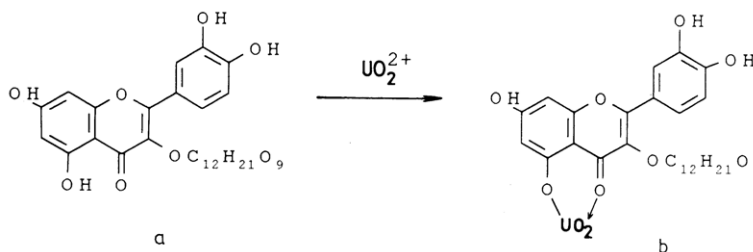


Fig. 4. Formation of uranyl-rutin complex in a 1:1 stoichiometric ratio: a) rutin, b) complex. Favored metal site is 5-hydroxypyran-4-one, rather than the *ortho*-hydroxyl groups in the B ring.¹⁰¹

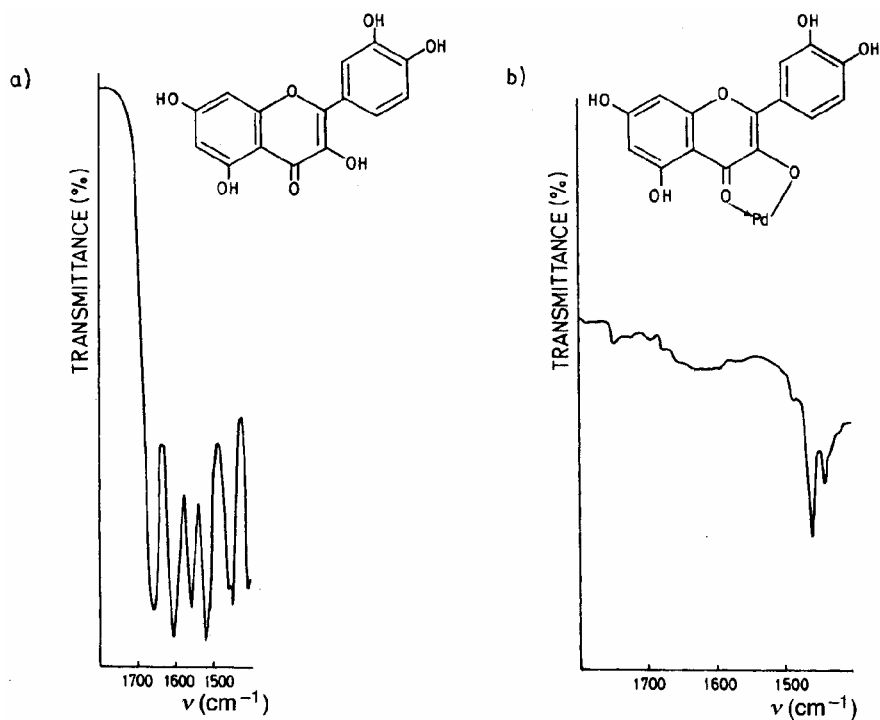


Fig. 5. Composition of the Pd(II)–quercetin complex. Favored metal site is 3-hydroxypyran-4-one, as confirmed by IR spectroscopy.¹⁰²

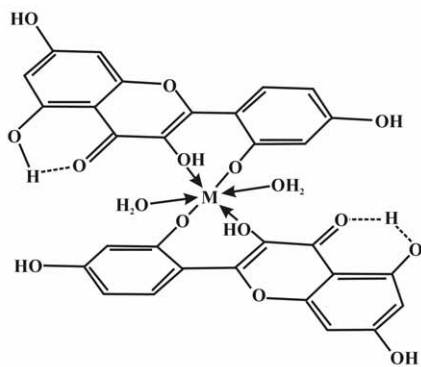


Fig. 6. Probable structure of M(II)–morin complexes M = Pt(II), Pd(II) and Zn(II). The structure is suggested due to the fixation of ring B caused by the effect of coordination after the complex was formed.⁶⁰

Composition of the complexes

Based on our research, only mononuclear complexes (with one central ion) were formed under the investigated experimental conditions (water–alcoholic solution, neutral or acidic media, maximum concentration of $0.0025 \text{ mol dm}^{-3}$ for rutin, quercetin, morin and 3-hydroxyflavone and $0.0015 \text{ mol dm}^{-3}$ for hesperidin). The maximum number of flavonoids in a complex never exceeded two. Though complexes comprising a greater number of flavonoids as ligands are

sterically unfavorable, Zhou and co-workers⁶² found by fluorescence spectroscopy 1:3 complexes of quercetin with eight rare-earth metal ions as the central ions.

The stoichiometric composition of flavonoid complexes is typically determined by the following methods: the method of continual variation of equimolar and non-equimolar solutions, the molar-ratio method, the Bent–French and Nach methods.^{114,115} According to longtime experience, the most reliable results were obtained by the method of continual variation of equimolar solutions, while the method of continual variation of non-equimolar solutions is not recommended for metal–flavonoids complexes because of low reproducibility. It was also found that the Bent–French method is not sufficiently accurate for complexes with a 1:2 stoichiometric ratio, but is acceptable for complexes with a 1:1 composition. According to recent literature, these methods were not widely utilized by other authors (only the molar ratio method and method of continual variation were used by Cornard and co-authors),^{69–71} but we find them still suitable taking into account their simplicity and inexpensiveness. The compositions of the investigated flavonoid complexes, as well as the methods used, are presented in Table I.

TABLE I. Composition of the metal–flavonoid complexes. MR: Mole ratio method, B–F: Bent–French method

Flavonoid	Method	Metal ion	Metal/flavonoid	pH	Ref.
Rutin	Job, MR	Cu(II)	1:2	6.1	78
	MR, B–F	Zn(II)	1:1	6.2	79
	MR, Nach, Job	Pb(II)	1:2	4.5	80
	MR, Nach, Job	Ni(II)	1:2	6.2	82
	MR, Nach	Co(II)	1:1	5.0	83
	B–F, Job, MR	MoO ₄ ²⁻	1:1	6.3	91
	MR	WO ₄ ²⁻	1:2	7.0	92
	Job, MR	Eu(III)	1:2	5.0	98
	Job, MR	UO ₂ (II)	1:1	6.8	101
	Job	Pd(II)	1:2	8.2	103
	Job, MR	TiO(C ₂ O ₄) ₂ ²⁻	1:2	6.4	107
	Quercetin	MR, Nach	Ni(II)	1:1	5.0
MR, Nach		Co(II)	1:1	5.0	84
Job, MR		Pd(II)	1:1	6.2	102
Job, MR		TiO(C ₂ O ₄) ₂ ²⁻	1:2	6.4	109, 111
Morin	Job, MR	Cu(II)	1:2	5.8	76
	Job, MR, Nach	Zn(II)	1:2	5.5	77
	Job	WO ₄ ²⁻	1:2	5.2	97
	Job	Pd(II)	1:1	5.5	106
	Job, MR	TiO(C ₂ O ₄) ₂ ²⁻	1:2	4.3	110
	MR, B–F	Ba(II)	1:1	4.2	85

TABLE I. Continued

Flavonoid	Method	Metal ion	Metal/flavonoid	pH	Ref.
3-Hydroxyflavone	Job	Zn(II)	1:1	5.8	75
	Job, MR, Nach	Pb(II)	1:1	6.1	93
	Job, MR	Ni(II)	1:1	6.1	95
	Job	Co(II)	1:1	6.2	86
	Job, MR	MoO ₄ ²⁻	1:2	6.3	90
	Job	WO ₄ ²⁻	1:2	8.6	94
	Job	Eu(III)	1:2	5.7	96
	Job, MR, B-F	UO ₂ (II)	1:1	3.5	88
	Job, MR	TiO(C ₂ O ₄) ₂ ²⁻	1:2	5.0	108
	Job, MR	Mn(II)	1:1	6.3	87
Hesperidin	Job, MR	Cu(II)	1:2	5.7	105
	Job, MR	UO ₂ (II)	1:2	3.7	104
	Job, MR	Al(III)	1:1	3.7	100
	Job, MR	Zr(IV)	1:1	3.6	99

The role of pH in complex formation

Flavonoids are weak polybasic acids that tend to protonate.¹¹⁴ Therefore, pH has a considerable impact on complex formation. According to our results, complexes with the highest coordination number are typically formed in slightly acidic or neutral pH, rarely in basic media. The optimal pH for complex formation, although strongly dependent on the features of the metal ion, is around pH 6. Complex formation at pH values lower than 3.0 is difficult because the flavonoids are predominantly present in their undissociated form. Although high pH values favor deprotonation of flavonoids and, consequently, more complex species, at higher pH values metal ions are often involved in side reaction (hydrolysis) and hydroxo-complexes are formed.⁷⁵⁻¹¹¹

Complexation with flavonoids as unidentate or bidentate ligands leads to the formation of complexes that contain protons in addition to the metal ion and ligand (so-called protonated complexes) which tend to dissociate at higher pH values. Thus, the bathochromic shift that can be observed in the absorption spectra of metal-flavonoid complexes at higher pH values can be attributed to the dissociation of the protonated complexes, rather than the formation of complexes with different stoichiometric compositions.¹⁰²⁻¹⁰⁹ The absorption spectra of the titanyl-oxalato-quercetin complex at different pH values are presented in Fig. 7. The majority of the investigated metal-flavonoid complexes follow this pattern.¹⁰²⁻¹⁰⁹

Stability of complexes

Several methods for spectrophotometric determination of the stability constants of metal-ligand complexes have been described, such as the Sommer,

Bent–French and Nach method, the method of continual variation of equimolar solutions, the molar-ratio method and the Bjerrum method.^{114–115} We found the Bjerrum method to be the most appropriate for metal–flavonoid complexes, having satisfactory reproducibility and accuracy. The method was modified and simplified by Malešev and the adopted method (denoted with Bjerrum* in Table II), described in detail in the literature,^{91,94,100,102} was extensively used in our research. The stability constant of approximately twenty metal–flavonoid complexes were calculated using this method, Table II (note that only one value for the stability constant is presented although two or more methods were applied in the study, but gave approximately equal results).

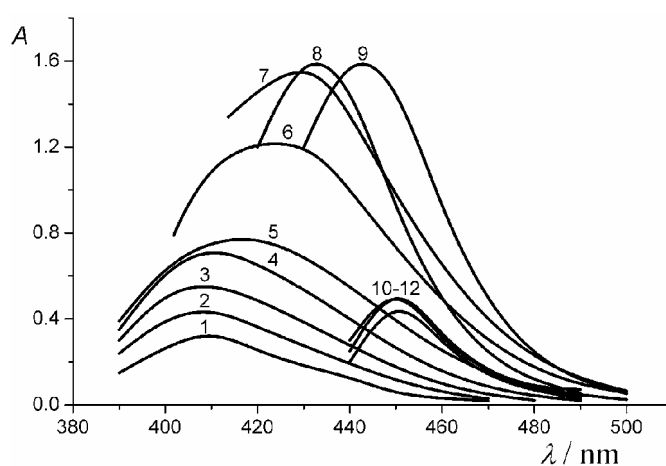


Fig. 7. Absorption spectra of the tityloxalato–quercetin complex obtained at different pH values; curves 1–12: pH: 3.6 (1), 4.3 (2), 5.0 (3), 5.6 (4), 6.8 (6), 7.2 (7), 8.2 (8) 9.2 (9), 10.0 (10), 12.2 (11), 10.6 (12). The bathochromic shift is due to dissociation of the complex.¹⁰⁹

In general, the majority of the investigated complexes can be characterized as moderately ($5 < \log\beta < 10$) or highly ($\log\beta > 10$) stable. It is interesting to note that in the highly stable complexes, the central ion is typically an anion, *i.e.*, tityloxalate $\text{TiO}(\text{C}_2\text{O}_4)_2^{2-}$ and WO_4^{2-} in complexes with rutin, morin and 3-hydroxyflavone and MoO_4^{2-} in the complex with 3-hydroxyflavone, rather than a cation. This is in discordance with the crystal field theory, which describes bonding in transition metal complexes and states that the interactions between ligand and metal are partly electrostatic. However, the molecular orbital theory allows overlapping of atomic orbitals with the same symmetry between the central ion and the ligands. Thus, bonding in metal–flavonoid complexes probably occurs by electron transfer from the d orbital of the metal ion to the π^* orbital of the flavonoid.¹¹⁵

For several investigated rutin complexes, the values of the thermodynamic parameters for complex formation were determined and they imply that the reaction between a flavonoid and a metal ion occurs spontaneously at room temperature.¹¹¹

TABLE II. Stability constants of metal–flavonoid complexes. Bjerrum* denotes Bjerrum's modified method

Flavonoid	Method	Metal ion	Stability constant $\log\beta$	pH
Rutin	Sommer, Nach	Cu(II)	10.76	6.1
	Nach, B–F	Zn(II)	4.68	6.2
	Sommer, Nach	Pb(II)	13.81	4.5
	MR, Nach	Ni(II)	8.95	6.2
	Nach, MR	Co(II)	6.04	5.0
	B–F, Bjerrum*	MoO ₄ ²⁻	8.01	4.0
	Bjerrum*	WO ₄ ²⁻	13.44	4.0
	Bjerrum*	Eu(III)	10.59	5.0
	Bjerrum*	UO ₂ (II)	6.57	4.0
	Bjerrum*	Pd(II)	10.15	8.0
Bjerrum*	TiO(C ₂ O ₄) ₂ ²⁻	10.80	6.5	
Quercetin	MR	Ni(II)	5.57	5.0
	Sommer	Co(II)	4.87	5.0
	Bjerrum*	Pd(II)	6.05	5.0
	Bjerrum*	TiO(C ₂ O ₄) ₂ ²⁻	11.84	6.5
Morin	Sommer	Cu(II)	4.94	5.8
	Sommer	Zn(II)	6.74	5.5
	Bjerrum*	WO ₄ ²⁻	11.6	3.0
	Bjerrum*	Pd(II)	4.55	4.0
	Bjerrum*	TiO(C ₂ O ₄) ₂ ²⁻	7.35	8.0
	MR, B–F	Ba(II)	4.55	4.2
3-Hydroxyflavone	Sommer	Zn(II)	8.51	5.8
	Nach	Pb(II)	7.74	6.1
	Nach	Ni(II)	7.63	6.1
	B–F, Nach	Co(II)	10.87	6.2
	Bjerrum*	MoO ₄ ²⁻	15.13	6.3
	Bjerrum*	WO ₄ ²⁻	16.45	4.0
	Bjerrum*	Eu(III)	13.47	6.0
	B–F, Bjerrum*	UO ₂ (II)	8.68	4.0
	Bjerrum*	TiO(C ₂ O ₄) ₂ ²⁻	16.65	5.0
	B–F, Bjerrum*	Mn(II)	5.43	6.0
	B–F, Bjerrum*	Cd(II)	5.90	6.2
Hesperidin	Bjerrum*	Cu(II)	5.78	7.0
	Bjerrum*	UO ₂ (II)	7.00	6.0
	Bjerrum*	Al(III)	4.54	5.0

Analytical appraisal

Due to their significant health benefits, sensitive analytical methods are required for the quantitative determination of flavonoids in crude plant materials/extracts, plant-based beverages and pharmaceutical preparations. Until now, a number of analytical techniques have been described for the quantification of flavonoids. Liquid chromatography is currently the most commonly applied method

for routine determination of flavonoids. Reversed phase RP-HPLC approaches established in the late 1980s¹¹⁶ aim at the separation, identification and quantization of flavonoids in crude plant materials/extracts and plant-based beverages.^{117–126}

Given that metal-flavonoid chelates are usually colored and absorb at a different wavelength, the complexing reactions of flavonoids with metal ions can be optimized and utilized for the quantitative determination by indirect spectrophotometric methods. By measuring the absorbance of the newly formed colored complex, the amount of the complex-forming constituent (metal ion or ligand flavonoid) can be quantified. Flavonoid-complexing reactions are particularly suitable for analytical purpose because the solutions of the complexes show excellent characteristics for detection by spectrophotometric techniques (intensive color, clear, translucent and rather stable in time).^{75–111} The intensity and the hue of the color of the complexes depend strongly on the chemical properties of the flavonoid, in particular the number and the position of the hydroxyl groups in the flavonoid molecules, as well as the properties of the metal ion. The length of the conjugated π -bond system which includes the reactive groups affects considerably the absorption intensity and hence sensitivity.

Several official methods for flavonoid determination recommend the employment of complexing reactions. For example, the Romanian Pharmacopoeia X established the usage of AlCl_3 as a colorimetric reagent for the quantitative analysis of flavonoids in *Cynarae folium*,¹²⁷ and a general color test for identification of flavonoids in extracts obtained from stems, leaves and flowers prescribes the reaction with 5 % FeCl_3 .¹²⁸ During the late 1960s and early 70s, interactions of flavonoids with metal ions were investigated for analytical purposes.^{129–145} In these articles, chelating reactions of flavones and flavonols were predominantly described, emphasizing their potential for analytical determination of metal ions in the atmosphere, natural water, biological materials and alloys. The following detection limits for some of the metal ions were achieved: 5.5 ppm for Zr(IV), 2.8 ppm for Mo(VI), 3.7 ppm for W(IV) and 0.5 ppm for Fe(III) based on complexing reaction with rutin.¹⁴⁵ To improve the sensitivity and selectivity of metal determination, multi-ligand complexes incorporating a metal, flavone and some other ligands (antipyrine, ClO_4^- , SO_4^{2-}) were synthesized.¹⁴⁵ Being suitable for metal determination, complexing reactions of flavonoids have been extensively investigated during last ten years.^{146–153} For this purpose, quercetin and morin were the most widely used flavonoids for the determination of Al(III), Cr(III), W(IV), Zn(II), Ti(IV), Fe(III) and Mo(VI).

Determination of flavonoids via colored complexing reactions

Numerous complexing reactions have been optimized and adjusted for spectrophotometric determination of the parent flavonoid.^{88–109} Alcohol-water mixtures were used as the solvent. The composition of the solvent was optimized to achieve complete dissolution of both components, and ranged typically between

50 to 80 % ethanol (methanol for hesperidin complexes). The ionic strength and pH were adjusted to a constant value. Parameters, such as linearity, interval (range), specificity, estimated limit of detection (*LOD*), estimated limit of quantization (*LOQ*), recovery (*R*, %), precision or relative standard deviation (*RSD*, %) were established.

Generally, the Beer law was obeyed in the range from 10^{-6} to 10^{-3} mol dm⁻³ for the considered flavonoid, with excellent linearity. Among a variety of selected metal salts, potassium titanyl oxalate is particularly suitable for analytical purposes.¹⁰⁹ For the determination of rutin *via* the titanyl oxalate complex, the best detection limit *LOD* = 0.67 µg ml⁻¹ was obtained.¹⁰⁷

Complexing reactions were also optimized in an attempt to develop a simple, rapid and inexpensive method for the routine determination of flavonoids in commercially available pharmaceutical preparations (Table III). Using the proposed method, it was possible to eliminate the matrix interference since the flavonoid molecules exclusively form the complex. A good selectivity (ability to accurately measure an analyte in the presence of other substances that may be present in the sample matrix) with respect to other constituents in the sample matrix (tablet excipients and diluents, other active principles) was achieved by the proposed assays. The low values of the obtained *RSD* (less than 3 %) and recovery lying in the stated range (Ph EUR 97), indicate good application of the method for flavonoid determination in oral dosage forms.

TABLE III. Spectrophotometric determination of rutin and quercetin in oral dosage forms, and hesperidin in orange juices *via* the complexing reaction

Metal ion	Rutin		Quercetin		Hesperidin in orange juice			Ref.
	Recovery %	<i>RSD</i> %	Recovery %	<i>RSD</i> %	Trade name	Found mg l ⁻¹	<i>SD</i>	
Al(III)	–	–	–	–	“Happy day”	268	168	100
					”Bravo”	6.79	7.88	
Pd(II)	102.5	0.57	–	–	–	–	–	103
UO ₂ (II)	97.9	0.75	–	–	–	–	–	101
TiO(C ₂ O ₄) ₂ ²⁻	97.3	0.87	104.5	2.80	–	–	–	107, 111

However, the selectivity with respect to other compounds which are structurally/chemically related to flavonoids is low in complex matrices, such as *Ginkgo biloba* preparations. However, in mixtures of flavonoids and other relevant components containing one component in a relatively large excess, the same procedure can be applied. For example, the content of hesperidin in orange juice is significantly higher than other flavonoids. Thus, using the complexing reaction with Al(III), it was possible to determine hesperidin in orange juice.¹⁰⁰ Since the amount of hesperidin differs significantly in different species, even in one and the same plant material, depending strongly on the region of growth and the sea-

son, the content of hesperidin is usually not declared by producers, but the concentration obtained in the investigated brands of orange juice with this particular reaction, corresponds to those found by other authors.¹⁵⁴

CONCLUSIONS

The overall anti-oxidant action of flavonoids is achieved through synergy between a direct reaction with free radicals and the chelation of metal ions which are responsible for the production of reactive oxygen species. To unravel the origin of their potent biological action, many metal-flavonoid complexes have been synthesized and characterized. Our research in metal-flavonoid complexes covers approximately 40 complexes of five flavonoids (rutin, quercetin, 3-hydroxyflavone, morin and hesperidin) with a number of metal ions or metal groups. Only mononuclear complexes were formed under the employed experimental conditions. The 3- or 5-hydroxy group and the 4-carbonyl group in the C ring are main metal complexing domains which interact with metal ions. The majority of the investigated complexes are moderate ($5 < \log\beta < 10$) or highly stable ($\log\beta > 10$) complexes. Some complexing reactions were utilized to develop simple methods for routine determination of rutin, quercetin or hesperidin in commercially available pharmaceutical preparations or beverages.

Acknowledgments: We gratefully acknowledge the partial financial support in grants No. 143012 and No. 142013 of the Ministry of Science of the Republic of Serbia.

ИЗВОД

ИСПИТИВАЊЕ МЕТАЛ-ФЛАВОНОИД ХЕЛАТА И ОДРЕЂИВАЊЕ ФЛАВОНОИДА ПРЕКО КОМПЛЕКСИРАЈУЋЕ РЕАКЦИЈЕ МЕТАЛ-ФЛАВОНОИД

ДУШАН МАЛЕШЕВ и ВЕСНА КУНТИЋ

*Institut za fizi-kemiju, Farmaceutski fakultet, Univerzitet u Beogradu,
Vojvode Stepe 450, 11000 Beograd*

Флавоноиди представљају велику групу полифенолних једињења биљног порекла, који имају антиоксидантна својства због директног «хватања» слободних радикала. Антиоксидантно дејство флавоноиди такође остварују стварањем хелата са јонима прелазних метала, првенствено са јонима Fe(II), Fe(III) и Cu(II), који сами учествују у реакцији стварања слободних радикала. Хелати метал-флавоноид су много ефикаснији «хватачи» слободних радикала од матичних флавоноида и могу заштитити потенцијалне мете у организму од оксидативног стреса. Да би се разјаснио механизам биолошког деловања комплекса метал-флавоноид, испитиване су физичко-хемијске карактеристике комплекса: место везивања јона метала, зависност структуре комплекса од односа метал/лиганд, афинитет флавоноида за везивање металног јона, итд. Међутим, подаци о саставу, структури и особинама комплекса су некомплетни и понекад контрадикторни. Стога је намера овог рада да кроз ретроспективу наших резултата дамо лични допринос у испитивању метал-флавоноид комплекса. У приказаном ревијалном раду сакупљени су сви наши резултати о приближно 40 комплекса образованих између пет флавоноида (рутин, кверцетин, 3-хидроксифлавоон, морин и хесперидин) и већег броја металних јона или металних група. Истакнути су подаци о месту везивања централног јона у комплексу, стехиометријском односу метал-лиганд, утицају рН на форми-

рање комплекса и константама стабилности комплекса. Такође, у овом раду приказали смо и примену метал–флавоноид комплекса у аналитичке сврхе.

(Примљено 2. јуна 2006, ревидирано 4. априла 2007)

REFERENCES

1. S. Rusznyak, A. Szent-Györgyi, *Nature* **138** (1936) 798
2. A. Szent-Györgyi, *Physiol. Chem.* **225** (1938) 126
3. E. Middleton, C. Kandaswami, in: *The Flavonoids: Advances in Research Since 1986*, J. B. Harborne, Ed., Chapman & Hall, London, 1994
4. L. Jurd, in: *The Chemistry of Flavonoid Compounds*, T. A. Geissman, Ed., Pergamon Press, New York, 1962
5. T. J. Mabry, K. R. Markham, M. B. Tomas, *The Systematic Identification of Flavonoids*, Springer-Verlag, Berlin, 1970
6. J. B. Harborne, H. Baxter, *The Handbook of Natural Flavonoids*, Wiley, Chichester, 1999
7. M. G. L. Hertog, P. C. H. Hollman, M. B. Katan, D. Kromhout, *Nutr. Cancer* **20** (1993) 21
8. M. G. L. Hertog, P. C. H. Hollman, M. B. Katan, *J. Agric. Food. Chem.* **40** (1992) 2379
9. N. C. Cook, S. Samman, *J. Nutr. Biochem.* **7** (1996) 66
10. J. Kuhnhan, *World Rev. Nutr. Diet.* **24** (1976) 24
11. J. A. Ross, C. M. Kasum, *Annu. Rev. Nutr.* **22** (2002) 19
12. A. R. Ness, J. W. Powles, *Int. J. Epidemiol.* **26** (1997) 1
13. A. L. Klatsky, G. D. Friedman, M. A. Armstrong, *Am. J. Epidemiol.* **132** (1990) 479
14. H. D. Sesso, J. M. Gaziano, J. E. Buring, C. H. Hennekens, *Am. J. Epidemiol.* **149** (1999) 162
15. C. A. Brown, C. Bolton-Smith, M. Woodward, H. Tunstall-Pedoe, *J. Epidemiol. Com. Health* **47** (1993) 171
16. D. A. Balentine, S. A. Wiseman, L. C. M. Bouwens, *Food Sci. Nutr.* **37** (1997) 693
17. M. L. Neuhouser, *Nutr. Cancer* **50** (2004) 1
18. N. Schmiedebergs, *Arch. Pharmacol.* **370** (2004) 290
19. M. Katan, *Am. J. Clin. Nutr.* **65** (1997) 1542
20. R. R. Huxley, H. A. Neil, *Eur. J. Clin. Nutr.* **57** (2003) 904
21. M. G. L. Hertog, E. J. M. Feskens, P. C. H. Hollman, M. B. Katan, D. Kromhout, *Lancet* **342** (1993) 1007
22. W. Ren, Z. Qiao, H. Wang, L. Zhu, L. Zhang, *Med. Res. Rev.* **23** (2003) 519
23. P. Knekt, R. Järvinen, A. Reunanen, J. Maatela, *Br. Med. J.* **312** (1996) 478
24. E. B. Rimm, M. B. Katan, A. Ascherio, M. J. Stampfer, W. C. Willett, *Ann. Intern. Med.* **125** (1996) 384
25. M. G. L. Hertog, E. J. M. Feskens, D. Kromhout, *Lancet* **349** (1997) 699
26. L. Yochum, H. Kushi, K. Meyer, A. R. Folsom, *Am. J. Epidemiol.* **149** (1999) 943
27. B. Starvic, *Clin. Biochem.* **27** (1994) 245
28. M. G. L. Hertog, P. C. H. Holmann, *Eur. J. Clin. Nutr.* **50** (1996) 63
29. C. Manach, F. Regeat, O. Texier, G. Agullo, C. Demigne, C. Remesy, *Nutr. Res.* **16** (1996) 517
30. N. C. Cook, S. Sammn, *J. Nutr. Biochem.* **7** (1996) 66
31. V. Kuntić, I. Filipović, D. Malešev, S. Jelić, *Yugoslav. Med. Biochem.* **18** (1999) 167
32. B. N. Ames, M. K. Shigenaga, T. M. Hagen, *Proc. Natl. Acad. Sci.* **90** (1993) 7915
33. D. Amic, D. Davidovic-Amic, D. Beslo, N. Trinajstic, *Croat. Chem. Acta* **76** (2003) 55
34. M. M. Silva, M. R. Santos, G. Caroco, R. Rocha, G. Justino, L. Mira, *Free Rad. Res.* **36** (2002) 1219
35. C. A. Rice-Evans, N. J. Miller, G. Paganga, *Free Rad. Biol. Med.* **20** (1996) 933
36. N. Salah, N. J. Miller, G. Paganga, L. Tijburg, G. P. Bolwell, C. Rice-Evans, *Arch. Biochem. Biophys.* **322** (1995) 399

37. I.B.Afanas'ev, E.A.Ostrachovitch, N.E.Abramova, L.G.Korkina, *Biochem. Pharmacol.* **50** (1995) 627
38. W. Bors, M. Saran, *Free Rad. Res. Commun.* **2** (1987) 289
39. L. Mira, M. Silva, C. F. Manso, *Biochem. Pharmacol.* **48** (1994) 753
40. G. Cao, E. Sofic, R. L. Prior, *Free Rad. Biol. Med.* **22** (1997) 749
41. S. R. Husain, J. Cillard, P. Cillard, *Phytochemistry* **26** (1987) 9
42. K. Ioku, T. Tsushida, Y. Takei, N. Nakatani, J. Terao, *Biochim. Biophys. Acta* **1234** (1995) 99
43. S. Renaud, M. deLorgeli, *Lancet* **339** (1992)1523
44. W. Bors, W. Heller, C. Michel, in: *Flavonoids in Health and Disease*, C. A. Rice-Evans, L. Packer, Eds., Marcel Dekker, New York, 1998, p. 111
45. *German Pharmacopoeia*, Deutscher Apotheker Verlag, Stuttgart, 2000
46. T. A. van Beek, *J. Chromatogr. A* **967** (2002) 25
47. H. J. H. Fenton, *J. Chem. Soc.* **65** (1894) 889
48. H. E. Hajji, E. Nkhili, V. Tomao, O. Danglas, *Free Rad. Res.* **40** (2006) 303
49. S. van Acker, G. P. van Balen, B. van der Berg, W. J. F. van der Vijgh, *Biochem. Pharmacol.* **56** (1998) 935
50. I. B. Afanas'ev, A. I. Dorozhko, A. V. Brodskii, V. A. Kostyuk, A. I. Potapovitch, *Biochem. Pharmacol.* **38** (1989) 1763
51. J. E. Brown, H. Khodr, R. C. Hider, C. A. Rice-Evans, *Biochem. J.* **330** (1998) 1173
52. M. Fiorani, R. De Sancitis, R. De Bellis, M. Dacha, *Free Rad. Biol. Med.* **32** (2002) 64
53. S. Fleschin, K. R. Jennings, *Free Rad. Res.* **36** (2002) 1199
54. L. Mira, M. T. Fernandez, M. Santos, R. Rocha, M. H. Florenico, K. R. Jennings, *Free Rad. Res.* **36** (2002) 1199
55. M. T. Fernandez, M. L. Mira, M. H. Florenco, K. R. Jennings, *J. Inorg. Biochem.* **92** (2002) 105
56. V. A. Kostyuk, A. I. Potapovich, E. N. Vladykovskaya, L. G. Korkina, I. B. Afanas'ev, *Arch. Biochem. Biophys.* **385** (2001) 129
57. M. Y. Moridani, J. Pourahmad, H. Bui, A. Siraki, P. J. O'Brien, *Free Rad. Biol. Med.* **34** (2003) 243
58. R. F. De Souza, W. F. De Giovanni, *Redox. Rep.* **9** (2004) 97
59. I. B. Anafas'ev, E. A. Ostrakhovitch, E. V. Mikhail, G. A. Ibragimova, L. G. Korkina, *Biochem. Pharmacol.* **61** (2001) 677
60. H. Tang, X. Wang, S. Yang, L. Wang, *Rare Metals* **23** (2004) 38
61. M. Kopacz, E. Woznicka, J. Gruszecka, *Acta Pol. Pharm.* **62** (2005) 65
62. J. Zhou, L. Wang, J. Wang, N. Tang, *J. Inorg. Biochem.* **83** (2001) 41
63. Z. Deng, C. Coudray, L. Gouzoux, A. Mazur, Y. Rayssiguier, D. Pepin, *Biol. Trace Elem. Res.* **76** (2000) 245
64. S. X. Wang, F. J. Zhang, Q. P. Feng, Y. L. Li, *J. Inorg. Biochem.* **46** (1992) 251
65. R. Kh. Yuldashev, Kh. M. Makhkamov, Kh. T. Sharipov, Kh. U. Aliev, *Chem. Nat. Comp.* **35** (1999) 420
66. P. Viswanathan, V. Sriram, *J. Agric. Food. Chem.* **48** (2000) 2802
67. A. C. Boudet, J. P. Cornard, J. C. Merlin, *Spectrochim. Acta* **56** (2000) 829
68. J. P. Cornard, J. C. Merlin, *J. Mol. Struct.* **569** (2001) 129
69. J. P. Cornard, A. C. Boudet, J. C. Merlin, *Spectrochim. Acta* **57** (2001) 591
70. J. P. Cornard, J. C. Merlin, *J. Inorg. Biochem.* **92** (2002) 19
71. R. F. De Souza, E. M. Sussuchi, W. F. De Giovanni, *Synth. Reac. Inorg. Met.-Org. Chem.* **33** (2003) 1125
72. A. Torreggiani, M. Tamba, A. Trincherro, S. Bonora, *J. Mol. Struct.* **744-747** (2005) 759
73. M. D. Engelman, E. R. Hutchenson, I. F. Cheng, *J. Agric. Food Chem.* **53** (2005) 2953

74. R. F. De Souza, W. F. De Giovanni, *Spectrochim. Acta* **61** (2005) 1985
75. Z. Radović, D. Malešev, *Arh. Farm.* **4** (1983) 147
76. Z. Radović, D. Malešev, *Arh. Farm.* **5** (1983) 221
77. D. Malešev, Z. Radović, *Bull. Soc. Chim.* **48** (1983) 745
78. Z. Radović, D. Malešev, *Pharmazie* **39** (1984) 870
79. D. Malešev, Z. Radović, *Pharmazie* **40** (1985) 133
80. Z. Radović, D. Malešev, *Mikrochim. Acta* **2** (1985) 247
81. Z. Radović, D. Malešev, *Arch. Pharm.* **320** (1987) 188
82. Z. Radović, D. Malešev, *Acta Polon. Pharm.* **XLIV** 5 (1987) 433
83. D. Malešev, Z. Radović, *Pharmazie* **42** (1987) 57
84. D. Malešev, Z. Radović, *Pharmazie* **42** (1987) 59
85. Z. Radović, D. Malešev, *Pharmazie* **43** (1988) 135
86. D. Malešev, Z. Radović, *Pharmazie* **44** (1989) 496
87. D. Malešev, Z. Radović, M. Jelikić-Stankov, *Pharmazie* **44** (1989) 863
88. D. Malešev, Z. Radović, M. Jelikić-Stankov, *Monatsh. Chem.* **121** (1990) 455
89. D. Malešev, Z. Radović, M. Jelikić-Stankov, *J. Serb. Chem. Soc.* **55** (1990) 607
90. D. Malešev, Z. Radović, M. Jelikić-Stankov, *Monatsh. Chem.* **122** (1991) 429
91. D. Malešev, Z. Radović, M. Jelikić-Stankov, M. Bogavac, *Anal. Lett.* **24** (1991) 1159
92. D. Malešev, Z. Radović, M. Jelikić-Stankov, *Pharmazie* **46** (1991) 534
93. D. Malešev, Z. Radović, M. Jelikić-Stankov, *Arh. Farm.* **46** (1991) 223
94. D. Malešev, Z. Radović, M. Jelikić-Stankov, *Spectrosc. Lett.* **25** (1992) 1089
95. Z. Radović, D. Malešev, *Arh. Farm.* **42** (1992) 27
96. D. Malešev, Z. Radović, M. Jelikić-Stankov, *Arh. Farm.* **42** (1992) 163
97. D. Malešev, Z. Radović, M. Jelikić-Stankov, *J. Serb. Chem. Soc.* **58** (1993) 557
98. D. Malešev, Z. Radović, M. Jelikić-Stankov, *Spectrosc. Lett.* **26** (1993) 1985
99. Z. Radović, D. Malešev, M. Jelikić-Stankov, *Pharmazie* **51** (1996) 8
100. D. Malešev, Z. Radović, V. Kuntić, M. Kosanić, *Anal. Lett.* **30** (1997) 917
101. V. S. Kuntić, D. L. Malešev, Z. V. Radović, M. M. Kosanić, U. B. Mioč, V. B. Vukojević, *J. Agric. Food Chem.* **46** (1998) 5139
102. V. Kuntić, S. Blagojević, D. Malešev, Z. Radović, M. Bogavac, *Monatsh. Chem.* **129** (1998) 41
103. V. Kuntić, M. Kosanić, D. Malešev, Z. Radović, *Pharmazie* **53** (1998) 724
104. V. Kuntić, M. Kosanić, D. Malešev, Z. Radović, U. Mioč, *J. Serb. Chem. Soc.* **63** (1998) 565
105. V. Kuntić, S. Blagojević, D. Malešev, Z. Radović, *Pharmazie* **54** (1999) 548
106. S. Blagojević, D. Malešev, Z. Radović, *Arh. Farm.* **5-6** (1999) 287
107. V. Kuntić, D. Malešev, Z. Radović, V. Vukojević, *Monatsh. Chem.* **131** (2000) 769
108. M. Aleksić, S. Blagojević, D. Malešev, Z. Radović, *J. Serb. Chem. Soc.* **65** (2000) 631
109. N. Pejić, V. Kuntić, D. Malešev, *Pharmazie* **57** (2002) 216
110. S. Blagojević, M. Aleksić, D. Malešev, Z. Radović, *Arh. Farm.* **5** (2003) 17
111. V. Kuntić, N. Pejić, S. Mičić, V. Vukojević, Z. Vujić, D. Malešev, *J. Serb. Chem. Soc.* **70** (2005) 753
112. P. G. Pietta, *J. Nat. Prod.* **63** (2000) 1035
113. M. E. Bodini, G. Copia, R. Tapia, F. Leighton, L. Herrera, *Polyhedron* **18** (1999) 2233
114. J. Inczedy, *Analytical applications of complex equilibria*, Ellis Horwood Ltd., New York, 1976
115. M. Obradović, D. Veselinović, P. Đurđević, *Fizičko-hemijske metode ispitivanja ravnoteža u kompleksirajućim sredinama*, Filozofski fakultet Niš, Fakultet za fizičku hemiju, Beograd, 1996
116. D. J. Daigle, E. J. Conkerton, *J. Liq. Chromatogr.* **11** (1988) 309
117. J. P. V. Leite, L. Rastrelli, G. Romussi, A. B. Oliveira, J. H. Y. Vilegas, C. Pizza, *J. Agric. Food Chem.* **49** (2001) 3796

118. W. K. Li, J. F. Fitzloff, *J. Chromatogr., B: Biomed. Appl.* **765** (2001) 99
119. C. Queija, M. A. Queiros, L. M. Rodrigues, *J. Chem. Educ.* **78** (2001) 236
120. C. L. Moreira, S. R. De Paiva, J. L. M. Da Costa, M. R. Figueiredo, *J. High. Resol. Chromatogr.* **22** (1999) 527
121. A. Crozier, E. Jensen, M. E. J. Lean, M. S. McDonald, *J. Chromatogr., A* **761**(1997) 315
122. U. Justesen, K. Pia, L. Torben, *J. Chrom. A* **799** (1997) 101
123. P. L. Menghinello, F. Cucchiarini, D. Palma, M. Agostini, V. Dacha, *J. Liq. Chromatogr. Relat. Technol.* **22** (1999) 3007
124. L. Bramati, F. Aquilano, P. Pietta, *J. Agric. Food. Chem.* **51** (2003) 7472
125. A. B. Teris, *J. Chromatogr., A* **967** (2002) 21
126. A. Hasler, O. Sticher, B. Meier, *J. Chromatogr., A* **605** (1992) 41
127. *XXX Romanian Pharmacopoeia X*, Ed. Medicală, București, 1993
128. M. Stanciu-Rotaru, M. Mititelu, M. Crasnaru, D. Balaban, *Roum. Biotech. Lett.* **8** (2003) 1093
129. V. A. Bandyukova, A. L. Shinkarenko, *Zh. Analit. Khim.* **21** (1966) 232
130. F. D. Drawert, W. Heimann, A. Ziegler, *Anal. Chem.* **217** (1966) 22
131. N. A. Tykavkina, K. I. Lapteva, N. G. Devyatko, *Zh. Analit. Khim.* **24** (1969) 777
132. A. B. Blank, I. I. Mirenskaya, *Zh. Analit. Khim.* **27** (1972) 1883
133. A. Korcuc, K. Lesz, *Chem. Anal.* **17** (1972) 855
134. E. P. Shkrobot, *Zh. Analit. Khim.* **17** (1962) 186
135. N. L. Olenovich, L. I. Kovalchuk, *Zh. Analit. Khim.* **28** (1973) 2162
136. A. B. Blank, I. I. Mirenskaya, L. M. Satanovsii, *Zh. Analit. Khim.* **30** (1975) 1116
137. A. B. Blank, I. I. Mirenskaya, L. P. Eksperiandova, *Zh. Analit. Khim.* **28** (1973) 1331
138. A. T. Pilipenko, T. U. Kukibaev, A. I. Volkova, T. E. Getman, *Ukr. Khim. Zh.* **39** (1973) 819
139. A. T. Pilipenko, T. U. Kukibaev, A. I. Volkova, *Zh. Analit. Khim.* **28** (1973) 510
140. A. P. Golovina, A. P. Tsintsevich, A. F. Karpovish, E. U. Kovalenko, N. B. Zorov, *Zh. Analit. Khim.* **28** (1973) 815
141. A. T. Pilipenko, A. I. Zhebentayev, A. I. Volkova, *Ukr. Khim. Zh.* **38** (1972) 363
142. M. Katyal, *Talanta* **15** (1968) 95
143. A. Korcuc, *Wiadom. Chem.* **23** (1969) 345
144. E. M. Nevskaya, V. A. Nazarenko, *Zh. Analit. Khim.* **27** (1972) 1699
145. M. Katyal, S. Prakash, *Talanta* **24** (1977) 367
146. E. A. Saad, L. H. Khalil, M. T. M. Zaki, A. A. Abu El-Ella, *Mikrochim. Acta* **140** (2002) 87
147. A. M. Jamaluddin, H. Jamail, *Talanta* **42** (1995) 1135
148. A. Saffavi, M. Mirzace, H. Abdollahi, *Anal. Lett.* **36** (2003) 699
149. M. Z. Gonzalez, M. E. Diaz Garcia, A. Sanz-Medel, *Talanta* **36** (1989) 919
150. A. Y. El-Sayed, E. A. Saad, B. M. M. Ibrahime, M. T. M. Zaki, *Mikrochim. Acta* **135** (2000) 19
151. N. Pourreza, K. Alizadeh, *J. Anal. Chem* **53** (1998) 520
152. A. Y. El-Sayed, M. M. H. Khalil, *Talanta* **43** (1996) 583
153. M. Tarek, M. Zaki, A. K. Abdel-Kader, M. M. Abdalla, *Fresenius J. Anal. Chem* **339** (1991) 197
154. D. Obendorf, E. Reichart, *Electroanalysis* **7** (1995) 1075.

SHORT COMMUNICATION

A mild and effective method for the conversion of alkenes into alcohols in subcritical water

RECEP OZEN* and NERMİN S. KUS

Mersin University, Department of Chemistry, Mersin, Turkey

(Received 18 December 2006)

Abstract: Alkenes were oxidized to alcohols in subcritical water. A number of alkenes were oxidized directly to their alcohols in excellent yields. The syntheses were performed in 215 cm³ stainless steel high pressure reactor at 120 °C in 150 cm³ water. The yields of alcohols increased with the nitrogen pressure.

Keywords: alkene, alcohol, subcritical water, oxidation.

INTRODUCTION

Several methods such as oxymercuration, hydroboration, treatment with water in the presence of an acid catalyst and addition of water to olefins in the presence of a transition metal catalyst as well as strong acid catalyzed reactions in subcritical water have been introduced in the literature for the hydration of alkenes.¹ Although the conversion of alkenes to alcohols have been known in subcritical media (Fig. 1),² many of the methods³ employ strong acids and metal catalysts which are not environmentally friendly. The use of subcritical water as a medium for chemical reactions has recently received a great deal of attention.^{4–5} In contrast to many other solvents, water not only provides a medium for solution chemistry but also often participates in chemical events. Water also offers practical advantages over organic solvents as it is inexpensive, readily available, non-toxic and non-flammable. A previous study,⁶ the oxidation of toluene to aromatic aldehydes with molecular oxygen in subcritical water was reported. In continuation of our recent work, oxidative coupling of thiols with molecular oxygen in subcritical water was performed⁷ and an alternative procedure for the conversion of alkenes into alcohols was reported.⁶

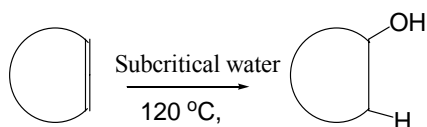


Fig. 1. Conversion of alkenes to alcohols.

* Corresponding author. E-mail: rozen@mersin.edu.tr
doi: 10.2298/JSC0710941O

EXPERIMENTAL

IR spectra were recorded on a Win First Satellite[®] model spectrophotometer. ¹H-NMR spectra were obtained using a 400 MHz Bruker DPX[®] instrument.

General Procedure

The reactions were performed at 120 °C and in a 215 cm³ stainless steel pressure reactor⁵ equipped with a N₂ pressure gauge, safety valve, digital temperature reader, heater and magnetic stirrer. The pressure was kept at 50 bar with N₂. A glass vessel was inserted into the reactor to avoid the catalytic effect of steel and corrosion. The reactor was charged with alkene (1 g) and 150 cm³ H₂O. N₂ was supplied through a tube directly into the liquid phase. After completion of the reaction, the reactor mixture was cooled to room temperature and extracted with ethyl acetate (3×25 cm³). The combined organic extracts were dried (MgSO₄) and evaporated on a rotary evaporator under reduced pressure. Then the desired products were chromatographed over silica gel using ethyl acetate as the eluent. Evaporation of the solvent gave fairly pure alcohols, which were identified by IR and ¹H-NMR spectroscopy.

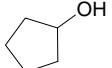
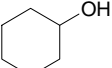
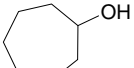
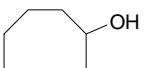
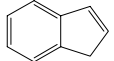
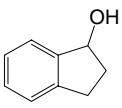
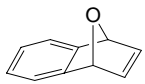
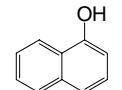
RESULTS AND DISCUSSION

In the present work, four monocyclic and four bicyclic olefins were converted into the corresponding alcohols in excellent yields. The reactions were performed at 120 °C under various pressures of nitrogen. The reactor was heated slightly before the reactions were commenced. Air oxygen and oxygen dissolved in water was removed from the reactor by bubbling nitrogen gas. Then, nitrogen gas was introduced into the reactor and the temperature was maintained at 120 °C. The reactions were monitored by TLC. In order to investigate effect of pressure on the yields, the reactions were carried out at different pressures. The yields were shown to depend on the nitrogen pressure. Reactions were performed at 20, 30, 40 and 50 bar of nitrogen. When the pressure was greater than 50 bar, the olefins polymerized. On the other hand, when the pressure was decreased below 20 bar, the reactions were incomplete. The ideal pressure was 50 bar of nitrogen. Similarly, different temperatures were examined. The best temperature was found to be 120 °C. All the products were characterized by their spectral data and comparison with reported data.⁸⁻¹⁰

As can be seen from Table I, the yields of alcohols from bicyclic olefins were slightly higher than from monocyclic olefins. The reactions times of the bicyclic olefins were shorter than those of the monocyclic olefins. It is assumed that these conversions proceeded *via* a radical mechanism, because the behavior of subcritical water as a radical oxidant in the presence of a metal catalyst has been known for a long time.² However, hitherto alkenes have not been converted to the corresponding alcohols in subcritical water without a metal catalyst. Oxabenzonorbornadiene (entry 8) was converted to 1-naphthol by the opening of the oxygen bridge, because the oxygen bridge is weaker than the methylene bridge. This result was to be expected.

The presented method is a simple, economic, environmentally friendly method for the transformation of olefins to alcohols.

Table I. Conversion of olefins into alcohols in subcritical water

Entry	Substrate	Product	τ / h	Yield / %			
				$p(\text{N}_2)$ / bar			
				20	30	40	50
1			8 ⁸	70	75	80	80
2			7 ⁸	75	80	85	85
3			8 ⁸	80	83	83	90
4			9 ⁸	78	85	82	85
5			4 ⁸	87	90	95	90
6			3 ⁹	73	78	80	85
7			3 ⁸	80	85	85	85
8			2 ¹⁰	75	80	83	85

Reactions conditions are exemplified in the general reaction procedure. Isolated yields obtained after chromatography. All products were characterized by ¹H-NMR and IR spectroscopic data and their physical data compared with literature data.

Acknowledgments: We are grateful to the Mersin University Research Council and TUBITAK (The Scientific and Technical Council of Turkey) for the supporting this work (Grant No: TBAG-2235).

ИЗВОД

ЈЕДНОСТАВАН И ЕФИКАСАН МЕТОД КОНВЕРЗИЈЕ АЛКЕНА
У АЛКОХОЛЕ У СУПКРИТИЧНОЈ ВОДИ

RECEP OZEN и NERMİN S. KUS

Mersin University, Department of Chemistry, Mersin, Turkey

У раду је приказан метод оксидације алкена до алкохола у супкритичној води. Већи број алкена је оксидован до оговарајућих алкохола са одличним приносом. Синтезе су обављене у реакторима од нерђајућег челика запремине од 215 cm³, који подноси високе притиске, при температури од 120 °C и запремини воде од 150 cm³. Принос алкохола растао је са притиском азота.

(Примљено 18. децембра 2006)

REFERENCES

1. J. March, *Advanced Organic Chemistry*, 4th ed., Wiley, New York, USA, 1992 p. 759
2. A. R. Katritzky, D. A. Nichols, M. Siskin, R. Murgan, M. Balasubramanian, *Chem. Rev.* **101** (2001) 837
3. R. C. Crittendon, E. J. Parsons, *Organometallics* **13** (1994) 2587
4. C. M. Kormos, N. E. Leadbeater, *Tetrahedron* **62** (2006) 4728
5. P. J. Gemperline, Y. Yang, Z. Bian, *Anal. Chem. Acta* **73** (2003) 485
6. B. Kayan, A. M. Gizir, R. Ozen, N. S. Kus, *Org. Prep. Proced. Int.* **37** (2005) 83
7. R. Ozen, F. Aydin, *Monatsh. Chem.* **137** (2006) 307
8. L. D. Ride, *CRC Handbook of Chemistry and Physics*, 72nd ed., Taylor and Francis, Boca Raton, 1991–1992
9. D. J. Sandman, K. Mislow, W. P. Giddings, J. Dirlam, G. C. Hanson, *J. Am. Chem. Soc.* **90** (1968) 4877
10. G. R. Ziegler, *J. Am. Chem. Soc.* **91** (1969) 446.

Do altered activities of superoxide dismutases and the level of NF- κ B modulate the effects of gamma radiation in HeLaS3 cells?

ANA NIĆIFOROVIĆ¹, MIROSLAV ADŽIĆ¹, SNEŽANA D. SPASIĆ^{2#} and
MARIJA B. RADOJČIĆ^{1*}

¹Department of Molecular Biology and Endocrinology, Vinča Institute of Nuclear Sciences, Belgrade and ²Centre of Chemistry, ICTM, Belgrade, Serbia

(Received 21 February 2007, revised 31 May 2007)

Abstract: Most experimental models, including cell culture studies, have demonstrated that over-expression of manganese superoxide dismutase (MnSOD) in cells bearing a carcinoma phenotype has anti-proliferative and tumour suppression characteristics. In contrast, when cervical carcinoma biopsies express MnSOD, there is a poor prognosis and resistance to radiation therapy. The results herein indicate that human cervical adenocarcinoma (HeLaS3) cells have increased MnSOD activity (up to 50 % of the total SOD activity) due to low expression of its repressor p53 and a high level of oxidative stress arising from the cell culture conditions. High MnSOD activity may be related to HeLaS3 cell radioresistance, illustrated by a high IC₅₀ of 3.4 Gy and by a relatively high level of cell viability after gamma irradiation. In contrast to MnSOD activity, cytosolic CuZnSOD activity decreased after ionising radiation. The catalase (Cat) activity was unchanged. IR also increased the nitric oxide synthase (NOS) activity. Such conditions lead to increased concentrations of the superoxide radical, hydrogen peroxide and NO[•], which together may be responsible for the decreased expression of NF- κ B and unaltered Cat activity. Therefore, the disturbed redox balance within HeLaS3 cells may be responsible for the cytotoxicity observed at higher irradiation doses. It could be concluded that inhibition of the CuZnSOD activity may be an important target for the selective killing of radioresistant cancer cells.

Keywords: gamma irradiation, antioxidant enzymes, NF- κ B, p53, HeLaS3 cells.

INTRODUCTION

Carcinoma of the uterine cervix is one of the most frequent malignancies in the human population with 500,000 newly diagnosed cases annually.^{1,2} It is usually treated by surgery in combination with subsequent ionising radiation (IR) therapy.^{3–5} Cervical carcinomas are characterised by the fact that approximately

[#] Serbian Chemical Society member.

* Corresponding author. E-mail: marija@vin.bg.ac.yu
doi: 10.2298/JSC0710945N

half of the biopsies express manganese superoxide dismutase (MnSOD) and there is significant association between MnSOD expression, poor prognosis and resistance to IR therapy.⁶ A cervical carcinoma cell culture model (HeLaS3 cells) constitutively possesses enhanced MnSOD activity, probably due to the inserted human papilloma virus E6 protein causing ubiquitination and degradation of p53.⁷ In p53-deficient cervical carcinoma cells, resistance to irradiation correlates with an increased expression of MnSOD and this enzyme is negatively regulated at the transcriptional level by p53.⁸ Adaptation of these cells grown in culture may lead to up-regulation of the antioxidant defence enzymes.⁹ Thus, induced over-expression of MnSOD in HeLaS3 cells could further influence their response to a free radical challenge.¹⁰

Elevated MnSOD activity represents a survival factor which is required for the maintenance of mitochondrial integrity in cells exposed to adverse conditions.^{11,12} It seems that there is an established molecular basis for the correlation of MnSOD expression in cervical carcinoma and resistance to IR therapy. As MnSOD is predominantly anti-apoptotic,^{13,14} MnSOD over-expression in tumours could offer a survival advantage to tumour cells, leading to their radioresistance due to their low apoptotic potential.¹⁵ High MnSOD activity leads to an increased amount of hydrogen peroxide (H₂O₂) which could *via* NF-κB activation and trans-activation of the MnSOD gene build up a positive feed-forward loop.¹⁶

NF-κB is considered to be a primary oxidative stress-responsive transcription factor which plays a critical role in balancing pro- and anti-apoptotic activities.^{17,18} NF-κB is sensitive to concentrations of ROS and can be activated by H₂O₂ in a cell type-specific manner.¹⁹ Increased activity of NF-κB may promote the survival of mutated cells.²⁰ In contrast, other studies have indicated that over-expression of MnSOD is closely associated with tumour regression *in vivo* and loss of malignant phenotype *in vitro*.^{21–23} The current prevailing theory of the tumour-suppressing ability of MnSOD is that an imbalance in the redox state of the cell leads to an inhibition of cell proliferation. One explanation for these growth-suppressive effects of MnSOD could be the resulting imbalance of the antioxidant enzymes, which favours H₂O₂ accumulation.²⁴ Possible mechanisms for the suggested tumour-suppressive consequences of MnSOD over-expression could be the modulation of specific oncogenes,²⁵ up-regulation of protease inhibitors²⁶ and inhibition of the transcription factors AP-1 and NF-κB.²⁷

In the present study, alterations in the expression of NF-κB and p53 and alterations in the activity of the major anti-oxidant enzymes MnSOD, CuZnSOD and catalase (Cat), and inducible nitric oxide (NO[•]) synthase activity (iNOS) in HeLaS3 cells exposed to IR were explored. The obtained data offer practical information concerning the therapeutic effects of IR when biopsies of human uterine cervical carcinoma express MnSOD.

EXPERIMENTAL

Cell culture. The human uterine cervical adenocarcinoma cell line HeLaS3 was obtained from the American Type Culture Collection (Rockville, MD, USA). The cells were maintained in 95 % Ham's F12 supplemented with 5 % heat-inactivated foetal calf serum, 100 IU ml⁻¹ penicillin and streptomycin and 2 mM L-glutamine (all obtained from Sigma-Aldrich, Taufkirchen, Germany). The cells were grown as a monolayer in a humidified atmosphere of 95 % air and 5 % CO₂ at 37 °C. Asynchronous cultures were chosen for all the experiments because techniques for the synchronisation of mammalian cell lines often lead to perturbation of cell cycle checkpoint mechanisms.²⁸

Cell irradiation. IR (2, 5 and 10 Gy of gamma-rays) was delivered during the exponential phase of cell growth using a ⁶⁰Co source at a fixed dose rate of 20 Gy h⁻¹.

Cell viability. Cell growth and viability were determined using the Trypan Blue exclusion assay.

Sample preparation and Western blot analyses. Trypsinised and washed cells were lysed using a buffer containing 10 mM Tris-HCl pH 7.4, 0.32 M sucrose, 5 mM MgCl₂, 1 % Triton X-100 and a protease inhibitor cocktail. The protein concentration in the cell lysates was determined by the Lowry method.²⁹ Aliquots of lysates were mixed with denaturing buffer according to Laemmli,³⁰ boiled (100 °C, 2 min), separated by SDS-polyacrylamide gel electrophoresis (60 µg of cell protein per gel lane) and transferred to nitrocellulose membranes. The membranes were blocked using 10 mM Tris buffer pH 7.4 supplemented with 150 mM NaCl, 1 % BSA and 0.1 % Tween-20. The membranes were separately incubated with rabbit anti-actin antibody (CSA-400), anti-mouse p53 antibody (KAM-CC002), both from Stressgen Biotechnologies, Victoria, BC, Canada, and rabbit anti-NF- κ B antibody (NF- κ B p65, C-20; SC-372, Santa Cruz Biotechnology, CA, USA), a secondary goat anti-rabbit IgG HRP conjugate (SAB-300) and an anti-mouse IgG HRP conjugate (SAB-100) (Stressgen Biotechnologies, Victoria, BC, Canada) were used for detection. The quantification of the specific antigen bands was performed using an UltroScan XL scanning laser densitometer and computer image processing. The level of detected proteins by Western blotting was expressed in arbitrary units (AU mg⁻¹ of protein).

Determination of enzyme activities. SOD activity in cell lysates was determined according to McCord and Fridovich as the percentage inhibition of superoxide (O₂⁻) formation induced by the xanthine-xanthine oxidase system.^{31,32} The results are expressed as units mg⁻¹ of total cellular protein. Cat activity was determined according to Claiborne.³³ One unit of Cat activity is defined as the amount of enzyme that degrades 1 µmol of H₂O₂ min⁻¹ mg⁻¹ of protein.

Citrulline assay. The L-citrulline assay was used to measure the inducible NOS activity by a colorimetric assay of deproteinised samples, as previously described by Boyde *et al.*³⁴ In parallel, L-citrulline was used as a standard and taken through the full assay procedure. All assay reagents were purchased from Sigma-Aldrich.

Statistical analysis. The values are presented as mean \pm standard deviation (SD) calculated from four individual experiments. Statistical significance was evaluated using the one-way analysis of variance and the Tukey post-hoc test; $p < 0.05$ was considered to be statistically significant.

RESULTS AND DISCUSSION

To investigate the effect of IR on cell viability and cell growth, HeLaS3 cells were irradiated with 2, 5 and 10 Gy, returned to normal culture conditions and then analysed 24, 48 and 72 h after irradiation. Cell growth inhibition, expressed as the cell viability index, V_i , was significantly reduced after IR treatment. This reduction was both time- and dose-dependent (Fig. 1B). The greatest effect of IR was observed after a dose of 10 Gy, which inhibited cell proliferation by 80 % (at 72 h after irradiation, $p < 0.001$). The calculations indicated that the V_i was 18.1 ± 3.0 ,

whilst the IR dose that decreased cell growth from 100 to 50 % (IC_{50}) was 3.4 ± 0.2 Gy. This relatively high IC_{50} classifies HeLaS3 as a radioresistant cell line. This was confirmed with the high cell viability, which decreased to only 60 % after 10 Gy at 72 h post irradiation (Fig. 1A). The results indicated that IR-mediated HeLaS3 tumour suppression occurred *via* a non-cytotoxic mechanism.

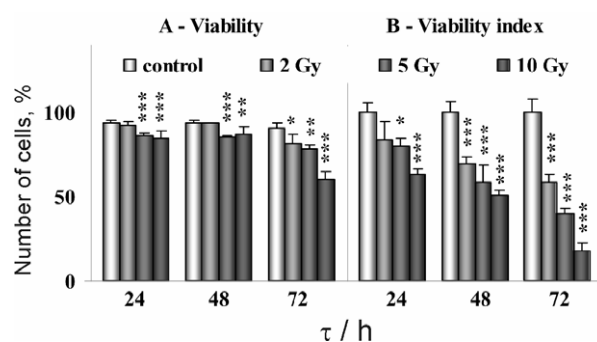


Fig. 1. The time- and the dose-dependence of cell viability (panel A) and cell viability index (panel B) of irradiated HeLaS3 cells. The results are presented as mean \pm SD, $n = 4$. * $p < 0.05$, ** $p < 0.01$ and *** $p < 0.001$, refer to differences between irradiated samples vs. the respective control.

In order to investigate the molecular basis of the anti-proliferative action of IR, the activity of the three anti-oxidant enzymes MnSOD, CuZnSOD and Cat, as well as of inducible NOS, was determined. It is known that selective elevation of MnSOD activity increases the resistance of both non-malignant and malignant cells to oxidants and oxidant-generating events such as IR³⁵⁻³⁷ but may, under unbalanced conditions culminate in increased sensitivity. The high constitutive MnSOD expression in HeLaS3 cells, potentiated with mild oxidative stress under the cell culture conditions,⁹ may be related to their observed radioresistance, illustrated by their high IC_{50} and V_i . However, IR caused a further increase in the MnSOD activity (which is in agreement with observations of other authors)³⁸ simultaneously with a decrease in the CuZnSOD activity (Fig. 2). Cytosolic CuZnSOD activity has generally not been found to be elevated in tumours. Furthermore, its expression is not dependent on the generation of reactive oxygen species (ROS).³⁹ This is in accordance with reports indicating that conditions generating O_2^- , such as IR, could induce the synthesis of MnSOD but not of CuZnSOD.⁴⁰ The present observations concerning SOD activities were similar to those previously found in HTE epithelial cells and MCF-7 human breast adenocarcinoma cells.⁴¹ As the Cat activity remained unchanged (Table I), such a situation led to unbalanced conditions with a high pro-oxidative potential of endogenously formed H_2O_2 . The high H_2O_2 concentration could also have been the reason for the inhibition of CuZnSOD activity, but not of MnSOD activity. Decreased CuZnSOD activity can contribute to decreased cell proliferation, as fibroblasts derived from CuZnSOD knockout animals proliferate more slowly (25 % less) than control cells, emphasising the importance of CuZnSOD activity in cell growth and survival.⁴² Inhibition of CuZnSOD activity may cause accumulation of endogenous O_2^- and lead to free radical-mediated mitochondrial membrane damage, release of mitochondrial

cytochrome *c* and increase apoptosis of cancer cells.⁴³ The present results also indicate that targeting CuZnSOD activity may be a promising approach to the selective killing of cancer cells.⁴³ Untoxified H₂O₂ may be related to cell cycle arrest in the S phase *via* Cip1 (p21) and cyclin D3 inhibition.⁴⁴ IR induces a late S phase arrest in HeLaS3 cells. This latter observation was noted in a previous study⁴⁵ as well as in an independent study.⁴⁶

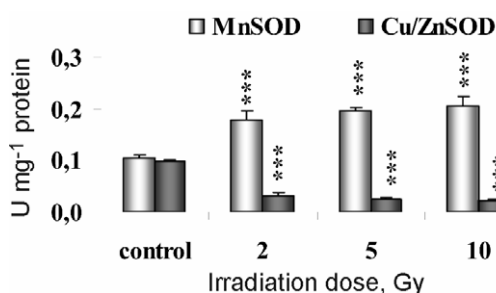


Fig. 2. IR-induced changes in MnSOD and CuZnSOD activity in irradiated HeLaS3 cells (analysed 72 h after irradiation). The results are presented as mean \pm SD, $n = 4$. *** $p < 0.001$ refers to differences between irradiated samples vs. the respective control.

TABLE I. Antioxidant enzyme activity and expression level of transcription factors in irradiated HeLaS3 cells (analysed 72 h after irradiation). The results are presented as mean \pm SD, $n = 4$. ** $p < 0.01$ and *** $p < 0.001$ refer to differences between irradiated samples vs. the respective control

	Catalase U mg ⁻¹	L-Citrulline % of control	NF- κ B AU mg ⁻¹	p53 AU mg ⁻¹
Control	12.2 \pm 1.0	100.0 \pm 1.7	100.0 \pm 2.9	100.0 \pm 0.7
2 Gy	12.8 \pm 1.8	107.5 \pm 2.5	89.8 \pm 4.6	99.5 \pm 1.2
5 Gy	13.3 \pm 2.2	112.9 \pm 2.6**	82.1 \pm 6.9**	94.5 \pm 6.4
10 Gy	13.9 \pm 1.6	115.2 \pm 0.8***	75.1 \pm 4.7***	94.1 \pm 3.7

Key signalling networks which regulate the response to IR also involve the redox-sensitive transcriptional factors p53 and NF- κ B. In the current HeLaS3 cell study, in contrast to some other cell lines,⁴⁷ IR did not induce expression of p53.⁸ However, it led to a decreased expression of NF- κ B, by approximately 25 % (Table I). It is well established that NF- κ B may protect against a variety of apoptotic signals. In addition, its decreased expression has been shown to enhance the sensitivity of tumours to apoptosis induced by IR. Furthermore, there is correlation between increased NO[•] production after IR, NF- κ B inhibition by NO[•] and induction of apoptosis in several cell lines. These findings could explain the IR-mediated down-regulation of NF- κ B observed in this study. Increased activity of iNOS, measured by the citrulline assay (Table I), could be one of the reasons for the decreased NF- κ B expression. Another reason may be a mechanism involving over-expression of MnSOD. Such a signalling pathway linking MnSOD over-expression with down-regulation of NF- κ B has been described in MCF-7 cells.⁴¹

CONCLUSIONS

In conclusion, IR-induced cellular perturbations in HeLaS3 cells involve down-regulation of NF- κ B (p65) expression, increased activity of mitochondrial

MnSOD and unchanged Cat activity. Such a situation leads to an increase in the endogenous level of H₂O₂, which may be related to cell cycle arrest in the S phase *via* Cip1 (p21) and cyclin D3 inhibition.³⁹ The present results also indicated that cytosolic CuZnSOD activity decreased upon IR treatment, which could have been a consequence of a high endogenous concentration of H₂O₂, leading to decreased cell proliferation. Therefore, it is proposed that targeting CuZnSOD with an inhibitory adjuvant drug may be a promising approach to the selective killing of cancer cells.

Acknowledgement: The work was supported by a project grant (number 143042B) from the Serbian Ministry of Science.

ИЗВОД

ДА ЛИ ИЗМЕЊЕНЕ АКТИВНОСТИ СУПЕРОКСИДНИХ ДИСМУТАЗА И НИВОА NF-κB У HeLaS3 ЋЕЛИЈАМА МОДУЛИШУ ЕФЕКТЕ ГАМА ЗРАЧЕЊА?

АНА НИЋИФОРОВИЋ¹, МИРОСЛАВ АЦИЋ¹, СНЕЖАНА Д. СПАСИЋ² И МАРИЈА Б. РАДОЉЧИЋ¹

¹Laboratorija za molekularnu bioloģiju i endokrinologiju, Institut za nuklearne nauke "Vin-a", Beograd i ²Centar za hemiju I HTM, Beograd

Највећи број експерименталних модела, који укључују и студије на ћелијама у култури, показује да повећана експресија манган-супероксид-дисмутазе (MnSOD), у ћелијама које имају малигни фенотип, има антипролиферативне и тумор-супресорске карактеристике. За разлику од тога када су биопсије карцинома цервикса утеруса MnSOD позитивне, постоји лоша прогноза и резистенција на терапију зрачењем. Наши резултати показују да ћелије хуманог аденокарцинома цервикса утеруса (HeLaS3) имају повећану MnSOD активност (до 50 % од укупне SOD активности) због ниске експресије њеног репресора p53 и високог нивоа оксидативног стреса, који проистиче из услова у ћелијској култури. Висока активност MnSOD може се повезати са њиховом радиорезистенцијом, која се огледа у високом IC₅₀ од 3,4 Гу и релативно високој вијабилности након озрачивања. За разлику од MnSOD активности, активност цитосолне CuZnSOD се смањује након озрачивања. Активност каталазе се не мења. Јонизујуће зрачење такође повећава активност азот-моноксид-синтазе. Такви услови воде повећању концентрације супероксидног радикала, водоник пероксида и азот монооксида, који заједно могу бити одговорни за смањену експресију NF-κB и неизмењену активност каталазе. Овако поремећена редокс равнотежа у HeLaS3 ћелијама може бити одговорна за цитотоксичност запажену при већим дозама зрачења. Стога се може закључити да инхибиција активности CuZnSOD ензима представља значајан фактор у селективној цитотоксичности радиорезистентних ћелија канцера.

(Примљено 21. фебруара 2007, ревидирано 31. маја 2007)

REFERENCES

1. P. Pisani, F. Bray, D. M. Parkin, *Int. J. Cancer* **97** (2002) 72
2. W. M. Schoell, M. F. Janicek, R. Mirhashemi, *Semin. Surg. Oncol.* **16** (1999) 203
3. D. Choy, L. C. Wong, J. Sham, H. Y. Ngan, H. K. Ma, *Gynecol. Oncol.* **49** (1993) 311
4. V. Kesic, *Eur. J. Surg. Oncol.* **32** (2006) 832
5. A. Papanikolaou, I. Kalogiannidis, D. Misailidou, M. Goutzioulis, P. Stamatopoulos, A. Makedos, A. Vatopoulou, G. Makedos, *Eur. J. Gynaecol. Oncol.* **27** (2006) 607

6. T. Nakano, K. Oka, N. Taniguchi, *Cancer Res.* **56** (1996) 2771
7. M. Scheffner, B. A. Werness, J. M. Huibregtse, A. J. Levine, P. M. Howley, *Cell* **63** (1990) 1129
8. G. Pani, B. Bedogni, R. Anzevino, R. Colavitti, B. Palazzotti, S. Borrello, T. Galeotti, *Cancer Res.* **60** (2000) 4654
9. B. Halliwell, *FEBS Lett.* **540** (2003) 3
10. G. Guo, Y. Yan–Sanders, B. D. Lyn–Cook, T. Wang, D. Tamae, J. Ogi, A. Khaletskiy, Z. Li, C. Weydert, J. A. Longmate., T. Huang, D. R. Spitz., L. W. Oberley, J. J. Li, *Mol. Cell Biol.* **23** (2003) 2362
11. S. Motoori, H. J. Majima, M. Ebara, H. Kato, F. Hirai, S. Kakinuma, C. Yamaguchi, T. Ozawa, T. Nagano, H. Tsujii, H. Saisho, *Cancer Res.* **61** (2001) 5382
12. M. R. Veldwijk, C. Herskind, S. Laufs, W. J. Zeller, S. Fruehauf, F. Wenz, *Radiother. Oncol.* **72** (2004) 341
13. S. K. Manna, H. J. Zhang, T. Yan, L. W. Oberley, B. B. Aggarwal, *J. Biol. Chem.* **273** (1998) 13245
14. R. Kahl, A. Kompkottter, W. Watien, Y. Chovolou, *Drug Metab. Rev.* **36** (2004) 747
15. M. W. Epperly, J. A. Bray, P. Esocobar, W. L. Bigbee, S. Watkins, J. S. Greenberger, *Radiat. Oncol. Invest.* **7** (1999) 331
16. M. Adžić, A. Nićiforović, V. Vučić, Z. Nešković–Konstantinović, S. D. Spasić, D. R. Jones, M. B. Radojčić, M. B. Spasić, *Redox Rep.* **11** (2006) 39
17. J. T. Wu, J. G. Kral, *J. Surg. Res.* **123** (2005) 158
18. F. Mercurio, A. Manning, *Oncogene* **18** (1999) 6163
19. R. Tolando, A. Jovanović, R. Brigelius–Flohé, F. Ursini, M. Maiorino, *Free Radical Biol. Med.* **28** (2000) 979
20. T. Criswell, K. Leskov, S. Miyamoto, G. Luo, D. Boothman, *Oncogene* **22** (2003) 5813
21. J. J. Li, L. W. Oberley, D. K. St. Clair, L. A. Ridnour, T. D. Oberley, *Oncogene* **10** (1995) 1989
22. N. Li, T. D. Oberley, L. W. Oberley, W. Zhong, *Prostate* **35** (1998) 221
23. T. Yan, L. W. Oberley, W. Zhong, D. K. St. Clair, *Cancer Res.* **56** (1996) 2864
24. N. Li, T. D. Oberley, L. W. Oberley, W. Zhong, *J. Cell Physiol.* **175** (1998) 359
25. K. K. Kinningham, D. K. St. Clair, *Cancer Res.* **57** (1998) 5265
26. J. J. Li, N. H. Colburn, L. W. Oberley, *Carcinogenesis* **19** (1998) 833
27. J. J. Li, L. W. Oberley, M. Fan, N. H. Colburn, *FASEB J.* **12** (1998) 1713
28. J. Gong, F. Traganos, Z. Darzynkiewicz, *Cell Growth Differ.* **6** (1995) 1485
29. O. H. Lowry, N. J. Rosebrough, A. L. Farr, R. J. Randall, *J. Biol. Chem.* **193** (1951) 265
30. U. K. Laemmli, *Nature* **227** (1970) 680
31. J. M. McCord, I. Fridovich, *J. Biol. Chem.* **224** (1969) 6049
32. J. D. Crapo, J. M. McCord, I. Fridovich, *Meth. Enzymol.* **53** (1978) 382
33. A. Claiborne in: *Handbook of Methods for Oxygen Radical Research*, R. A. Greenwald, Ed., CRC, Boca Raton, 1985, p. 283
34. T. R. Boyde, M. Rahmatullah, *Anal. Biochem.* **107** (1980) 424
35. Y. Takada, M. Hachiya, S. Park, Y. Osawa, T. Ozawa, M. Akashi, *Mol. Cancer Res.* **1** (2002) 137
36. K. Hirose, D. L. Longo, J. J. Oppenheim, K. Matsushima, *FASEB J.* **7** (1993) 361
37. B. Palazzotti, G. Pani, R. Coavitti, M. E. De Leo, B. Bedogni, S. Borrello, T. Galeotti *Int. J. Cancer* **82** (1999) 145
38. M. Akashi, M. Hachiya, R. L. Paquette, Y. Osawa, S. Shimizu, G. Suzuki, *J. Biol. Chem.* **270** (1995) 15864

39. K. Isoherranen, V. Peltola, L. Laurikainen, J. Punnonen, J. Laihia, M. Ahotupa, K. Punnonen, *J. Photochem. Photobiol. B* **40** (1997) 288
40. S. Shull, N. H. Heintz, M. Periasamy, M. Manohar, Y. M. W. Janssen, J. P. Marsh, B. T. Mossman, *J. Biol. Chem.* **266** (1991) 24398
41. H. E. Marshall, J. S. Stamler, *J. Biol. Chem.* **277** (2002) 34223
42. T. T. Huang, M. Yasunami, E. J. Carlson, A. M. Gillespie, A. G. Reaume, E. K. Hoffman, P. H. Chan, R. W. Scott, C. J. Epstein, *Arch. Biochem. Biophys.* **344** (1997) 424
43. P. Huang, L. Feng, A. E. Oldham, J. M. Keating, W. Plunkett, *Nature* **407** (2000) 390
44. D. Joyce, C. Albanese, J. Steer, M. Fu, B. Bouzahzah, R.G. Pestell, *Cytokine Growth Factor Rev.* **12** (2001) 73
45. A. Nićiforović, M. Adžić, B. Zarić, M. B. Radojčić, *Russ. J. Phys. Chem.* **81** (2007) 1
46. F. Ianzini, M. A. Mackey, *Int. J. Radiat. Biol.* **72** (1997) 409
47. Y. Yaginuma, H. Westphal, *Cancer Res.* **52** (1992) 4196.

Biochemical changes in cuttings of *Robinia pseudoacacia* after treatment with naphthenate

SLAVKO KEVREŠAN^{1*#}, BRANISLAV KOVAČEVIĆ², VERA ĆIRIN-NOVTA^{3#}, KSENIJA KUHAJDA^{3#}, JULIJAN KANDRAČ^{1#}, KSENIJA PAVLOVIĆ^{3#} and LJUBICA GRBOVIĆ^{3#}

¹Faculty of Agriculture, University of Novi Sad, Trg D. Obradovića 8, 21000 Novi Sad, ²Institute of Lowland Forestry and Environment, Antona Čehova 1, 21000 Novi Sad and

³Department of Chemistry, Faculty of Sciences, University of Novi Sad, Trg D. Obradovića 3, 21000 Novi Sad, Serbia

(Received 18 December 2006, revised 27 February 2007)

Abstract: Naphthenic acids were isolated from gas oil fractions (distillation interval 168–290 °C) of Vojvodina crude oil “Velebit”, characterized and their biological activity evaluated by the biochemical changes in cuttings of *Robinia pseudoacacia* after treatment with naphthenate. The activities of IAA peroxidase, total peroxidases and amylase, as well as the contents of reducing sugars and total proteins, were determined in the basal parts of soft wood cuttings of black locust after treatment with sodium naphthenate or the sodium salt of 1-naphthaleneacetic acid (NAA), concentration 10^{-7} mol dm⁻³ for 3 or 6 h. High activities of IAA oxidase and amylase, together with a low activity of peroxidase (which is known as being stimulatory for the initiation and activation of primordia) were obtained after the three-hour treatment with sodium naphthenate. Six-hour treatment had an inhibitory effect on the examined biochemical markers. The effects of three- and six-hour treatments with NAA were between those of the corresponding treatment with naphthenic acids.

Keywords: naphthenate, rooting, biochemical markers, black locust.

INTRODUCTION

Naphthenic acids represent a complex mixture of cycloalkyl and alkyl carboxylic acids which are found in raw oil and fractions obtained by its distillation. In previous studies, it was shown that naphthenic acids from the fraction boiling in the temperature range 168–290 °C during the atmospheric distillation temperatures of Vojvodina crude oil “Velebit” exhibited certain biological activity in respect of the uptake of various ions,^{1,2} as well as an activity similar to that of the plant hormones auxin and gibberelline.³ Naphthenic acids from this oil fraction stimulate the rooting of cuttings and the lateral branches of sunflower,⁴ as well as of poplar hardwood cuttings.⁵

* Corresponding author. E-mail: kevresan@polj.ns.ac.yu

Serbian Chemical Society member.

doi: 10.2298/JSC0710953K

rity of the investigated acids and esters were determined using ASTM-standardized methods,^{14,15} elemental microanalysis performed according to Densted, structural analysis by the standard n-d-M-analysis.^{14,15} The density was measured using a DE 40 Density meter, Mettler, at 25 °C and the refraction index on an Abe refractometer, Oficine Galileo.

The FTIR spectra were obtained using a Nicolet termo IR 670 Spectrometer and the band positions (λ_{max}) are given in cm^{-1} . Low resolution mass spectra were obtained on a Varian MAT-311A mass spectrometer, using chemical ionization (CI) as the ion source. The spectra recorded employing a CI source gave almost exclusively signals of the $[\text{M}+1]^+$ ions. In this case, the sample introduced into the chamber was diluted with a large quantity of gas carrier (isobutane). The resulting sample concentration was approximately 1 % and the pressure was about 0.07–0.12 kPa.

Plant material

Softwood cuttings were taken from adult trees of black locust, genotype Rozaszin-AC. The softwood cuttings were soaked in a solution of sodium naphthenate, concentration of $10^{-7} \text{ mol dm}^{-3}$, for 3 h for the first group of cuttings and 6 h for the second group. Subsequently, the cuttings were transferred into distilled water, whereas control cuttings were kept all the time in distilled water. For comparison, the cuttings were also treated in the same manner with 1-naphthaleneacetic acid (NAA) of the same concentration as sodium naphthenate. The cuttings were kept in a greenhouse at 25 °C and relative humidity of 80 %. After 1, 3 and 6 days, the lower 2 cm of the cuttings were taken for biochemical analyses.

Biochemical parameters and statistics

Samples were subjected to extraction,¹⁶ to determine the peroxidase activity,¹⁶ amylase activity¹⁷ and activity of IAA oxidase¹⁸ in the extract. One unit of peroxidase activity (U) was defined as the increase of one unit of absorbance per minute under the assay conditions, the enzymatic activity being referred to fresh mass. The content of soluble proteins was determined,¹⁹ as was the content of reducing sugars after Miller.²⁰ The experiments were carried out in five replicates and the data were treated using the analysis of the variance and LSD test.

RESULTS AND DISCUSSION

The physicochemical characteristics and structural n-d-M analysis of the raw material and isolated naphthenic acids are shown in Table I. The raw material used for the isolation of crude naphthenic acids is the fraction with characteristics very close to those of diesel fuel (Table I). The content of naphthenic acids in the raw oil distillate, calculated on the basis of the acid number, average molecular mass and density of the raw material, was 0.25 % (2.12 g dm^{-3}). The average molecular mass of the naphthenic acids was determined to be 266 and this value was used to prepare solutions and for the biological experiments. The composition of the mixture of naphthenic acids was determined on the basis of low resolution mass spectra, which showed that the largest portion of the naphthenic acids belonged to the bicyclic class of carboxylic acids (Table II).

In all cases, the activities of IAA oxidase and amylase increased until the third day and thereafter decreased. The effect was more pronounced after the three-hour treatment with sodium naphthenate, compared to the six-hour treatment and control (Fig. 2A and 2B). The total peroxidase activity was increased on the first day after the treatment, but exhibited a decrease three days thereafter. The effect was the most pronounced after the three-hour treatment with sodium

naphthenate (Fig. 2C). For all treatments, including control as well, the content of soluble proteins increased one day after the treatment, decreased to the third and again increased to the sixth day, except for the six-hour treatment with sodium naphthenate, when the effect was completely the opposite (Fig. 3A). The changes in the content of reducing sugars were not so clear (Fig. 3B). The effects of three- and six-hour treatments with NAA were between those of the corresponding treatments with sodium naphthenate.

TABLE I. Physicochemical characteristics and structural n-d-M analysis of the raw material and isolated naphthenic acids

	Oil fraction	Naphthenic acids
Distillation interval, °C	168–290	190–390
Density, kg m ⁻³	848.2	947.1
Refraction index	1.4639	1.4903
Acid number, mg KOH g ⁻¹	0.51	201.15
Structural n-d-M analysis (Content, mass %)		
C_A	–	1.1
C_N	–	59.7
C_P	–	39.2
Average molecular C-atoms	16	16–17
Average relative molecular mass	248	266
Elemental microanalysis (Content, mass %)		
C		76.69
H		11.28
O		12.00
Average molecular formula		C ₁₇ H ₃₀ O ₂

TABLE II. Low resolution mass spectra of naphthenic acids using the CI method

Class of carboxylic acids	Z series $C_nH_{2n+z}O_2$	Series of molecular peaks (M+1) ⁺	No. of C-atoms in molecule Z-series	Z-series content in total acid mixture mass %
Aliphatic	Z = 0 $C_nH_{2n}O_2$	257(0.3); 271(0.5); 285(1.0); 299(0.2)	15–18	2.0
Monocyclic	Z = –2 $C_nH_{2n-2}O_2$	241(1.0); 255(2.6); 269(2.8); 283(3.2); 297(3.6); 311(3.0); 325(2.5); 339(1.4); 353(0.7)	14–22	20.8
Bicyclic	Z = –4 $C_nH_{2n-4}O_2$	225(1.2); 239(3.0); 253(5.5); 267(7.3); 281(8.0); 295(6.2); 309(5.0); 323(3.2); 337(1.7); 351(0.8)	13–22	41.9
Tricyclic	Z = –6 $C_nH_{2n-6}O_2$	237(1.2); 251(2.6); 265(4.4); 279(6.4); 293(7.1); 307(4.6); 321(2.1); 335(0.8); 349(0.5)	14–22	29.7
Tetracyclic	Z = –8 $C_nH_{2n-8}O_2$	263(1.4); 277 (1.6); 291(1.9); 305(1.2)	16–19	6.1

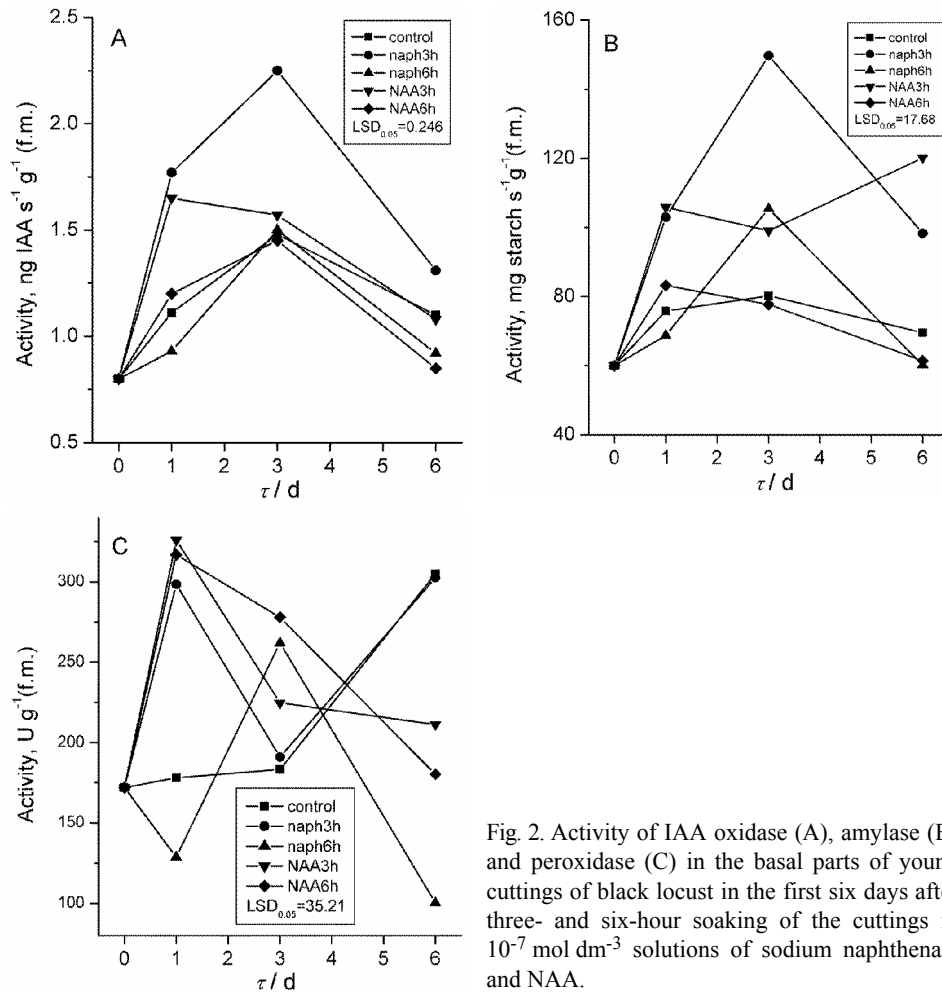


Fig. 2. Activity of IAA oxidase (A), amylase (B) and peroxidase (C) in the basal parts of young cuttings of black locust in the first six days after three- and six-hour soaking of the cuttings in 10^{-7} mol dm⁻³ solutions of sodium naphthenate and NAA.

The results obtained three days after the treatment show that the highest activities of IAA oxidase and amylase and the lowest activity of peroxidase were obtained after the three-hour treatment with 10^{-7} mol dm⁻³ solution of sodium naphthenate. Such an effect is well known as a stimulatory for the initiation and activation of primordial.^{7,8,21} The effect was more pronounced compared to that of the treatment with NAA. These results are also in concordance with the results of Loh and Severson,²² who observed a stimulatory effect of a one-day treatment with potassium naphthenate on IAA oxidase. There were no clear changes in the content of reducing sugars, which is probably caused by the nature of the softwood cuttings (constant income of assimilates from the leaves). It is opposite to the observations of Tschaplinski and Blake,¹¹ who worked with poplar hardwood cuttings which had no leaves at the beginning of rooting and the content of

reducing sugars depended on the intensity of activation of the starch reserves. However, Severson²³ found that potassium naphthenates stimulated glucose uptake in beans roots.

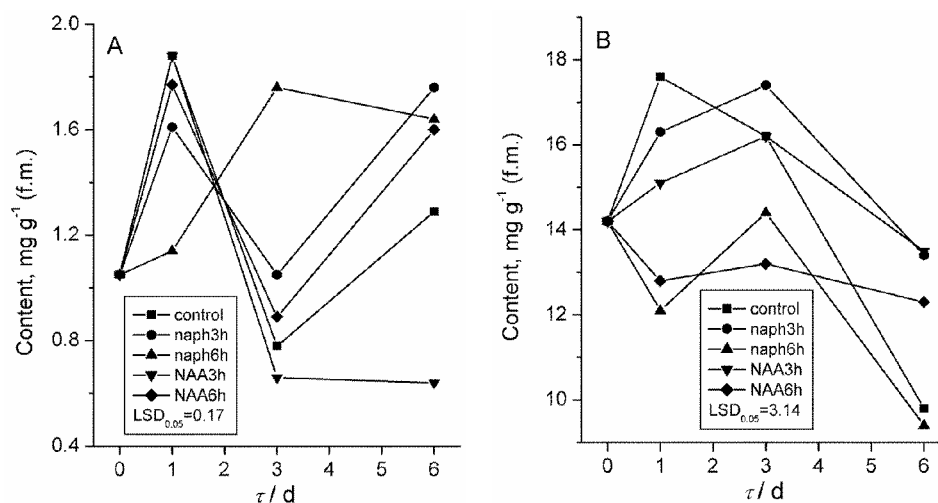


Fig. 3. Contents of soluble proteins (A) and reducing sugars (B) in the basal parts of young cuttings of black locust in the first six days after three- and six-hour soaking of the cuttings in 10^{-7} mol dm⁻³ solutions of sodium naphthenate and NAA.

In contrast to the stimulatory effect of a three-hour treatment, a six-hour treatment had an inhibitory effect on the examined biochemical markers (*e.g.*, the lowest level of soluble proteins one day after the treatment), which is in agreement with previous results.^{5,24} Thus, despite of its low concentration, sodium naphthenate during prolonged treatment showed some harmful effects.

The presented results suggest that sodium naphthenate can exhibit a stimulatory effect on several biochemical markers of rooting. Complete information could be obtained with experiments in a greenhouse and with tissue cultures.

Acknowledgement: This study was supported by the Ministry of Science of the Republic of Serbia, project No. 142005B.

ИЗВОД

БИОХЕМИЈСКЕ ПРОМЕНЕ У РЕЗНИЦАМА *Robinia pseudoacacia* НАКОН ТРЕТМАНА СА НАФТЕНАТОМ

СЛАВКО КЕВРЕШАН¹, БРАНИСЛАВ КОВАЧЕВИЋ², ВЕРА ЋИРИН-НОВТА³, КСЕНИЈА КУХАЈДА³,
ЛУЛИЈАН КАНДРАЧ¹, КСЕНИЈА ПАВЛОВИЋ³ И ЉУБИЦА ГРБОВИЋ³

¹ Пољопривредни факултет, Универзитет у Новом Саду, Трг Д. Обрадови Ја 8, Нови Сад, ² Институт за низијско земљоправство и заштитивне средине, Антона Радвића 1, Нови Сад и ³ Департаман за хемију, Природно-математички факултет, Универзитет у Новом Саду, Трг Д. Обрадови Ја 8, Нови Сад

Нафтенске киселине су изоловане из гасне фракције (интервал дестилације 168–290 °C) војвођанске нафте “Велебит”, окарактерисане и њихова биолошка активност испитана путем

биохемијских промена у резницама *Robinia pseudoacacia* након третмана са натријум-нафтенатом. Активности IAA пероксидазе, укупна пероксидазна активност и активност амилазе заједно са садржајем редукујућих шећера и протеина одређене су у базалним деловима резница багрема након третмана са натријум-нафтенатом и натријумовом соли (1-нафтил)сирћетне киселине у концентрацији од 10^{-7} mol dm⁻³ у току 3 или 6 сати. Високе активности IAA оксидазе и амилазе праћене ниском активиношћу пероксидазе (што је познато као стимулативно за иницијацију и активацију коренских примордија) добијене су након трочасовног третмана натријум-нафтенатом. Шесточасовни третман је испољио инхибиторни ефекат на испитане биохемијске маркере. Ефекти трочасовног и шесточасовног третмана са NAA су били између одговарајућих третмана са нафтенским киселинама.

(Примљено 18. децембра 2006, ревидирано 27. фебруара 2007)

REFERENCES

1. S. Kevrešan, V. Ćirin–Novta, K. Kuhajda, J. Kandrač, N. Petrović, Lj. Grbović, Ž. Kevrešan, *Biol. Plant.* **48** (2004) 453
2. S. Kevrešan, V. Ćirin–Novta, K. Kuhajda, J. Kandrač, N. Petrović, Lj. Grbović, Ž. Kevrešan, *Belgian J. Bot.* **138** (2005) 11
3. V. Ćirin–Novta, K. Kuhajda, S. Kevrešan, J. Kandrač, Lj. Radić, *Acta Period. Technol.* **33** (2002) 135
4. S. Kevrešan, V. Ćirin–Novta, D. Vasić, K. Kuhajda, J. Kandrač, N. Petrović, Lj. Radić, *Helia* **26** (2003) 18
5. S. Kevrešan, V. Ćirin–Novta, B. Kovačević, D. Vasić, K. Kuhajda, J. Kandrač, N. Petrović, Lj. Radić, *Topola* **171/172** (2003) 63
6. M. Kamaluddin, J. J. Zwiazek, *Tree Physiol.* **22** (2002) 1265
7. N. C. Bhattacharya, in *Adventitious root formation in cuttings*, T. D. Davis, B. E. Haissig, N. Sanklila, Eds., Dioscorides Press, Portland, 1989, p. 88
8. T. Güneş, *Turk. J. Bot.* **24** (2000) 97
9. A. N. Molassiotis, K. Dimassi, G. Diamantidis, I. Therios, *Biol. Plant.* **48** (2004) 1
10. C. Saxena, S. Samantaray, G. R. Rout, P. Das, *Biol. Plant.* **43** (2000) 121
11. T. J. Tschaplinski, T. J. Blake, *Can. J. Bot.* **67** (1989) 2168
12. V. Ćirin–Novta, K. Kuhajda, S. Kevrešan, J. Kandrač, Lj. Grbović, P. Rodić, *Acta Period. Technol.* **35** (2004) 87
13. V. Ćirin–Novta, S. Kevrešan, K. Kuhajda, J. Kandrač, Lj. Radić, P. Rodić, *Acta Period. Technol.* **34** (2003) 49
14. R. V. Anbroh, *Petrol. Chem.* **12** (1972) 230
15. D. M. Shopov, K. I. Kovaceva, N. P. Dimov, *Petrol. Chem.* **24** (1984) 169
16. U. C. Basak, A. B. Das, P. Das, *Marine Biol.* **136** (2000) 185
17. B. Panjabi, R. N. Basu, *Indian Biologist* **10** (1978) 65
18. M. A. Quesada, C. Sanchez–Roldan, A. Heredia, V. Valpuesta, M. Bukovac, *J. Plant Growth Regul.* **11** (1992) 1
19. M. M. Bradford, *Anal. Biochem.* **72** (1976) 248
20. G. L. Miller, *Anal. Chem.* **31** (1959) 426
21. T. Gaspar, M. Hofinger, in *Adventitious root formation in cuttings*, T. D. Davis, B. E. Haissig, N. Sanklila, Eds., Dioscorides Press, Portland, 1989, p. 117
22. J. W. C. Loh, J. G. Severson, *Phytochemistry* **14** (1975) 1265
23. J. G. Severson, *Phytochemistry* **11** (1972) 71
24. S. Kevrešan, B. Kovačević, D. Vasić, V. Ćirin–Novta, K. Kuhajda, *Cercetari stiintifice – Horticultura*, Seria A IX-A, Partea a II-a (2005) 1.

Essential oil analysis of two endemic *Eryngium* species from Serbia

CHRYSOSTOMOS CAPETANOS¹, VASILIKI SAROGLOU¹, PETAR D. MARIN²,
ANA SIMIĆ² and HELEN D. SKAL TSA^{1*}

¹Division of Pharmacognosy and Chemistry of Natural Products, School of Pharmacy, University of Athens, Panepistimiopolis Zografou, 15771 Athens, Greece and ²Faculty of Biology, Institute of Botany and Botanical Garden “Jevremovac”, University of Belgrade, Studentski trg 16, 11000 Belgrade, Serbia

(Received 7 November 2006, revised 13 March 2007)

Abstract: The volatile composition of two *Eryngium* species was studied. The essential oils were obtained by hydrodistillation in a modified Clevenger-type apparatus, and their analyses were performed by GC and GC–MS. A total of 58 different compounds were identified. Their main constituents were as follows: *E. serbicum*: germacrene D (19.7 %), β -elemene (10.0 %) and spathulenol (6.9 %); *E. palmatum*: sesquicineole (21.3 %), caryophyllene oxide (16.0 %), spathulenol (16.0 %) and sabinene (5.5 %). The main portion in both studied taxa consisted of sesquiterpenes.

Keywords: *E. palmatum* Vis. et Pančić, *E. serbicum* Pančić, Apiaceae, volatile constituents, sesquiterpene hydrocarbons.

INTRODUCTION

The genus *Eryngium* L. comprises 220–250 species. It belongs to the tribe Saniculeae, subfamily Saniculoideae of the Apiaceae family. In the flora of Europe, ca. 26 species are present,¹ among them five species are found in the flora of Serbia.²

In the present study, two endemic taxa were examined: *E. palmatum* Vis. et Pančić and *E. serbicum* Pančić. *E. palmatum* is an endemic perennial herb, growing in dry places and woods, which is distributed in the central part of the Balkan Peninsula (Serbia, Bulgaria, FYROM and Albania).^{1,2} *E. serbicum* is an endemic perennial plant growing only in Serbia in dry habitats.^{1,2}

Hitherto, the composition of the volatile compounds is known in only three species: *E. billardieri* F. Delaroché,³ *E. paniculatum* Cav.⁴ and *E. foetidum* L.^{4–9}

EXPERIMENTAL

Analysis of volatile compounds

The air-dried plant material (100 g) from each population was cut into small pieces and the essential oils were obtained by hydrodistillation in 500 ml H₂O for 2 h, in a modified Clevenger

* Corresponding author. E-mail: skaltsa@pharm.uoa.gr
doi: 10.2298/JSC0710961C

apparatus with a water-cooled oil receiver to reduce over-heating artifacts of hydrodistillation.¹⁰ The oils were taken in 2 ml of capillary GC grade *n*-pentane, dried over anhydrous sodium sulfate and stored at -20°C . The composition of the volatiles was determined utilizing GC and GC-MS analyses. The GC analysis was carried out on a Perkin Elmer 8500 gas chromatograph with a FID, fitted with a Supelcowax-10 fused silica capillary column ($30\text{ m} \times 0.32\text{ mm}$ (i.d.); film thickness: $0.25\text{ }\mu\text{m}$). The column temperature was programmed from 75 to 260°C at a rate of $2.5^{\circ}\text{C min}^{-1}$. The injector and detector temperatures were set at 230 and 300°C , respectively.

GC-MS analyses were performed on a Hewlett-Packard 5973-6890 system operating in EI mode (70 eV) equipped with a split/splitless injector (220°C), a split ratio 1/10, using two different columns: a fused silica HP-5 MS capillary column ($30\text{ m} \times 0.32\text{ mm}$ (i.d.), film thickness: $0.25\text{ }\mu\text{m}$) and a HP-Innowax capillary column ($30\text{ m} \times 0.32\text{ mm}$ (i.d.), film thickness: $0.50\text{ }\mu\text{m}$). The temperature program for the HP-5 MS column was from 60°C (5 min) to 280°C at a rate of $4^{\circ}\text{C min}^{-1}$ and for the HP-Innowax column from 60°C to 260°C at a rate of $3^{\circ}\text{C min}^{-1}$. Helium was used as the carrier gas at a flow rate of 0.8 ml min^{-1} . Injection volume of each sample was $2\text{ }\mu\text{l}$. Retention indices for all compounds were determined according to the Van den Dool approach,¹¹ using *n*-alkanes as standards. The identification of the components was based on comparison of their mass spectra with those of the Wiley Library¹² and those described by Adams,¹³ as well as by comparison of their retention indices with literature data.^{13,14} In many cases, the essential oils were subject to co-chromatography with authentic compounds (Fluka, Sigma).

Optical rotation values were determined at 25°C at 589 nm in dichloromethane.

Plant Material

Aerial parts of both taxa were collected from natural populations during the flowering stage as follows: *E. serbicum* Pančić (ery-1) at Kosovska Mitrovica in June 2003 and *E. palmatum* Vis. et Pančić (ery-2) at Ozren in June 2003.

Voucher specimens of the *Eryngium* species were determined by Dr. P. D. Marin and deposited in the Herbarium of Institute of Botany and Botanical Garden "Jevremovac", Faculty of Biology, University of Belgrade, under the code numbers: ES 6039 and EP 60310, respectively.

RESULTS AND DISCUSSION

As shown in Table I, both essential oils were complex mixtures of about fifty constituents in each investigated case, with the contributions of the main compounds never exceeding 20 % of the total. Among them, sesquiterpenes were the main constituents in both studied taxa (Table II).

The main constituents of the investigated *Eryngium* essential oils are the following: in *E. serbicum* germacrene D (19.7 %), β -elemene (10.0 %) and spathulenol (6.9 %); in *E. palmatum* sesquicineole (21.3 %), caryophyllene oxide (16.0 %), spathulenol (6.6 %) and sabinene (4.4 %).

Previously investigated *Eryngium* essential oils had different compositions. In the essential oil of *E. paniculatum*, (*E*)-anethole (52.6 %) was found as main component,⁴ while in *E. billardieri*, α -muurolene was dominant.³ Previously, several investigations of the essential oils of *E. foetidum* revealed that fatty acids and aldehydes were the main constituents. Thus, Leclercq *et al.*⁹ reported (*E*)-2-dodecenal (45.5 %), dodecanoic acid (15.5 %) and 2-dodecenoic acid (8.6 %) as the main compounds. Wong *et al.*⁸ found (*E*)-2-dodecenal (59.7 %) in the leaves, while 2,3,6-trimethylbenzaldehyde was dominant in the root (37.6 %). Martins *et al.*⁶ found 2,3,6-trimethylbenzaldehyde (37.5 %) and (*E*)-2-dodecenal (23.7 %)

as the main constituents in different plant parts. More recent investigations⁵ also revealed 2,4,5-trimethylbenzaldehyde (27.7 %) and (*E*)-2-dodecenal (27.5 %) as the dominant components. In contrast, Pino *et al.*⁷ reported that caryophyllene oxide (19.3 %) was one of the main compounds.

TABLE I. Qualitative and quantitative composition (% v/v) of volatile compounds

	<i>R</i> ^a	<i>R</i> ^b	Ery-1	Ery-2
Heptanal	897		–	0.4
α -Thujene	927		1.4	0.3
α -Pinene	935		5.7	4.4
β -Thujene	966		–	0.2
Sabinene	971	1123	1.5	5.5
β -Pinene	975	1112	4.3	–
2-Pentylfuran	987		–	1.2
Myrcene	989	1160	4.3	–
Octanal	999	1289	3.8	4.4
α -Terpinene	1016	1180	–	0.2
<i>p</i> -Cymene	1024	1268	0.5	0.2
Limonene	1027	1201	1.1	0.6
γ -Terpinene	1055	1243	–	0.4
2-Nonanone	1090	1385	0.4	–
Undecane	1100		–	0.3
Nonanal	1101	1390	0.4	0.8
Pinocarvone	1161	1559	0.3	–
Tepinen-4-ol	1174	1591	–	0.1
Dodecane	1200		–	0.6
2-Decenal	1263	1639	1.2	–
Perillaldehyde	1271	1288	–	0.7
(–)-Bornyl acetate	1288	1570	–	1.6
Tridecane	1300		–	0.3
2,4,5-Trimethylbenzaldehyde	1357	1901	2.2	–
α -Copaene	1375	1481	1.1	0.7
β -Bourbonene	1384	1507	1.1	–
β -Elemene	1390	1578	10.0	0.9
β -Caryophyllene	1416	1584	1.2	2.2
Calarene	1431	1559	0.4	–
α -Humulene	1452	1662	0.4	1.1
<i>trans</i> - β -Farnesene	1454	1659	0.6	–
Germacrene D	1476	1709	19.7	0.6
Ar-curcumene	1479		–	0.2
β -Selinene	1489	1717	1.7	–
α -Selinene	1497	1722	1.0	–

TABLE I. Continued

	<i>RI</i> ^a	<i>RI</i> ^b	Ery-1	Ery-2
Bicyclogermacrene	1497	1732	2.4	–
Ledene	1498	1716	–	0.4
Germacrene A	1499		0.8	–
α -Muurolene	1501		–	0.2
β -Bisabolene	1503	1724	0.7	0.2
Sesquicineole	1515		–	21.3
δ -Cadinene	1520	1755	1.2	0.4
Elemol	1550	2082	–	1.5
1,5-Epoxyalvial-4(14)-ene	1564	1924	1.1	1.2
Spathulenol	1578	2128	6.9	6.6
Caryophyllene oxide	1581	1987	2.6	16.0
β -Copaene-4- α -ol	1590		1.2	–
Salvial-4(14)-en-1-one	1593	2013	3.4	0.6
Nor-copaanone	1597	2156	2.2	–
Vulgarol B	1605		1.3	–
β -Oplopenone	1607	1964	0.5	–
Humulene epoxide II	1608		–	4.8
α -Copaen-8-ol	1626		–	2.5
T-muurolol	1642	2236	–	1.5
Ageratochromene	1656		2.2	–
Caryophylla-4(12),8(13)-dien-5- β -ol	1668	2299	0.9	0.3
Eudesma-4(15),7-dien-1- β -ol	1684		3.9	–
α -Bisabolol	1685	2222	–	6.8
TOTAL			95.6	92.2
$[\alpha]_D^{20}$			-2.55 (CH ₂ Cl ₂ <i>c</i> 0.10)	-2.12 (CH ₂ Cl ₂ <i>c</i> 0.07)

^aComponents listed in order of elution from a HP 5MS column.

^b*RRI*, relative retention indices calculated against C₉–C₂₄ *n*-alkanes on the HP 5MS column (1) and HP Innowax (2) capillary columns, respectively.

TABLE II. Grouped components

	Ery-1	Ery-2
<i>Aliphatics</i>		
Alkanes, alkenes	–	1.2
Aldehydes	7.6	5.7
Ketones	0.4	–
<i>Terpenoids</i>		
Monoterpene hydrocarbons	18.8	11.8
Oxygenated monoterpene	0.3	2.4
Sesquiterpene hydrocarbons	42.3	6.9
Oxygenated sesquiterpene	24.0	63.1
Miscellaneous	–	1.2
Compounds with 13 C	2.2	–

According to the present results, the essential oils of *E. serbicum* and *E. palmatum* have several differences between them, as their main components

differ significantly. *E. palmatum* is characterized by an abundance of sesquiterpene (21.3 %), which was absent in *E. serbicum*.

Acknowledgements: The authors thank Dr Z. Krivosej for the plant collection. P.D.M and A.S. are grateful for financial support from the Ministry of Science of the Republic of Serbia (Project No. 143049B).

ИЗВОД

АНАЛИЗА ЕТАРСКИХ УЉА ДВЕ ЕНДЕМСКЕ *ERYNGIUM* ВРСТЕ ИЗ СРБИЈЕ

CHRYSOSTOMOS CAPETANOS¹, VASILIKI SAROGLOU¹, ПЕТАР Д. МАРИН²,
АНА СИМИЋ² и HELEN D. SKAL TSA¹

¹Division of Pharmacognosy and Chemistry of Natural Products, School of Pharmacy, University of Athens, Panepistimiopolis Zografou, 15771 Athens, Greece i ²Biološki fakultet, Institut za botaniku i Botanički vrt "Jevremovac", Univerzitet u Beogradu, Studentski trg 16, 11000 Beograd

У раду су испитивани испарљиви састојци две *Eryngium* врсте. Етарска уља су изолована хидродестилацијом у модификованом апарату типа Clevenger и анализирана методама GC и GC-MS. Укупно је идентификовано 58 различитих једињења. Главни састојци испитиваних врста су: у *E. serbicum*: гермакрен D (19,7 %), β-елемен (10,0 %) и спатуленол (6,9 %); у *E. palmatum*: сесквицинео (21,3 %), кариофилен-оксид (16,0 %), спатуленол (16,0 %) и сабинен (5,5 %). Велики део обе испитиване јединке састоји се од сесквитерпена.

(Примљено 7. новембра 2006, ревидирано 13. марта 2007)

REFERENCES

1. A. O. Chater, in *Flora Europaea* 1968, 2, p. 320
2. L. V. Nikolić, in *Flora SR Srbije* 1973, 5, p. 193
3. F. Sefidkon, M. Dabiri, A. Alamshahi, *J. Essent. Oil Res.* **16** (2004) 42
4. M. I. Cobos, J. L. Rodriguez, A. Petre, E. Spahn, J. Casermeiro, A. G. Lopez, J. A. Zygadlo, *J. Ess. Oil Res.* **14** (2002) 82
5. E. Cardozo, M. Rubio, L. B. Rojas, A. Usubillaga, *J. Essent. Oil Res.* **16** (2004) 33
6. A. P. Martins, L. R. Salgueiro, A. Proença de Cunha, R. Vila, S. Cañigüeral, F. Tomi, J. Casanova, *J. Essent. Oil Res.* **15** (2003) 93
7. J. A. Pino, A. Rosado, V. Fuentes, *J. Essent. Oil Res.* **9** (1997) 123
8. K. C. Wong, M. C. Feng, T. W. Sam, G. L. Tan, *J. Essent. Oil Res.* **6** (1994) 369
9. P. A. Leclercq, N. X. Duñg, V. N. Lô, N. V. Toanh, *J. Essent. Oil Res.* **4** (1992) 423
10. *Hellenic Pharmacopoeia V*, Chapter 28:12, National Organization for Medicines of Greece, Athens, 2002
11. H. Van den Dool, P. D. Kratz, *J. Chromat.* **11** (1963) 463
12. Y. Massada, *Analysis of essential oil by gas chromatography and spectrometry*, Wiley, New York, 1976
13. R. Adams, *Identification of Essential Oil Components by Gas Chromatography/Mass Spectroscopy*, Allured Publishing Co, Carol Stream, Illinois, 2001
14. N. N. Davies, *J. Chromatogr.* **503** (1990) 1.

The McClelland approximation and the distribution of π -electron molecular orbital energy levels

IVAN GUTMAN^{*,#}

Faculty of Science, University of Kragujevac, P.O. Box 60, 34000 Kragujevac, Serbia

(Received 29 March 2007)

Abstract: The total π -electron energy E of a conjugated hydrocarbon with n carbon atoms and m carbon–carbon bonds can be approximately calculated by means of the McClelland formula $E \approx g\sqrt{2mn}$, where g is an empirical fitting constant, $g \approx 0.9$. It was claimed that the good quality of the McClelland approximation is a consequence of the fact that the π -electron molecular orbital energy levels are distributed in a nearly uniform manner. It will now be shown that the McClelland approximation does not depend on the nature of the distribution of energy levels, *i.e.*, that it is compatible with a large variety of such distributions.

Keywords: total π -electron energy, McClelland formula, Hückel molecular orbital theory.

The total π -electron energy E is one of the most thoroughly studied theoretical characteristics of conjugated molecules that can be calculated within the Hückel molecular orbital (HMO) approximation.^{1,2} Research on E is currently very active.^{3–8} Long time ago McClelland proposed the simple approximate formula:⁹

$$E \approx g\sqrt{2mn} \quad (1)$$

where n is the number of carbon atoms and m the number of carbon–carbon bonds, and where g is an empirically determined fitting parameter, $g \approx 0.9$. In the meantime a large number of other (n,m) -type approximate expressions for E have been proposed, but, as demonstrated by detailed comparative studies,^{10–13} none of these could exceed the accuracy of Eq. (1).

In 1983 the present author discovered¹⁴ that a result closely similar to Eq. (1) can be obtained by assuming that the HMO energy levels are uniformly distributed. Eventually such a distribution-based approach to E was elaborated in more detail.^{15,16} The conclusion of the works^{14–16} was that the McClelland approximation (Eq. (1)) is connected with the assumption that the HMO π -electron energy levels of conjugated hydrocarbons are distributed in a (nearly) uniform manner.

* E-mail: gutman@kg.ac.yu

Serbian Chemical Society member.

doi: 10.2298/JSC0710967G

The reasoning by means of which this conclusion was obtained will be briefly repeated.

If $\lambda_1, \lambda_2, \dots, \lambda_n$ are the Eigen values of the molecular graph representing the respective conjugated molecule, then:¹⁻³

$$E = \sum_{i=1}^n |\lambda_i| \quad (2)$$

As is well known,^{1,2} the graph Eigen values satisfy the relation:

$$E = \sum_{i=1}^n (\lambda_i)^2 = 2m \quad (3)$$

Without loss of generality, Eqs. (2) and (3) may be rewritten as:

$$E = n \int_{-\infty}^{+\infty} |x| \Gamma(x) dx$$

and

$$E = n \int_{-\infty}^{+\infty} x^2 \Gamma(x) dx = 2m$$

where $\Gamma(x)$ is the probability density of the distribution of the graph Eigen values. It should be mentioned in passing that the exact expression for $\Gamma(x)$ is:

$$\Gamma(x) = \frac{1}{n} \sum_{i=1}^n \delta(x - \lambda_i)$$

with δ denoting the Dirac delta-function.

In situations when the actual form of the probability density $\Gamma(x)$ is not known (*i.e.*, when the spectrum of the molecular graph is not known), one tries to guess an approximate expression for it, denoted by $\Gamma^*(x)$, which must satisfy the conditions:

$$\int_{-\infty}^{+\infty} \Gamma^*(x) dx = 1 \quad (4)$$

$$\int_{-\infty}^{+\infty} x^2 \Gamma^*(x) dx = \frac{2m}{n} \quad (5)$$

and, of course, $\Gamma^*(x) \geq 0$ for all values of x . Then the quantity E^* ,

$$E^* = n \int_{-\infty}^{+\infty} |x| \Gamma^*(x) dx \quad (6)$$

is expected to provide a reasonably good approximation for the total π -electron energy E . In the works,^{14,16} the simplest possible choice for $\Gamma^*(x)$ was tested, namely,

$$\Gamma^*(x) = b \quad \text{for } -a \leq x \leq +a \quad \text{and otherwise } \Gamma^*(x) = 0 \quad (7)$$

The form of the function (7) is shown in Fig. 1.

The parameters a and b can easily be determined from the conditions Eq. (4) and (5), resulting in

$$a = \sqrt{\frac{6m}{n}} \quad \text{and} \quad b = \sqrt{\frac{n}{24m}} \quad (8)$$

By inserting the conditions given by Eq. (7) back into Eq. (6), one obtains:

$$E^* = a^2bn$$

which combined with Eq. (8) yields:

$$E^* = g^* \sqrt{2mn} \quad (9)$$

with g^* being a constant equal to $\sqrt{3}/2$. Not only is the algebraic form of the expression (9) identical to the McClelland approximation (Eq. (1)), but also the value of the multiplier $g^* = 0.8660$ is remarkably close to the (earlier) empirically determined value for g .

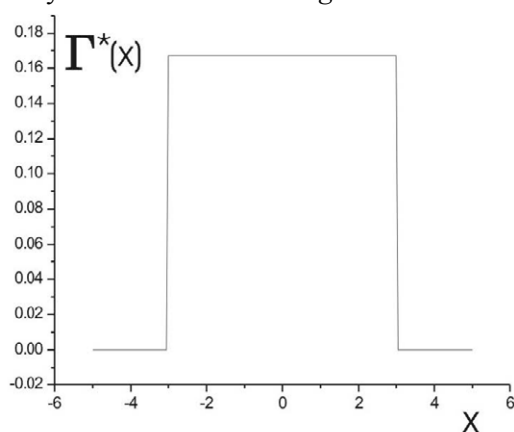


Fig. 1. The form of the probability density (Eq. 7) for $a = 3$ and $b = 1/6$. The Eigen values of the molecular graph are assumed to be uniformly distributed within the interval $(-a, +a)$, i.e., within the interval $(a, -a)$, the probability density is assumed to be constant (equal to b). Outside this interval, the probability density is set to be equal to zero.

Thus, it can be seen that by assuming a uniform distribution of the Eigen values of a molecular graph, the McClelland formula (Eq. (1)) can be reproduced. What has hitherto been overlooked is that formula (1) can also be deduced by using many other probability densities.

OBTAINING FORMULA (1) FROM A VARIETY OF MODEL FUNCTIONS $\Gamma^*(x)$

Suppose that the model based on Eq. (7) is required to be upgraded by including the information that the MO energies around the non-bonding level (corresponding to $x = 0$) are more numerous than those far from the non-bonding level, see diagram 1 in Fig. 2. This can be achieved by means of the function:

$$\Gamma^*(x) = b \left[1 - \left(\frac{x}{a} \right)^2 \right] \quad \text{for} \quad -a \leq x \leq +a \quad \text{and otherwise} \quad \Gamma^*(x) = 0 \quad (10)$$

Then, by direct calculation in a fully analogous manner as described in the preceding section, formula (9) is obtained with $g^* = \sqrt{5}/4$.

If, however, the opposite is assumed, namely that the MO energies around the non-bonding level are less numerous than those far from the non-bonding level (see diagram 2 in Fig. 2), and therefore set

$$\Gamma^*(x) = b \left(\frac{x}{a} \right)^2 \quad \text{for } -a \leq x \leq +a \quad \text{and otherwise } \Gamma^*(x) = 0 \quad (11)$$

then Eq. (9) is again obtained, this time for $g^* = \sqrt{15}/4$.

The model function Γ^* may be made still more complicated, with two minima or two maxima (diagrams 3 and 4 in Fig. 2), *i.e.*,

$$\Gamma^*(x) = b \left(\frac{x}{a} \right)^2 \left[1 - \left(\frac{x}{a} \right)^2 \right] \quad \text{for } -a \leq x \leq +a \quad \text{and otherwise } \Gamma^*(x) = 0 \quad (12)$$

or

$$\Gamma^*(x) = b \left[\left(\frac{x}{a} \right)^2 - \frac{1}{2} \right]^2 \quad \text{for } -a \leq x \leq +a \quad \text{and otherwise } \Gamma^*(x) = 0 \quad (13)$$

but Eq. (9) is still obtained with $g^* = 5\sqrt{21}/(12\sqrt{2})$ and $g^* = 5\sqrt{7}/(2\sqrt{187})$, respectively.

Hitherto, it was required that the model function be symmetric with regard to $x = 0$, *i.e.*, that $\Gamma^*(-x) = \Gamma^*(x)$, *i.e.*, that the pairing theorem be obeyed.^{1,2} However, even this plausible restriction is not necessary, as shown by the examples:

$$\Gamma^*(x) = b \left[\left(\frac{x}{a} \right)^2 - 1 \right]^2 \quad \text{for } -a \leq x \leq +a \quad \text{and otherwise } \Gamma^*(x) = 0 \quad (14)$$

and

$$\Gamma^*(x) = b \left[\left(\frac{x}{a} \right)^2 + 1 \right]^2 \quad \text{for } -a \leq x \leq +a \quad \text{and otherwise } \Gamma^*(x) = 0 \quad (15)$$

Also the functions (14) and (15) imply the validity of Eq. (9), with $g^* = 3\sqrt{3}/16$ and $g^* = 9\sqrt{5}/(16\sqrt{2})$, respectively. The forms of the functions (14) and (15) are shown in diagrams 5 and 6 in Fig. 2.

In order to further demonstrate the arbitrariness of the form of the model function that leads to the McClelland approximation, an example with a singularity at $x = 0$ was constructed (see diagram 7 in Fig. 2):

$$\Gamma^*(x) = b \left(\frac{|x|}{a} \right)^{-1/2} \quad \text{for } -a \leq x \leq +a \quad \text{and otherwise } \Gamma^*(x) = 0 \quad (16)$$

In spite of the (physically impossible) property of the model function (16) that $\Gamma(x) \rightarrow \infty$ for $x \rightarrow 0$, Eq. (9) is also obtained with $g^* = \sqrt{5}/3$.

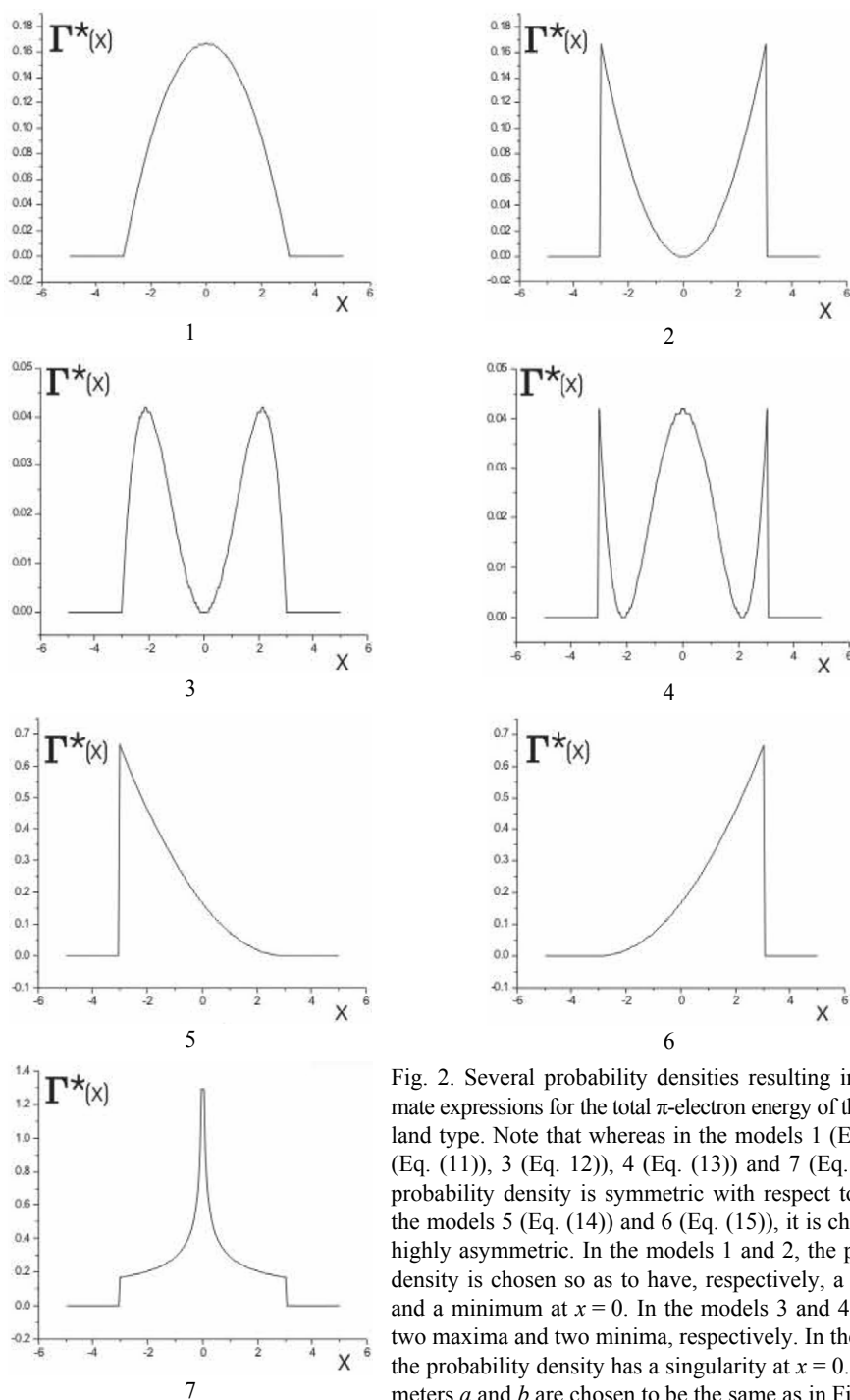


Fig. 2. Several probability densities resulting in approximate expressions for the total π -electron energy of the McClelland type. Note that whereas in the models 1 (Eq. (10)), 2 (Eq. (11)), 3 (Eq. (12)), 4 (Eq. (13)) and 7 (Eq. (16)), the probability density is symmetric with respect to $x = 0$. In the models 5 (Eq. (14)) and 6 (Eq. (15)), it is chosen to be highly asymmetric. In the models 1 and 2, the probability density is chosen so as to have, respectively, a maximum and a minimum at $x = 0$. In the models 3 and 4, there are two maxima and two minima, respectively. In the model 7, the probability density has a singularity at $x = 0$. The parameters a and b are chosen to be the same as in Fig. 1.

CONCLUDING REMARKS

In the seven examples for $\Gamma^*(x)$ given in the preceding section, Eq. (9) is always arrived at, but the multiplier g^* assumes different numerical values. In our opinion this detail is of lesser importance. Namely, it is possible to construct model functions $\Gamma^*(x)$, such that g^* in Eq. (9) has any desired value.

For instance, if for some $t \geq -1$,

$$\Gamma^*(x) = b \left[1 + t \left(\frac{x}{a} \right)^2 \right] \quad \text{for } -a \leq x \leq +a \quad \text{and otherwise } \Gamma^*(x) = 0 \quad (17)$$

then

$$g^* = \frac{3\sqrt{5}}{4} \frac{t+2}{\sqrt{(t+3)(3t+5)}}$$

By varying the parameter t , the multiplier in Eq. (9) assumes values between $3\sqrt{5}/8 = 0.8385$ and $\sqrt{15}/4 = 0.9682$, see Fig. 3. Therefore, the model function (17) can always be chosen so as to exactly "reproduce" the empirically determined value of g in the McClelland formula (Eq. (1)). This, of course, would be fully artificial and without any scientific justification.

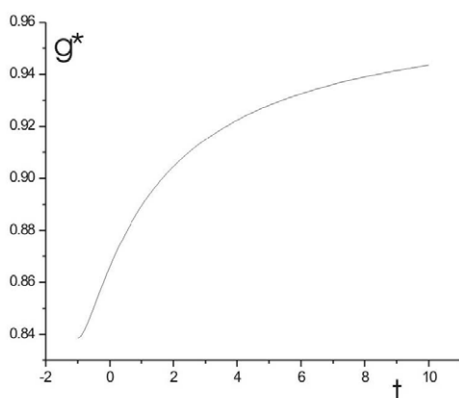


Fig. 3. Dependence of the multiplier g^* in Eq. (9) on the parameter t of the probability density (17). In order that $\Gamma^*(x)$ be positive valued, it must be $t > -1$.

The main conclusion of the present work is that the McClelland approximation (Eq.(1)) has nothing to do with the distribution of the HMO π -electron energy levels and that no inference on this distribution can be made based on the fact that Eq. (1) in a surprisingly accurate manner reproduces the actual E -values.

Acknowledgement: This work was supported by the Serbian Ministry of Science, through Grant No. 144015G, "Graph Theory and Mathematical Programming with Applications to Chemistry and Engineering".

ИЗВОД

МЕКЛЕЛАНДОВА АПРОКСИМАЦИЈА И РАСПОДЕЛА π -ЕЛЕКТРОНСКИХ
МОЛЕКУЛСКО ОРБИТАЛНИХ ЕНЕРГЕТСКИХ НИВОА

ИВАНГУТМАН

Prirodno-matemati-ki Fakultet Univerzitet u Kragujevcu

Укупна π -електронска енергија E конјугованих угљководоника са n угљеникових атома и m угљеник–угљеник веза може се приближно израчунати помоћу формуле $E \approx g\sqrt{2mn}$, где је g емпиријска константа, $g \approx 0,9$. Раније је изнета тврдња да је добар квалитет Мекле-ландове апроксимације заснован на чињеници да су π -електронски молекулско орбитални енергетски нивои расподељени приближно униформно. Сада показујемо да Меклеландова апроксимација не зависи од природе расподеле енергетских нивоа, то јест да је она компати-билна са бројним, веома различитим расподелама.

(Примљено 29. марта 2007)

REFERENCES

1. A. Graovac, I. Gutman, N. Trinajstić, *Topological Approach to the Chemistry of Conjugated Molecules*, Springer-Verlag, Berlin, 1977
2. I. Gutman, O. E. Polansky, *Mathematical Concepts in Organic Chemistry*, Springer-Verlag, Berlin, 1986
3. I. Gutman, *J. Serb. Chem. Soc.* **70** (2005) 441
4. M. Perić, I. Gutman, J. Radić-Perić, *J. Serb. Chem. Soc.* **71** (2006) 771
5. G. Indulal, A. Vijayakumar, *MATCH Commun. Math. Comput. Chem.* **55** (2006) 83
6. B. Zhou, *MATCH Commun. Math. Comput. Chem.* **55** (2006) 91
7. A. Chen, A. Chang, W. C. Shiu, *MATCH Commun. Math. Comput. Chem.* **55** (2006) 95
8. J. A. de la Peña, L. Mendoza, *MATCH Commun. Math. Comput. Chem.* **56** (2006) 113
9. B. J. McClelland, *J. Chem. Phys.* **54** (1971) 640
10. I. Gutman, L. Nedeljković, A. V. Teodorović, *J. Serb. Chem. Soc.* **48** (1983) 495
11. I. Gutman, S. Marković, A. V. Teodorović, Z. Bugarčić, *J. Serb. Chem. Soc.* **51** (1986) 145
12. I. Gutman, *Topics Curr. Chem.* **162** (1992) 29
13. I. Gutman, T. Soldatović, *MATCH Commun. Math. Comput. Chem.* **44** (2001) 169
14. M. Fischermann, I. Gutman, A. Hoffmann, D. Rautenbach, D. Vidović, L. Volkmann, *Z. Naturforsch.* **57a** (2002) 49
15. I. Gutman, *MATCH Commun. Math. Comput. Chem.* **14** (1983) 71
16. I. Gutman, M. Rašković, *Z. Naturforsch.* **40a** (1985) 1059
17. A. Graovac, I. Gutman, P. E. John, D. Vidović, I. Vlah, *Z. Naturforsch.* **56a** (2001) 307.

Spectrophotometric study of Co(II), Ni(II), Cu(II), Zn(II), Pd(II) and Hg(II) complexes with isatin- β -thiosemicarbazone

SANDRA S. KONSTANTINOVIĆ^{1*}, BLAGA C. RADOVANOVIĆ²,
ZORAN B. TODOROVIĆ^{1#} and SLAVICA B. ILIĆ¹

¹Faculty of Technology, Bulevar Oslobođenja 124, 16000 Leskovac and ²Faculty of Science,
Department of Chemistry, Višegradaska 33, 18000 Niš, Serbia

(Received 20 July 2006, revised 15 March 2007)

Abstract: The composition and stability of the complexes of isatin- β -thiosemicarbazone with Co(II), Ni(II), Cu(II), Zn(II), Pd(II) and Hg(II) have been investigated using spectrophotometric method at 30 °C and constant ionic strength of 0.1 mol dm⁻³ (KNO₃) in 70 % ethanol. Experimental results indicate the formation of MeL and MeL₂ complexes for Ni(II) and Co(II), and MeL for Cu(II), Zn(II), Pd(II) and Hg(II) complexes, whose stability constants, β_n , have been calculated using a computerized iterative method of successive approximation.

Keywords: isatin- β -thiosemicarbazone, complexes, spectrophotometric study, stability constant.

INTRODUCTION

It is known that aromatic azo and azomethine compounds (Schiff bases) are widely used because of their very good chelatogenic characteristics. In addition to the commercially available compounds, there are a large number of new synthesized ones which are of interest for the study of their complexation reactions and practical applications.¹ The synthetic versatility of isatin has led to an extensive use of this compound in organic synthesis. It stemmed from the interest in the biological and pharmacological properties of its derivatives.^{2–6} Also, thiosemicarbazones are of considerable interest because of their chemistry and potentially beneficial biological activities, such as anti-tumor, antibacterial, antiviral and anti-malarial activities.^{2–6} The activity of thiosemicarbazones is thought to be due to their power of chelation with traces of metal ions present in biological systems. In recent thermodynamic studies of some metal complexes, potentiometric methods were used.^{7,8} Also thermodynamic studies on transition metal ion complexes of some thiosemicarbazones using a spectrophotometric method have been reported.^{7,8}

* Corresponding author. E-mail: andjelkovic_s@yahoo.com

Serbian Chemical Society member.

doi: 10.2298/JSC0710975K

In this study, isatin- β -thiosemicarbazone (ITC) was synthesized and the stability constants of the complexes of this ligand with Co(II), Ni(II), Cu(II), Zn(II), Pd(II) and Hg(II) were evaluated by spectrophotometry.

EXPERIMENTAL

Preparation of isatin- β -thiosemicarbazone, C₉H₈N₄SO, (ITC)

Isatin-2,3-indolinedione and thiosemicarbazide, in a 1:1 molar ratio were dissolved in 95 % ethanol. The mixture was refluxed over a water bath for 1 h. After cooling to room temperature, the yellow microcrystalline solid was separated, washed with ethanol, diethyl ether and dried over silica gel.⁹

UV/VIS (DMF, $\nu(\text{cm}^{-1}/\epsilon \times 10^3 (\text{mol}^{-1} \text{dm}^3 \text{cm}))$): 28.6/0.946 $\pi \rightarrow \pi^*$, 27.3/1.325 $n \rightarrow \pi^*$; IR (KBr, cm^{-1}): 3422, 3290, 3229, 3141 $\nu(\text{NH}) + \nu(\text{NH}_2)$, 1699 $\nu(\text{C}=\text{O})$, 1607 $\nu(\text{C}=\text{N})$, 854 $\nu(\text{C}=\text{S})$. ¹H-NMR (DMSO, δ / ppm) 6.9–7.6 (*m*, 4H, Ar), 8.69, 9.04 (*s*, 2H, NH₂), 11.21 (2, 1H, NH), 12.47 (*s*, 1H, NH). Analysis: Calculated: 49.08 % C, 3.66 % H, 25.44 % N, 14.56 % S. Found: 48.95 % C, 3.75 % H, 25.30 % N, 14.61 % S; m.p. 239–241 °C.

Solutions

All reagents and solvents were of analytical grade.

ITC solutions were prepared by dissolving an exactly weighted amount of the substances in 70 % ethanol and in buffers prepared with 70 % ethanol.

Stock solutions of metal ions, $c_M = 0.1 \text{ mol dm}^{-3}$ were prepared by dissolving metal(II) chloride in doubly distilled water. The copper(II) solution was standardized iodometrically, while solutions of the other metals were standardized gravimetrically. Solutions of required concentrations were obtained by precisely diluting the stock solutions with the solvent.

The ionic strength, $I = 0.1 \text{ mol dm}^{-3}$, of the ligand and metal salt solutions was adjusted with potassium nitrate (1 M, prepared in distilled water). The following buffer solutions were prepared: pH 3.9, by mixing CH₃COOH (0.2 mol dm⁻³) and CH₃COONa (0.2 mol dm⁻³) in the required ratios; pH 5.8, 6.9, 7.6, 8.1 and 9.0, by mixing in different ratios a solution containing 0.2 mol dm⁻³ H₃BO₃, 0.05 mol dm⁻³ H₂C₄H₄O₆ and 0.05 mol dm⁻³ Na₂SO₄ with a solution containing 0.05 mol dm⁻³ Na₂B₄O₇; pH 9.9, by mixing the required volumes of a 0.05 mol dm⁻³ solution of Na₂B₄O₇ and a 0.05 mol dm⁻³ solution of Na₂CO₃; pH 11 and 12, by mixing 0.05 mol dm⁻³ solutions of tris-HCl.

Determination of pH

The actual pH values of the buffers prepared in 70 % ethanol, as well as the pH of solutions of the ligand and its complexes without buffers, were measured with a combined pH electrode calibrated using pH standard solutions prepared in 70 % ethanol. Since the solvent has a relative permittivity different to that of pure water, all pH values are relative and valid only for the solvent used (70 % ethanol).

UV/Vis Spectroscopy

Absorption spectra of isatin- β -thiosemicarbazone and its complexes with metal(II) ions were investigated in the solvent with the buffers, at pH 3.9–9.9, and the ionic strength of 0.1 mol dm⁻³ (KNO₃). UV/Vis Spectra were recorded on a Varian Cary-100 UV/VIS spectrophotometer using adequate solutions. A blank for the spectrophotometric measurement of the ligand was prepared with the solvent and the corresponding buffer. The absorbance of solutions with complexes was measured against the blank having the same composition as the complex solutions except for the metal ion. In order to prove the stability of the absorbance, measurements were repeated after 30, 60 and 90 min.

RESULTS AND DISCUSSION

Absorption spectra

The electronic spectra of isatin- β -thiosemicarbazone (Fig. 1) show reference absorption bands ($\lambda_1 = 251 \text{ nm}$ and $\lambda_2 = 281 \text{ nm}$) of the aromatic ring and the

indole moiety due to transitions of the $\pi-\pi^*$ type and an absorption band at $\lambda_3 = 355$ nm, also due to a transition of the $\pi-\pi^*$ type but from the thiosemicarbazone part of the molecule. No transitions which could be assigned to an $n-\pi^*$ type were observed in the spectra, since they are covered with the more intensive $\pi-\pi^*$ type. The absorption spectra of isatin-3-thiosemicarbazone at different values of pH exhibit one isobestic point at 325 nm (Fig. 1). This reveals that at last two species (thione–thiol tautomerism) exist in equilibrium in a solution of isatin- β -thiosemicarbazone depending on the pH of the medium (Scheme 1). Species B is present at high pH values and has a bathochromic shift, as a result of the increased extent of chain conjugation.⁸

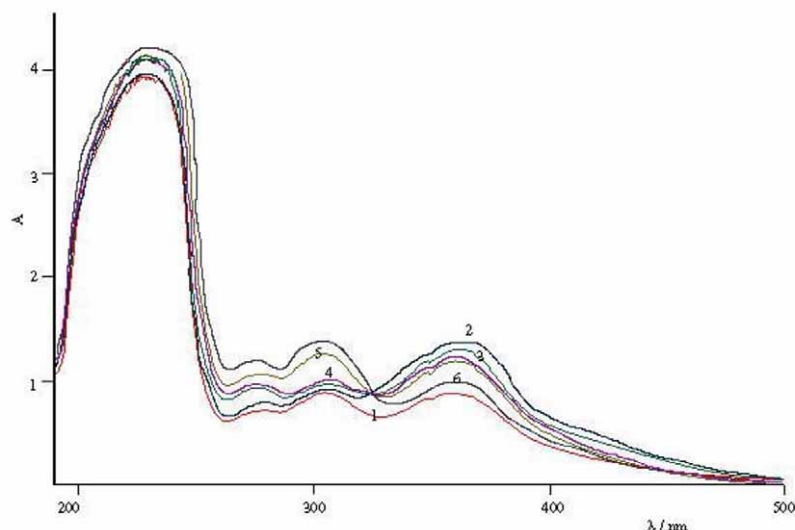
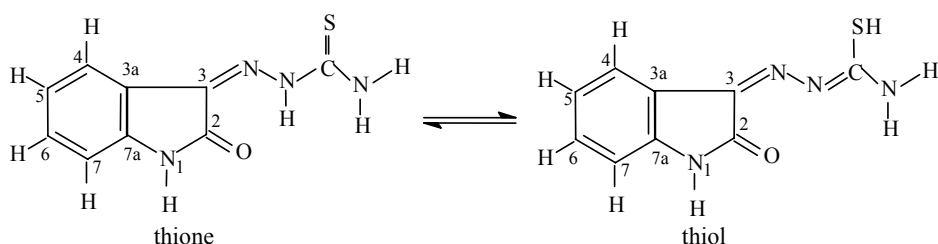


Fig. 1. UV/Vis spectra of isatin- β -thiosemicarbazone (10^{-4} mol dm $^{-3}$ in 70 % ethanol) at pH 6.89 without buffer (1), and at pH 8.1 (2), pH 9.0 (3), pH 9.9 (4), pH 11.0 (5) and pH 12.0 (6).



Scheme 1.

The absorption spectra of the ITC complex with Co(II) in solutions of different pH values are shown in Fig. 2. The optimal pH value for the formation of the Co(II) and Ni(II) complexes ($c_M = c_L = 1.0 \times 10^{-4}$ mol dm $^{-3}$) is 7.3 with buffer, whereas without buffer it is 7.5 for Ni(II) and 7.1 for Co(II). The maximum absorbance at 412 nm for Co(II) and 455 nm for Ni(II) decreases at higher pH values than these.

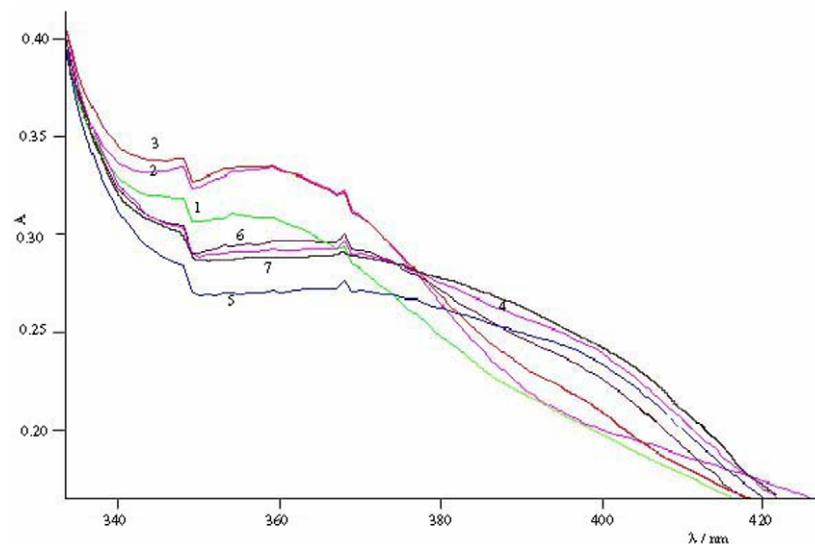


Fig. 2. Absorption spectra of the Co(II) complex in 70 % ethanol at pH 7.1 without buffer (7), and at pH 3.9 (1), 5.5 (2), 6.9 (3), 7.3 (4), 8.1 (5) and 9.9 (6) with buffer.

The best pH value for the formation of the Zn(II) and Hg(II) complexes ($c_M = c_L = 1.0 \times 10^{-4} \text{ mol dm}^{-3}$) is at 6.2 and 6.1 without buffer, respectively, and at 6.3 with buffer. The maximum absorbance at 402 nm for the Zn(II) complex does not change uniformly, while the maximum absorbance at 398 nm for the Hg(II) complex decreases at higher pH than these.

Absorption spectra of the ITC complex with Cu(II) in solutions of different pH values are shown in Fig. 3. The optimal pH values for the formation of the Cu(II) and Pd(II) complexes ($c_M = c_L = 1.0 \times 10^{-4} \text{ mol dm}^{-3}$) formation are at 4.9 for Cu(II) and 5.1 for Pd(II) without buffer and at 5.5 with buffer. Maximum absorbance at 450 nm for Cu(II) and 378 nm for Pd(II) decreases at higher pH than these.

The dependence of the absorbance of the complexes on pH is shown in Fig. 4. An analysis of the curves shows the optimal for complex formation. These pH values are in good agreement with those obtained from the absorption spectra of the complexes.

Under the optimum conditions, using a constant concentration of ITC ($1.0 \times 10^{-3} \text{ mol dm}^{-3}$) and the varying the Ni(II), Co(II), Cu(II), Zn(II), Pd(II) and Hg(II) concentrations in ethanol–water solutions, it was found that the system obeys the Beer law with standard deviations of 0.002, 0.003, 0.002, 0.004, 0.003, and 0.006, respectively, within the metal concentration range 1.0×10^{-5} – 2×10^{-4} for the Ni(II) and Co(II) complexes, 1.0×10^{-5} – 4×10^{-4} for the Cu(II) and Pd(II) complexes, 0.40×10^{-4} – 2.0×10^{-4} for the Zn(II) complex and 0.20×10^{-5} – 1.00×10^{-4} for the Hg(II) complex. The molar absorptivity (ϵ) values at 455 nm for Ni(II) was $1.2 \times 10^3 \text{ dm}^3 \text{ mol}^{-1} \text{ cm}^{-1}$, at 415 nm for Co(II) was $0.39 \times 10^3 \text{ dm}^3 \text{ mol}^{-1} \text{ cm}^{-1}$, at

402 nm for Zn(II) was $0.29 \times 10^3 \text{ dm}^3 \text{ mol}^{-1} \text{ cm}^{-1}$, at 450 nm for Cu(II) was $0.6 \times 10^3 \text{ dm}^3 \text{ mol}^{-1} \text{ cm}^{-1}$, at 378 nm for Pd(II) was $0.35 \times 10^3 \text{ dm}^3 \text{ mol}^{-1} \text{ cm}^{-1}$ and at 398 nm for Hg(II) was $0.37 \times 10^3 \text{ dm}^3 \text{ mol}^{-1} \text{ cm}^{-1}$, indicating that ITC can be readily utilized as a sensitive reagent for the micro-analytical determination of these metal ions.

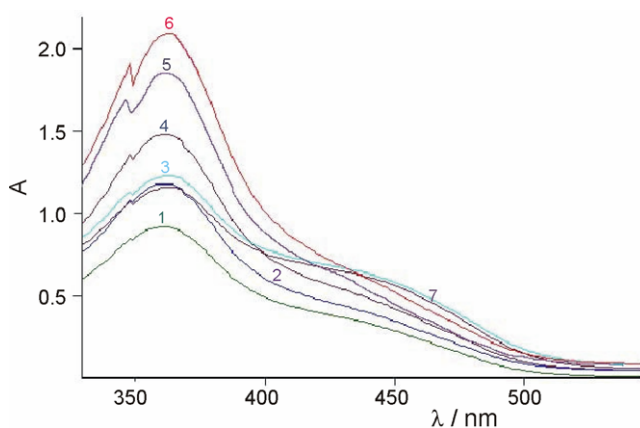


Fig. 3. Absorption spectra of the Cu(II) complex in 70 % ethanol at pH 4.9 without buffer (7), and at pH 3.9 (1), 5.5 (2), 6.9 (3), 7.3 (4), 8.1 (5) and 9.9 (6) with buffer.

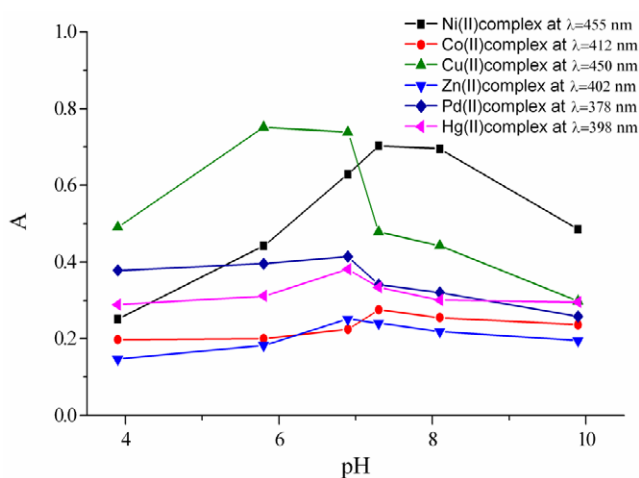


Fig. 4 Absorbance vs. pH of a mixture of ITC with metal ions in 70 % ethanol solution and $I = 0.10 \text{ mol dm}^{-3}$ with KNO_3 .

Composition and stability of the complexes

The composition and values of the stability constant of the formed complexes were determined in 70 % ethanol at $I = 0.10 \text{ mol dm}^{-3}$ (KNO_3) and at a constant temperature of $30 \text{ }^\circ\text{C}$ using a modified Job's method.¹⁰

The Job's curves (Fig. 5) were obtained using equimolar solutions of metal(II) ions and ITC in solutions without buffer. As can be seen, the observed maxima indicate the formation of MeL and MeL_2 complexes for Ni(II) and Co(II), and MeL for Cu(II), Zn(II), Pd(II) and Hg(II) complexes.

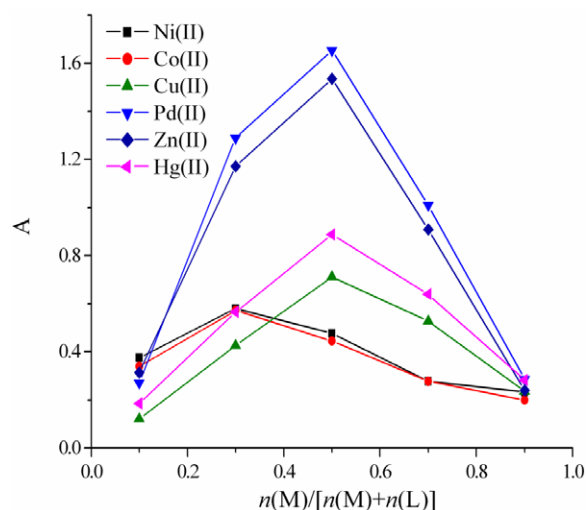


Fig. 5 Job curves for the complexes at pH 7.1 and $\lambda = 412$ nm for Co(II), at pH 7.5 and $\lambda = 455$ nm for Ni(II), at pH 4.9 and $\lambda = 450$ nm for Cu(II), at pH 6.2 and $\lambda = 402$ nm for Zn(II), at pH 5.2 and $\lambda = 378$ nm for Pd(II) and at pH 6.1 and $\lambda = 398$ nm for Hg(II).

The stability constants of the complexes predominant in solution were calculated according to a computerized iterative method of successive approximations.^{11,12} The obtained composition and $\log \beta_n$ values with standard errors are presented in Table I. The values of the stability constants are relative, since the dissociation of the ligand was not taken into consideration.

TABLE I. Composition and stability of the complex of metal(II) ions with ITC in 70 % ethanol ($t = 30$ °C)

Complex	Me:L	$\beta_n / 10^6 \text{ dm}^3 \text{ mol}^{-1}$	$\log \beta_n$	$-\Delta G / \text{kJ mol}^{-1}$
Cu(ITC)Cl ₂	1:1	27.1	7.43	43.13
Zn(ITC)Cl ₂		1.76	6.24	36.24
Pd(ITC)Cl ₂		0.341	5.53	32.08
Hg(ITC)Cl ₂		5.85	6.76	39.27
$\beta_n / 10^5 \text{ dm}^6 \text{ mol}^{-2}$				
Co(ITC) ₂ Cl ₂	1:2	6.39	6.98	40.51
Ni(ITC) ₂ Cl ₂		8.40	7.00	40.63

Thus, the trend of the stability of the complexes follows the order Cu > Ni > Co > Hg > Zn > Pd. This order agrees with the conclusions reached by Irving and William.¹³

The Cu(II) complex is the most stable of the studied complexes, probably due to its 3d⁹ configuration and well-known Jahn–Teller effect.^{14,15} The complexes formed by Ni(II) and Co(II) ions in 1:2 stoichiometry with ITS are more stable than the coordination compounds of a 1:1 type of mercury, zinc and palladium. The information gained from the values of ΔG at 30 °C indicates that the formation of the complexes is spontaneous, exothermic and follows the order of decreasing complex stability.

ИЗВОД

СПЕКТРОФОТОМЕТРИЈСКО ПРОУЧАВАЊЕ И АНАЛИТИЧКА ПРИМЕНА
КОМПЛЕКСА Co(II), Ni(II), Cu(II), Zn(II), Pd(II) И Hg(II) СА
ИЗАТИН- β -ТИОСЕМИКАРБАЗОНОМСАНДРА С. КОНСТАНТИНОВИЋ¹, БЛАГА Ц. РАДОВАНОВИЋ², ЗОРАН Б. ТОДОРОВИЋ¹ И СЛАВИЦА Б. ИЛИЋ¹¹ Tehnološki fakultet, Bulevar oslobođenja 124, 16000 Leskovac i ² Prirodno-matematički fakultet, Odsek za hemiju, Višegradska 33, 18000 Niš

Састав и стабилност наведених комплекса су испитани коришћењем спектрофотометријске методе при температури од 30 °C и константној јонској јачини 70 % раствора етанола 0,1 mol dm⁻³ (KNO₃). Резултати сугеришу формирање MeL и MeL₂ код Ni(II) и Co(II), и MeL код Cu(II), Zn(II), Pd(II) и Hg(II) комплекса, чије су константе стабилности β_n одређене коришћењем рачунарске итеративне методе sukcesivних апроксимација. Испитана је и могућност примене истраживаног азометина као реагенса за спектрофотометријска одређивања микроколичина метала.

(Примљено 20. јула 2006, ревидирано 15. марта 2007)

REFERENCES

1. G. S. Aćamović–Djoković, *J. Serb. Chem. Soc.* **60** (1995) 317
2. J. F. M. da Silva, S. J. Garden, A. C. Pinto, *J. Braz. Chem. Soc.* **12** (2001) 273
3. E. M. Jouad, G. Larcher, M. Allain, A. Riou, G. M. Bouet, M. A. Khan, X. Do Thanh, *J. Inorg. Biochem.* **86** (2001) 565
4. S. N. Pandeya, D. Sriram, P. Yogeewari, S. Ananthan, *Chemotherapy* **47** (2001) 266
5. S. N. Pandeya, D. Sriram, G. Nath, E. De Clercq, *Arzneim–Forsch./Drug Res.* **50** (2000) 55
6. S. S. Konstantinović, B. C. Radovanović, Z. Cakić, V. Vasić, *J. Serb. Chem. Soc.* **68** (2003) 641
7. E. G. Akgemci, T. Atalay, *Turk. J. Chem.* **24** (2000) 89
8. M. Mashaly, H. A. Bayoumi, A. Taha, *Chem. Papers* **53** (1999) 299
9. S. S. Konstantinović, B. C. Radovanović, A. Krklješ, *J. Therm. Anal. Cal.* (2007), doi: 10.1007/s10973-006-7794-9
10. K. Momoki, J. Sekino, H. Sato, N. Yamaguchi, *Anal. Chem.* **41** (1969) 1286
11. N. Rahman, S. N. H. Azmi, *Anal. Sci.* **16** (2000) 1353
12. J. Burgess, C. D. Hubbard, P. H. Miyares, T. L. Cole, T. P. Dasgupta, S. Leebert, *Tran. Met. Chem.* **30** (2005) 957
13. H. M. Irwing, R. J. P. Williams, *J. Chem. Soc.* **11** (1953) 3192
14. M. Mashaly, H. A. Bayoumi, A. Taha, *J. Serb. Chem. Soc.* **64** (1999) 621
15. T. Atalay, E. Akgemci, *Tr. J. Chem.* **22** (1998) 123.

DNA cleavage, structural elucidation and anti-microbial studies of three novel mixed ligand Schiff base complexes of copper(II)

N. RAMAN* and S. JOHNSON RAJA

Research Department of Chemistry, VHNSN College, Virudhunagar–626 001, India

(Received 10 November 2006, revised 20 April 2007)

Abstract: Three new copper complexes of mixed ligands derived from Schiff bases (condensation of *p*-aminoacetanilide and substituted benzaldehydes) with 1,10-phenanthroline have been synthesized and characterized by elemental analysis, IR, UV–Vis, magnetic moments, conductivity and electrochemical measurements. The spectral techniques suggest that all the copper complexes exhibit octahedral geometry. The low electrical conductance of the complexes supports their neutral nature. The monomeric nature of the complexes was assessed from their magnetic susceptibility values. The *in vitro* biological screening effects of the investigated compounds were tested against the bacteria *Escherichia coli*, *Staphylococcus aureus*, and *Salmonella typhi* and the fungi *Rhizopus stolonifer* and *Candida albicans* by the serial dilution method. A comparative study of the MIC values of the Schiff bases and their copper complexes indicates that the metal complexes exhibited higher antibacterial activity than the free ligands. The DNA cleavage ability of the complexes was monitored by the gel electrophoresis technique. It was found that electron withdrawing group substituted copper complex had higher DNA cleavage activity than the other copper complexes.

Keywords: *p*-aminoacetanilide, benzaldehyde, *p*-methoxybenzaldehyde, 2-chlorobenzaldehyde, CT DNA, copper(II) complexes.

INTRODUCTION

Transition metals are essential for the normal functioning of living organisms. Therefore, it is not surprising that transition metal compounds are of great interest as potential drugs. Many complexes, including the platinum group, have been synthesized and tested in a number of biological systems after the discovery of the inorganic anti-cancer agent, cisplatin. Thus, interest in the complexes of copper has arisen for the following reasons: copper complexes are known to have a broad spectrum of biological action¹ and copper is considered as an essential trace element but its concentrations as free metal ion inside cells should be lower than 10^{-15} M (calculated)/ 10^{-12} M (observed), since concentrations higher than 10^{-9} M in the cytoplasm can be poisonous.² The free copper concentration in the cyto-

* Corresponding author. E-mail: drn_raman@yahoo.co.in
doi: 10.2298/JSC0710983R

plasm is regulated by different mechanisms, including pumps, exchangers and by protein expression, which use copper in their active sites.³ The great majority of the copper proteins are involved mainly in oxidation/reduction reaction as well as in dioxygen transport.⁴ The development of mimic system for copper metalloenzymes has provided similar activities to that of natural metalloenzymes.⁵⁻⁷ Copper has proved to be a valuable metal center in the development of artificial nuclease systems, as reported in the literature.⁸⁻¹¹ Thus, synthetic copper compounds have been investigated on their ability to promote nucleic acid cleavage, as well as receiving special attention for their action on DNA.¹² The potential scope of the utility of these compounds is enormous and ranges from the creation of synthetic restriction enzymes for use by molecular biologists to the development of chemotherapeutic agents which may be effective against a variety of diseases, sensitive chemical probes for DNA structure in solution and tools for the molecular biologist to dissect genetic systems.¹³ Especially, a number of metal complexes of a variety of ligands have been studied in view of their possibility to lead to advanced functional materials, tuning the redox potentials, affinity towards DNA, and specificity for DNA base sequence recognition.¹⁴⁻¹⁶ Investigations of the interaction of DNA with small molecules are basic work in the design of new types of pharmaceutical molecules. Some types of metal complexes interacted with DNA could induce the breakage of DNA strands as shown by the gel electrophoresis technique. Thus, in cancer genes, after a cleavage of a DNA strand, the DNA double strands breaks. The replication ability of cancer gene is thereby destroyed.

It is well known from the literature that compounds containing an amide moiety have a strong ability to form metal complexes and exhibit a wide range of biological activities. Hence, in this work, the synthesis of three Schiff base copper complexes containing an amide moiety and 1,10-phenanthroline was attempted and the biological activities, such as anti-microbial and DNA cleavage, of the resulting complexes were studied.

EXPERIMENTAL

Synthesis of the Schiff bases

The Schiff base was prepared by the dropwise addition of an ethanolic solution (50 ml) of *p*-aminoacetanilide into a solution of benzaldehyde (L¹)/*p*-methoxybenzaldehyde (L²)/2-chlorobenzaldehyde (L³) (1:1 molar ratio of 10 mM) in ethanol. After completion of the addition, the solution was refluxed on a water bath for 1 h and allowed to cool by standing at room temperature. The formed solid product was removed by filtration and recrystallized from ethanol (Yield: 75 % for L¹; 70 % for L²; 78 % for L³).

Synthesis of the copper complexes

A solution of Schiff base and 1,10-phenanthroline in ethanol was added to a solution of CuCl₂·2H₂O (1:1:1 molar ratio of 10 mM) in ethanol and the mixture was stirred for 1 h. The solid product so-formed was separated by filtration and washed thoroughly with ethanol and dried *in vacuo* (Yield: 52 % for [CuL¹(Phen)Cl₂]; 55 % for [CuL²(Phen)Cl₂]; 60 % for [CuL³(Phen)Cl₂]).

Nuclease activity

The DNA cleavage experiment was conducted using CT DNA by gel electrophoresis with the corresponding copper complex in the presence of H₂O₂ as an oxidant. The reaction mixture was incubated at 35 °C for 1.5 h before the electrophoresis experiment as follows: CT DNA 10 μM, 5 μM each complex, 1 μM H₂O₂ in 50 mM tris-HCl buffer (pH 7.0) and 34 μM of double distilled water. The samples were electrophoresed for 2 h at 50 V on 1 % agarose gel using tris-acetic acid-EDTA buffer, pH 8.3. After electrophoresis, the gel was stained using 1 μg cm⁻³ EB and photographed under UV light.

Anti-microbial activity

The *in vitro* biological screening effects of the investigated compounds were tested against *Staphylococcus aureus*, *Escherichia coli*, *Salmonella typhi* by the well diffusion method using agar nutrient as the medium and amphotericin as the control.

The *in vitro* anti-fungal assay was performed by the disc diffusion method. The complexes and ligand were tested against the fungi *Rhizopus stolonifer* and *Candida albicans*, cultured on potato dextrose agar as medium. In a typical procedure, a well was made on the agar medium inoculated with the fungi. The well was filled with the test solution using a micropipette and the plate was incubated at 30 °C for 72 h. During this period, the test solution diffused and the growth of the inoculated fungi was affected. The inhibition zone developed on the plate was measured. The MIC of the complexes was determined by the serial dilution technique.

Apparatus and reagents

All reagents were Merck products and were used as supplied. For the voltammetric experiments, the tetrabutylammonium perchlorate (TBAP) used as the supporting electrolyte, was purchased from Sigma. Anhydrous grade methanol and DMSO were obtained from Fisher Scientific Company. The metal contents of the complexes were estimated gravimetrically as their oxides,¹⁷ by fusion with AnalaR ammonium oxalate. Microanalytical data and FAB mass spectra of the compounds were recorded at the Regional Sophisticated Instrumentation Center, Central Drug Research Institute (RSIC, CDRI), Lucknow. Microanalyses were performed using a Carlo Erba 1108 CHN Elemental Analyser. The FAB mass spectra of the complexes were recorded on a JEOL SX 102/DA-6000 mass spectrometer/data system using argon/xenon (6 kV, 10 mA) as the FAB gas. The accelerating voltage was 10 kV and the spectra were recorded at room temperature using *m*-nitrobenzyl alcohol (NBA) as the matrix. The IR spectra of the samples were recorded on a Perkin-Elmer 783 spectrophotometer in 4000–200 cm⁻¹ range using the KBr pellet technique. The UV-Vis spectra were recorded on a Shimadzu UV-1601 spectrophotometer using DMSO as the solvent in the wave range of 200–800 nm. The X-band ESR spectra of the complexes were recorded at 77 K at IIT, Mumbai using TCNE (tetracyanoethylene) as the *g*-marker. Magnetic susceptibility measurements of the complexes were carried out using a Guoy balance with copper sulfate as the calibrant. Electrochemical studies were carried out using a EG&G Princeton Applied Research Potentiostat/Galvanostat Model 273A, controlled by M270 software. The measurements were carried out under oxygen-free condition using a three electrode cell, in which glassy carbon was the working electrode, a saturated Ag/AgCl was the reference electrode and a platinum wire was used as the auxiliary electrode. All solutions (10⁻³ M) were purged with N₂ for 30 min prior to each set of experiments. The molar conductivity was measured with a Systronic conductivity bridge, using freshly prepared solutions of the complexes in DMSO solution (10⁻³ M). Solutions of CT-DNA in 50 mM NaCl/50 mM tris-HCl (pH 7.0) gave a ratio of UV absorbance at 260 and 280 nm, A₂₆₀/A₂₈₀ of *ca.* 1.8–1.9, indicating that the DNA was sufficiently free of protein contamination. The DNA concentration was determined by the UV absorbance at 260 nm after 1:100 dilutions. Stock solutions were kept at 4 °C and doubly distilled H₂O was used to prepare the buffer.

RESULTS AND DISCUSSION

All the complexes were air stable, insoluble in water and soluble in DMSO. They were identified by their physical and analytical data. The analytical data (Table I) are in good agreement with the general formula $[\text{CuL}(\text{Phen})\text{Cl}_2]$. The monomeric nature of the complexes was evidenced from their magnetic susceptibility values. The study of the magnetic and electronic spectral data was quite informative in characterizing the geometry of the complexes. These complexes are non-electrolytic due to their low conductivity values.¹⁸

TABLE I. Physical characterization, analytical, molar conductance and magnetic susceptibility data of the complexes

Compound	Color	Composition found (calcd), %				$A_m \times 10^3$ S cm ² mol ⁻¹	μ_{eff} / μ_B
		M	C	H	N		
L ¹	Yellow	–	75.69 (75.63)	5.81 (5.88)	11.80 (11.76)	1.3	–
$[\text{CuL}^1(\text{Phen})\text{Cl}_2]$	Dark green	11.49 (11.50)	58.60 (58.64)	3.95 (3.98)	10.11 (10.13)	1.6	1.85
L ²	White	–	71.10 (71.91)	5.65 (5.62)	10.42 (10.49)	1.2	–
$[\text{CuL}^2(\text{Phen})\text{Cl}_2]$	Brown	10.80 (10.85)	57.61 (57.68)	4.10 (4.12)	9.63 (9.61)	1.8	1.75
L ³	Glittering white	–	67.10 (67.16)	4.80 (4.85)	8.99 (8.95)	1.4	–
$[\text{CuL}^3(\text{Phen})\text{Cl}_2]$	Pale green	10.86 (10.85)	55.15 (55.33)	3.52 (3.59)	9.51 (9.56)	1.7	1.79

The FAB mass spectra of the Schiff bases and their copper complexes were used to compare their stoichiometric composition. The Schiff base L² shows a molecular ion peak M⁺ at $m/z = 268$. The molecular ion peak, observed at $m/z = 581$ for the copper complex confirms the molecular formula of the copper complex as $[\text{CuL}^2(\text{Phen})\text{Cl}_2]$. This was also supported by the FAB mass spectra of the other complexes.

The elemental analysis values are in close agreement with the values calculated from molecular formula assigned to these complexes, which is further supported by the FAB-mass studies of the complexes.

The electronic spectra of the Schiff base ligands and their copper complexes were recorded in DMSO solution at 300 K. The spectra of copper complexes show a d-d transition in the region 700–750 nm, assigned to a ${}^2\text{B}_{1g} \rightarrow {}^2\text{A}_{2g}$ transition. The position of this band in the spectra suggests a distorted octahedral geometry for the complexes.¹⁹ A moderately intensive band observed in the range 330–360 nm is due to a ligand-to-metal charge transfer transition²⁰ and the strong band observed in the range 250–280 nm is due to an intra-ligand charge transfer transition for these copper complexes.²¹

The IR spectra of the free Schiff base ligands were compared with the spectra of the complexes. The IR spectra of the Schiff bases show a prominent absorption peak at *ca.* 1700 cm⁻¹ corresponding to $\nu(\text{C}=\text{O})$ of acetanilide, which is shifted to a lower frequency 1680 cm⁻¹ in the spectra of the copper complexes, indicating coordination to the metal ion. The ligands show their characteristics $\nu(\text{C}=\text{N})$ bands in the region 1610–1590 cm⁻¹, which are also shifted to lower frequencies in the spectra of all the complexes (1580–1550 cm⁻¹). The IR spectra of the copper complexes show some new bands in the region 490–510 cm⁻¹ and 450–460 cm⁻¹, which are probably due to Cu–O and Cu–N bonds respectively.²² The weak band at 350 cm⁻¹ is probably due to the formation of Cu–Cl bonds.²³

The ESR spectrum of metal complexes provides information about hyperfine and superhyperfine structures which are of importance in the study of the environment of the metal ion in the complex, *i.e.*, the geometry and nature of the ligating sites of the Schiff base and the metal. The X-band ESR spectrum of the polycrystalline copper complex recorded at 77 K shows a well-resolved hyperfine splitting and exhibits two different *g*-values, indicating the magnetic anisotropy in the complex. The magnetic susceptibility value reveals that the copper complex has a magnetic moment, 1.85 μ_{B} , corresponding to that of one unpaired electron, indicating that the complex is mononuclear. This fact was also evident from the absence of a half field signal, observed in the spectrum at 1600 G due to $m_s = \pm 2$ transitions, ruling out any Cu–Cu interaction.²⁴

The *g*-tensor value of the $[\text{CuL}^3(\text{Phen})\text{Cl}_2]$ complex can be used to derive the ground state. In octahedral complexes, the unpaired electron lies in the $d_{x^2-y^2}$ orbital. In the present copper complex, the observed *g*-tensor values are $g_{\parallel}(2.256) > g_{\perp}(2.052) > g_e(2.002)$, which suggest that this complex has a distorted octahedral geometry. The ESR parameters of the complex also coincide well with related systems for which it was suggested that the complexes have a distorted octahedral geometry and that the systems are axially symmetric.²⁵ In the axial spectra, the *g* values are related to the exchange interaction coupling constant (*G*) by the expression:

$$G = g_{\parallel} - \frac{2}{g_{\perp} - 2}$$

According to Hathaway,²⁶ if the *G* value is larger than four, the exchange interaction is negligible because the local tetragonal axes are aligned parallel or are slightly misaligned. If its value is less than four, the exchange interaction is considerable and the local tetragonal axes are misaligned. For the present copper complex, it is 4.9, which suggests that the local tetragonal axes are aligned parallel or are slightly misaligned and are consistent with a $d_{x^2-y^2}$ ground state.

Based on the above spectral data, the structures of these complexes are assigned as shown in Fig. 1.

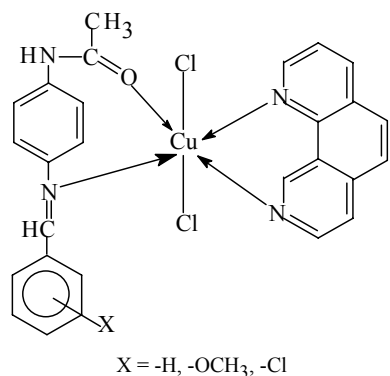


Fig. 1. Proposed structure of the synthesized copper(II) complexes.

Cyclic voltammetry is the most versatile electrochemical technique for the study of electroactive species. The cyclic voltammogram of the $[\text{CuL}^3(\text{Phen})\text{Cl}_2]$ (0.01 M) complex in DMSO at 300 K in the potential range 0.8 to -0.4 V at a scan rate 100 mV s^{-1} is shown in Fig. 2, which shows one quasi-reversible reduction peak at 0.31 V (E_{pc}), corresponding to the formation of Cu(III)/Cu(II) and an oxidation peak at 0.49 V (E_{pa}), corresponding to the formation of the Cu(II)/Cu(III) couple. The peak potential difference ($\Delta E_{\text{p}} = 130 \text{ mV}$) shows one quasi-reversible couple. The number of electrons of the complex transferred was established by the current heights ($I_{\text{pc}}/I_{\text{pa}} = 0.91$) which shows that the copper complex has one electron transfer.

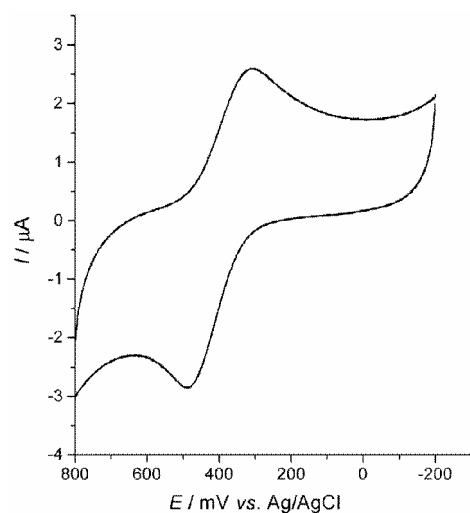


Fig. 2. Cyclic voltammogram of $[\text{CuL}^3(\text{Phen})\text{Cl}_2]$ in DMSO at room temperature.

The *in vitro* anti-microbial activity of the investigated compounds was tested against the microorganisms *E. coli*, *S. typhi*, *S. aureus*, *C. albicans* and *R. stolnifer* by the serial dilution method. The minimum inhibitory concentration (MIC) values of the compounds against the growth of micro-organisms are summarized

in Table II. A comparative study of the ligands and their copper complexes (MIC values) indicates that all the copper complexes exhibited higher anti-microbial activity than the free ligands. Such increased activity of the complexes can be explained on the basis of the Overtone concept²⁷ and the Tweedy chelation theory.²⁸ According to the Overtone concept of cell permeability, the lipid membrane surrounding the cell favors the passage of only lipid-soluble materials, due to which liposolubility is an important factor controlling the anti-microbial activity. On chelation, the polarity of the metal ion will be reduced to a greater extent due to the overlap of the ligand orbital and partial sharing of the positive charge of the metal ion with donor groups. Furthermore, the mode of action of the compound may involve formation of a hydrogen bond through the azomethine group with the active centre of cell constituents, resulting in interference with normal cell processes.

TABLE II. Anti-microbial data of the investigated compounds (MIC $\times 10^3$ M)

Compound	<i>E. coli</i>	<i>S. typhi</i>	<i>S. aureus</i>	<i>R. stolonifer</i>	<i>C. albicans</i>
L ¹	4.2	5.9	5.1	4.6	3.8
[CuL ¹ (Phen)Cl ₂]	3.2	0.8	1.6	2.2	2.6
L ²	4.5	3.9	5.9	4.0	6.2
[CuL ² (Phen)Cl ₂]	2.6	1.5	1.0	2.2	1.8
L ³	4.0	2.9	4.2	3.4	5.2
[CuL ³ (Phen)Cl ₂]	1.4	1.8	2.1	0.6	2.8
Amphotericin	3.2	2.0	1.8	1.5	2.5

The nuclease activity of the present copper complexes was investigated using CT DNA by agarose gel electrophoresis in the presence of an oxidant (H₂O₂), as shown in Fig. 3.

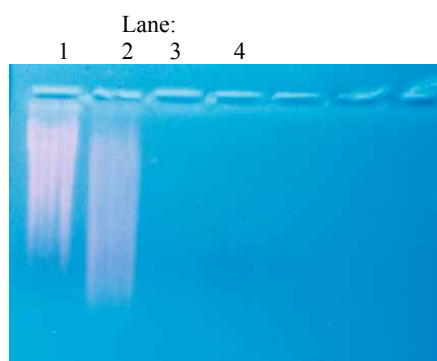


Fig. 3. Agarose gel (1 %) showing the changes in the agarose gel electrophoretic pattern of CT DNA induced by H₂O₂. Lane 1: DNA alone, Lane 2: DNA + [CuL¹(Phen)Cl₂], Lane 3: DNA + [CuL²(Phen)Cl₂] and Lane 4: DNA + [CuL³(Phen)Cl₂].

As can be seen from the results (Fig. 3), the electron withdrawing substituted complex had a higher DNA cleavage activity than the other copper complexes (*i.e.*, [CuL³(Phen)Cl₂] > [CuL²(Phen)Cl₂] > [CuL¹(Phen)Cl₂]). Due to the presence of an electron withdrawing group in the ligand, the positive charge of the copper ion increases, and this enhances the ability of the copper ion to interact

with DNA. The samples in lanes 3 and 4 were completely degraded. This shows that a slight increase in the concentration over the optimal value (*i.e.*, the value at which a 100 % cleavage efficiency was observed) led to extensive degradation, resulting in the disappearance of the bands on the agarose gel. The other copper complex (lane 2) degrades DNA efficiently. To understand the active oxygen species in the reactions, inhibition experiments were performed with standard scavengers for reactive oxygen intermediates using degradation experiments with the Rhodamine B dye test (Fig. 4).

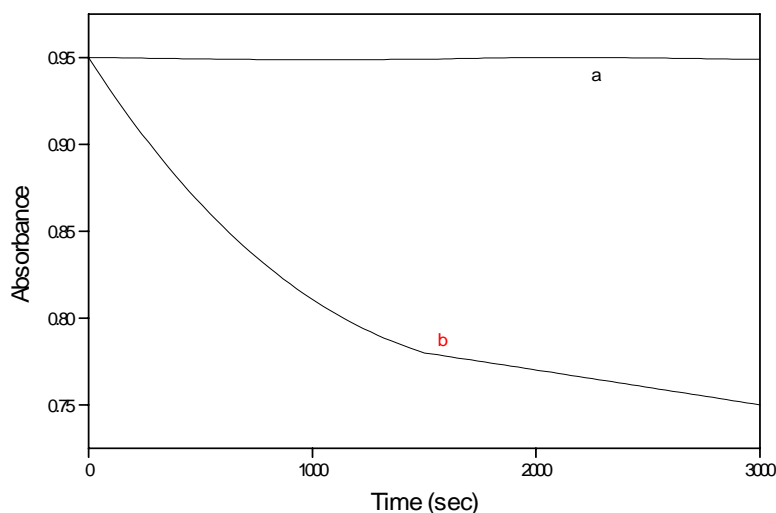


Fig. 4. Rhodamine B degradation followed by the decrease of the absorbance at 552 nm at pH 8.1 in 10 mM phosphate buffer: (a) in the presence of 0.1 mM $[\text{CuL}^1(\text{Phen})\text{Cl}_2]$; (b) in the presence of 0.1 mM $[\text{CuL}^1(\text{Phen})]^{2+}$, 10 mM H_2O_2 , 1 mM ascorbic acid.

The degradation of the dye provides a direct measure of the concentrations of hydroxyl radicals in the reaction mixture. From the observation, it is suggested that reactive oxygen species can be produced by the $[\text{CuL}^1(\text{Phen})\text{Cl}_2]$ complex under redox conditions.²⁹

CONCLUSIONS

A new series of mixed ligand complexes of copper was synthesized and their octahedral geometry was inferred from their spectral data. A comparative study of the MIC values of the ligands and their complexes indicates that the copper complexes exhibit higher anti-microbial activity than the free ligands. The Rhodamine B dye test clearly indicates that the increase of the cleavage reactivity is related to the presence of reactive radicals. Electrochemical experiments neatly demonstrate that the present ligand system is ideally suited for stabilizing the higher oxidation states of the copper ion.

Acknowledgements: The authors express their sincere thanks to the Head, Department of Chemistry, Principal and College Managing Board of VHNSN College, Virudhunagar for their constant encouragement and providing the research facilities. SJ thanks the Tamilnadu Government for financial support.

ИЗВОД

РАЗЛАГАЊЕ ДНК, ОДРЕЂИВАЊЕ СТРУКТУРЕ И АНТИМИКРОБНА ИСПИТИВАЊА ТРИ НОВА МЕШОВИТА КОМПЛЕКСА БАКРА(II) СА ЛИГАНДИМА ЗАСНОВАНИМ НА ШИФОВИМ БАЗАМА

N. RAMAN и S. JOHNSON RAJA

Research Department of Chemistry, VHNSN College, Virudhunagar-626 001, India

Синтетисана су три нова комплекса бакра са мешовитим лигандима од Шифових база (кондензација *p*-аминоацетанилида и супституисаних бензалдехида) са 1,10-фенантролином и окарактерисана елементалном анализом, IR, UV-Vis, одређивањем магнетних момената и проводљивости, као и електрохемијским мерењима. Спектралне технике указују на то да су сви комплекси бакра октаедарске геометрије. Ниска електрична проводљивост комплекса указује на њихову неутралну природу. Вредности магнетне суцептибилности указују на мономерну природу комплекса. Биолошка активност добијених једињења испитивана је *in vitro* на бактеријама *Escherichia coli*, *Staphylococcus aureus* и *Salmonella typhi* и гљивама *Rhizopus stolonifer* и *Candida albicans* методом серијског разблажења. Упоредна анализа МИС вредности Шифових база и њихових комплекса бакра указују на то да су метални комплекси антибактеријски активнији од слободних лиганата. Способност комплекса за везивање ДНК испитивана је техником гел-електрофорезе. Утврђено је да супституисани комплекси бакра мање електронске густине јаче везују ДНК од осталих комплекса бакра.

(Примљено 10. новембра 2006, ревидирано 20. априла 2007)

REFERENCES

1. R. K. Crouch, T. W. Oberley, J. R. J. Sorenson, in *Possible Medicinal Uses of Copper Complexes: Biological and Inorganic Copper Chemistry*, K. D. Karlin, J. Zubieta, Eds., Adenine Press, NY, 1986
2. R. J. P. Williams, J. J. R. Frausto da Silva, *Coord. Chem. Rev.* **200** (2000) 247
3. R. J. P. Williams, *Coord. Chem. Rev.* **216** (2001) 583
4. E. I. Solomon, U. M. Sundaram, T. E. Machonkin, *Chem. Rev.* **96** (1996) 2563
5. E. A. Lewis, W. B. Tolman, *Chem. Rev.* **104** (2004) 1047
6. R. Than, A. A. Feldmann, B. Krebs, *Coord. Chem. Rev.* **182** (1999) 211
7. K. Selmeczi, M. Reglier, M. Giorgi, G. Speier, *Coord. Chem. Rev.* **245** (2003) 191
8. E. L. Hegg, J. N. Burstyn, *Coord. Chem. Rev.* **173** (1998) 133
9. R. Kramer, *Coord. Chem. Rev.* **182** (1999) 243
10. A. Sreedhara, J. A. Cowan, *J. Biol. Inorg. Chem. Rev.* (2001) 337
11. C. Liu, M. Wang, T. Zhang, H. Sun, *Coord. Chem. Rev.* **248** (2004) 147
12. F. Liang, C. Wu, H. Lin, D. Gao, Z. Li, J. Wei, C. Zheng, M. Sun, *Bioorg. Med. Chem. Lett.* **13** (2003) 2469
13. P. B. Dervan, *Science* **232** (1986) 464
14. M. J. Clarke, F. Zhu, D. R. Frasca, *Chem. Rev.* **99** (1999) 2511
15. D. S. Sigman, A. Mazumder, D. M. Perrin, *Chem. Rev.* **93** (1993) 2295
16. S. Routier, N. Cotelle, J. P. Catteau, J. L. Bernier, M. J. Waring, J. F. Riou, C. Bailly, *Bioorg. Med. Chem.* **4** (1996) 1185

17. R. J. Angelici, *Synthesis and Techniques in Inorganic Chemistry*, W. B. Saunders Company, 1969
18. W. J. Geary, *Coord. Chem. Rev.* **7** (1971) 81
19. K. R. Krishnapriya, M. Kandaswamy, *Polyhedron* **24** (2005) 113
20. C. Fernandes, G. L. Parrilha, J. A. Lessa, L. J. M. Santiago, M. M. Kanashiro, F. S. Boniolo, A. J. Bortoluzzi, N. V. Vugman, M. H. Herbst, A. Horn Jr., *Inorg. Chim. Acta* **359** (2006) 3167
21. K. N. Srivastava, S. Das, R. A. Lal, *Indian J. Chem.* **25A** (1986) 85
22. K. Nakamoto, *Infrared and Raman Spectra of Inorganic and Coordination Compounds, Part B*, 5th ed., Wiley, New York, 1997, p. 59
23. D. M. Adams, *Metal-Ligand and Related Vibrations*, St. Martin's Press, New York, 1968
24. A. L. Sharma, I. O. Singh, M. A. Singh, H. R. Singh, R. M. Kadam, M. K. Bhide, M. D. Sastry, *Transition Met. Chem.* **26** (2001) 532
25. B. T. Thaker, P. K. Tankel, A. S. Patel, C. J. Vyas, M. S. Jesani, D. M. Patel, *Indian J. Chem.* **44A** (2005) 241
26. B. J. Hathaway, A. A. G. Tomlinson, *Coord. Chem. Rev.* **5** (1970) 1
27. Y. Anjaneyulu, R. P. Rao, *Synth. React. Inorg. Met.-Org. Chem.* **16** (1986) 257
28. B. G. Tweedy, *Phytopathology* **55** (1964) 910
29. C. Sissi, F. Mancin, M. Gatos, M. Palumbo, P. Tecilla, U. Tonellato, *Inorg. Chem.* **44** (2005) 2310.

Preparation and characterization of carbon paste electrode modified with tin and hexacyanoferrate ions

REZA E. SABZI*, ALL HASANZADEH, KHOSROW GHASEMLU and PARVANEH HERAVI

Department of Chemistry, Faculty of Science, Urmia University, Urmia, Iran

(Received 9 June 2006, revised 27 March 2007)

Abstract: A carbon paste electrode was modified chemically using Sn(II) or Sn(IV) chlorides and hexacyanoferrate(II) or hexacyanoferrate(III). The electrochemical behavior of such SnHCF carbon paste electrodes was studied by cyclic voltammetry. The study revealed that Sn(IV) and hexacyanoferrate(II) yield the best results. This electrode showed one pair of peaks: the anodic and cathodic peak at the potentials of 0.195 and 0.154 V vs. SCE, respectively, at a scan rate of 20 mV s⁻¹ in a 0.5 M phosphate buffer as the supporting electrolyte. The SnHCF modified electrodes were very stable under potential scanning. The effects of pH and alkali metal cations of the supporting electrolyte on the electrochemical characteristics of the modified electrode were studied. The results showed that cations have a considerable effect on the electrochemical behavior of the modified electrode. The diffusion coefficients of hydrated K⁺ and Na⁺ in the film, the transfer coefficient and the electron transfer rate constant were determined.

Keywords: carbon paste electrode, modified electrode, tin, hexacyanoferrate.

INTRODUCTION

To date various inorganic materials,¹ organometals² and polynuclear cyanometalate^{3–44} have been used to make modified electrodes (MEs). Among the various mediators used for electrode modification, solid metal hexacyanoferrates have attracted the attention of electrochemists as excellent electron transfer mediators. Ever since the work of Neff *et al.* on Prussian blue (PB) modified electrode (ME),^{45,46} there have been many papers published over the years on the preparation and characterization of metal hexacyanoferrates as electroactive materials.^{3–44} Various transition metal cations have been used with hexacyanoferrate to fabricate metal hexacyanoferrate (MHCF) modified electrodes, in which M can be: cadmium,³ chromium,^{4,5} cobalt,^{6–9} copper,^{10–12} dysprosium,¹³ gallium,¹⁴ indium,^{15–17} iron HCF (PB),^{18–20} lanthanum,²¹ manganese,^{22,23} molybdenum,²⁴ nickel,^{25–28} osmium,²⁹ palladium,^{30,31} platinum,³² ruthenium,³³ samarium(III),³⁴ silver,^{35,36} mixed-valent titanium,³⁷ vanadium,^{38–40} zinc,⁴¹ zirconium,^{42,43} and Ket–HCF (ketotifen-hexacyanoferrate).⁴⁴

* Corresponding author. E-mail: rezasabzi@yahoo.com
doi: 10.2298/JSC0710993S

The aim of the present study was to propose and examine the preparation of SnHCF MEs as a carbon paste electrode and study of the electrochemical behavior of the electrode in detail.

EXPERIMENTAL

Chemicals and instrumentation

$K_3[Fe(CN)_6]$ (HCF(III)), $K_4[Fe(CN)_6]$ (HCF(II)), KNO_3 , $SnCl_2$, $SnCl_4$ and other chemicals were of analytical grade and were obtained from Merck and used without further purification. A solution of 0.5 M phosphate buffer solution was used as supporting electrolyte. The buffer was prepared using phosphoric acid and pH adjusted with KOH. The electrochemical experiments were carried out using a potentiostat/galvanostat (BHP-2063 electrochemical analysis system, Behpa-joo, Iran). A conventional three-electrode cell was used at 25 °C (room temperature). A saturated calomel electrode and platinum wire (from Azar electrode Co., Iran) were used as reference and auxiliary electrodes, respectively.

Electrode preparation

The SnHCF carbon paste electrode was prepared using tin(IV) chloride. For the preparation of SnHCF, 50 ml of 0.1 M tin(IV) chloride solution containing 0.1 M KNO_3 was slowly added to 50 ml of 0.1 M HCF(II) with agitation. The formed SnHCF precipitate was filtered, washed, and dried. Then 0.05 g of the obtained precipitate was mixed with 0.5 g graphite (1:10) and a few drops of paraffin oil were added to the mixture. The mixture was housed in a polyethylene tube (inner diameter 2.4 mm) and polished on a smooth paper layer. An electric contact was made by a copper wire through the back of the electrode. The obtained SnHCF precipitate was a light green powder which was stable in aqueous solutions.

RESULTS AND DISCUSSION

Electrochemical behavior of the modified electrode

The SnHCF ME was prepared using Sn(II) and Sn(IV) chlorides with HCF(II) and HCF(III). The experimental results revealed that Sn(IV) chloride and HCF(II) after about 20 cycles at a scan rate 100 mV s^{-1} yielded a stable cyclic voltammogram with symmetric peaks with a small peak separation. To maintain the electroneutrality of the metal hexacyanoferrate modified electrode, it is important to equilibrate the compounds with the electrolyte by repeated oxidation and reduction because the starting compounds may contain metal ions in their channels from the synthesis, which must be excluded from lattice to the solution by potential scanning. The modified electrodes prepared with these two salts were characterized by cyclic voltammetry. MEs were also prepared from Sn(IV) with HCF(III), but no peaks were observed, and from Sn(II) with HCF(II) and HCF(III), but the ME had large peak separations. The cyclic voltammograms of SnHCF with Sn(II) and Sn(IV) salts are shown in Fig. 1. It seems that when Sn(IV) was used for the preparation of the ME, the following electrochemical reaction can occur:



However, when Sn(II) and HCF(II) were used for the preparation of the ME, a large peak separation was observed. This character of the ME may be due to the migration of K^+ from the lattice to the solution.

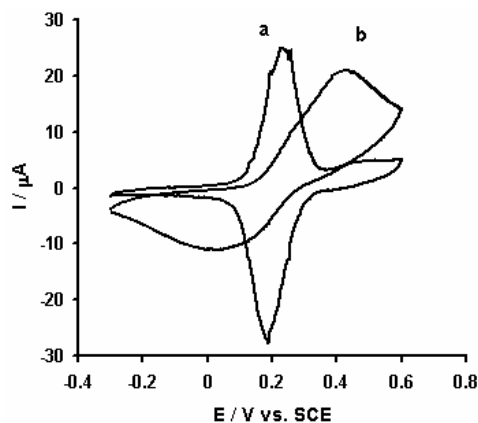
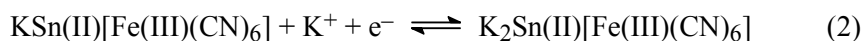


Fig. 1. Cyclic voltammograms of a) the Sn(IV)HCF(II) electrode and b) the Sn(II)HCF(II) electrode, both in a 0.5 M phosphate buffer solution pH 7 (with K^+ cations) at a scan rate of 60 mV s^{-1} .

The cyclic voltammograms of SnHCF in the presence of 0.5 M phosphate buffer, containing no deliberately added electroactive material, were recorded between -0.25 and 0.6 V vs. SCE at various scan rates 10 – 350 mV s^{-1} (Fig. 2A). As can be seen, a single and well-defined redox couple was observed. The anodic and cathodic peak potential were 0.195 and 0.154 V vs. SCE , respectively, at a scan rate of 20 mV s^{-1} . The formal potential, taken as the average of the anodic and cathodic peak potential, $E_0 = (E_{\text{pa}} + E_{\text{pc}})/2$, was about 174 mV and was almost independent of the potential scan rate for sweep rates ranging from 20 to 1000 mV s^{-1} . The formal potential for SnHCF was in order of that of PB. The formal potential for all hexacyanoferrate ME are compared in Table I. The $I_{\text{pa}}/I_{\text{pc}}$ ratio remained almost unity and the peak separation, $\Delta E_{\text{p}} = E_{\text{pa}} - E_{\text{pc}}$, was 41 mV at a scan rate of 20 mV s^{-1} ; at higher scan rates, the peak separation increased (327 mV for 1 V s^{-1}) indicating a limitation arising from the charge transfer kinetics. The peak currents of the voltammogram were linearly proportional to the scan rate up to 350 mV s^{-1} , which is expected for a surface confined redox process (Fig. 2B). For scan rates higher than 350 mV s^{-1} , the anodic and cathodic peak currents were proportional to the square root of the scan rate, which is expected for a diffusion-controlled electrode process. The electrode reaction was similar to those reported for other hexacyanoferrates. The redox couple was observed at relatively lower potential. The redox couple, corresponding to the surface-confined iron centers (Fe(III)/Fe(II)), has a formal potential of $E_0 = 0.174 \text{ V vs. SCE}$. The electrochemical reaction process can be expressed as follows:



As indicated in Table I, the formal potential of most transition metals are higher than 0.5 V vs. SCE , but the formal potential for SnHCF is low and in the order of that of PB. Therefore, it can be used for the electrocatalysis of some substrates which can not be catalyzed by other MHCF.

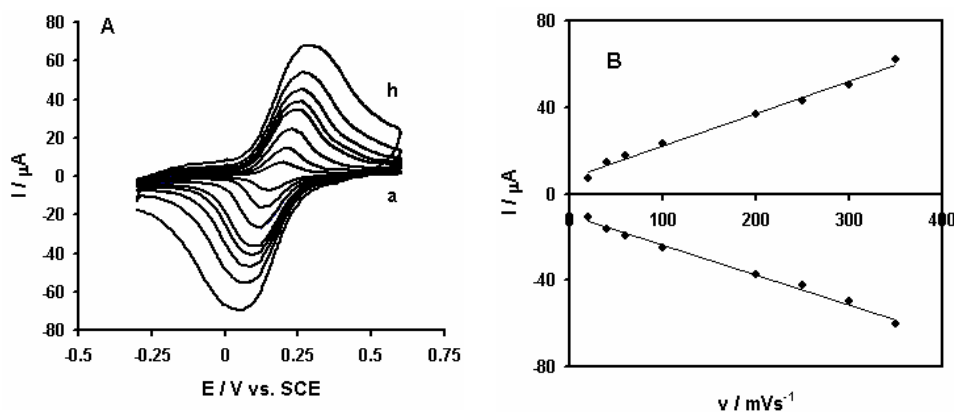


Fig. 2. A) Cyclic voltammograms of the SnHCF electrode in 0.5 M phosphate buffer solution, pH 7; potential scan rates: a) 20, b) 40, c) 60, d) 100, e) 200, f) 250, g) 300 and h) 350 mV s⁻¹ and B) plot of the anodic and cathodic peak currents vs. potential scan rate. Electrode diameter was 2 mm.

TABLE I. Formal potential of MHCf modified electrodes that have been reported until now

Modifier	Substrate	Electrolyte	Formal potential V vs. SCE or Ag/AgCl ^a	Ref.
PB: FeHCF	Pt	1.0 M KCl	0.2	18
Ag ₃ HCF	Pt, Au	1.0 M KNO ₃	0.739	35
CdHCF	Pt	1.0 M KNO ₃	0.58	3
CrHCF	GC ^b	1.0 M KCl	0.62	4
CoHCF	GC	1.0 M NaCl	0.38	6
CuHCF	GC	1 M KCl	0.70	10
DyHCF	GC	0.2 M KCl	0.21, 0.362	13
GaHCF	Ga	1.0 M KCl	0.931 V	14
InHCF	GC	0.5 M KCl	0.74 ^a	15
LaHCF	Pt	1 M KCl	0.32	21
MnHCF	Sol-gel	0.1 M KCl	0.545 ^a	22
MoHCF	Pt	0.5 M H ₂ SO ₄	0.15 ^a	24
NiHCF	Al	0.5 M NaNO ₃	0.44	27
OsHCF	GC	0.1 M KCl	0.44 ^a	29
PdHCF	Al	0.5 M KNO ₃	0.697	31
PtHCF	GC	1 M KCl	0.76	32
RuHCF	GC	0.1 M KCl	0.31 ^a , 0.96 ^a	33
SmHCF	GE ^c	0.2 M NaCl	0.18	34
SnHCF	CPE ^d	0.5 M Phosp. buffer (K)	0.174	This Article
TiHCF	GC	1 M HCl	-0.01	37
VHCF	Pt	5 M H ₂ SO ₄	0.9 ^a , 1.06 ^a	38
ZnHCF	WIGE ^e	0.5 M KCl	0.63	41
ZrHCF	Au	1 M KCl	0.23	42
Ket-HCF ^f	CPE	0.1 M Phosp. buffer (K)	0.64	44

^bGlassy carbon; ^cgraphite electrode; ^dcarbon paste electrode; ^ewax impregnated graphite electrode; ^fketothio-phenyl-hexacyanoferrate

The surface coverage of the SnHCF modified electrode, Γ , represent the moles of SnHCF redox site per unit area of the electrode surface. The amount of charge, Q , consumed for the anodic peak recorded at 50 mV s^{-1} , was measured with respect to the base line and used to calculate Γ from the following equation:

$$\Gamma = Q/nFA \quad (3)$$

where n , and F are the number of electrons transferred in the surface redox reaction and the Faraday constant, respectively. It should be pointed out that the calculated surface coverage is an efficiency characteristic (per cross section of the electrode) and does not reflect the actual amount of SnHCF per area of carbon paste electrode. Increasing the scan rate in the range from 20 to 5000 mV s^{-1} causes a continual decrease of the apparent coverage from 5.0×10^{-7} to $5.0 \times 10^{-8} \text{ mol cm}^{-2}$. The decrease of the apparent coverage with increasing scan rate is probably related to the decrease of the time window and charge transfers through the modified electrode layer, which become rate limiting at higher scan rates.

Effect of pH

Cyclic voltammetry was also used to study the effect of pH of phosphate buffers on the peak currents. The results are illustrated in Fig. 3, from which it can be seen that the peak currents increase with increasing pH up to 10. A 0.5 M phosphate buffer solution (pH 8) was selected and used as the pH for the further studies. Most MHCFs are stable in neutral or weakly acidic solutions, but this modified electrode shows a larger peak current and stability in basic solutions. This can be related to the stability of SnHCF in basic solutions, whereas other metal hexacyanoferrates hydrolyze at higher pH values and are gradually dissolved.

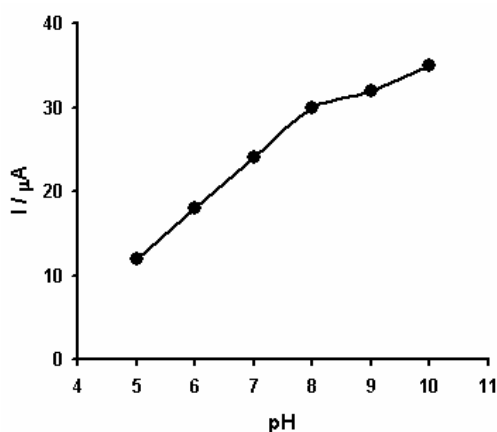


Fig. 3. Effect of pH on the peak currents of SnHCF in 0.5 M phosphate buffer solution.

Stability of modified electrode

The stability of the SnHCF modified electrode was examined by repetitive scans in the 0.5 M phosphate buffer solution. During the first few scans, the peak

current increased with continuous scanning. Subsequently, negligible variation in the height and separation of the cyclic voltammetric peaks was observed. The SnHCF modified electrode was stable under repeated CV scanning. The response of modified electrode had decreased by 5 % after 100 cycles. Furthermore, there was no loss of redox activity after storing the modified electrode in air for a month.

Ion effect on electrochemical behavior of SnHCF

In order to maintain the electroneutrality of the SnHCF film, motion of counter cations always accompanies electron transfer during the redox process. Thus, cations can have a considerable effect on the electrochemical behavior of SnHCF films. In this study, the cations Li^+ , Na^+ and K^+ at the same concentration (0.5 M) were examined (Fig. 4). The obtained results showed that the peak currents were higher and the peak separation larger in the presence of Na^+ cations than in the presence of K^+ cations, while the peaks are completely depressed in the presence of Li^+ . It is feasible that hydrated Li^+ ions enter the channels of the SnHCF lattice where they become trapped, thus blocking access to all channels into the lattice. Therefore, even by changing the counter ion of the bulk electrolyte, no redox signal was observed. Therefore, it can be concluded that the SnHCF modified electrode exhibits a preference for alkali metal cations in order $\text{K}^+ > \text{Na}^+ > \text{Li}^+$ in aqueous solution. The results also lead to the conclusion that sodium and potassium cations can freely penetrate into the SnHCF crystal lattice. The results of the study also showed that the voltammetric characteristic of the SnHCF electrode was strongly affected by the nature of anions present in the solution. Therefore, the effect of various anions, such as NO_3^- , Cl^- and phosphate was studied. The obtained results showed well-defined and reproducible cyclic voltammograms in 0.5 M phosphate buffer solution.

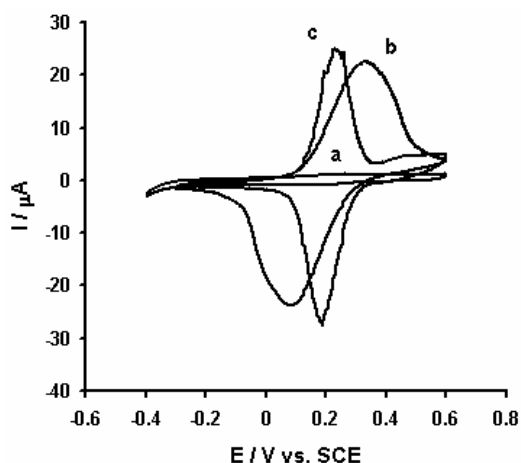


Fig. 4. Cyclic voltammograms of the SnHCF electrode in the presence of 0.5 M alkali metal cations (a) LiCl , (b) phosphate buffer solution containing Na^+ cations (c) phosphate buffer solution containing K^+ cations; scan rate: 60 mV s^{-1} .

Charge transfer rate in the film

Laviron derived general expressions for the linear potential sweep voltammetric response for the case of surface-confined electro-active species.⁴⁷ From these expressions, it is possible to determine the transfer coefficient (α) by measuring the variation of the peak potentials with scan rate, ν , as well as the apparent charge transfer rate constant (k_s) for electron transfer between the electrode and a surface deposited layer. According to Laviron's expressions, a plot of $E_p - E_0 = f(\log \nu)$ yields two straight lines with a slope equal to $2.3RT/\alpha nF$ for the cathodic peak and $2.3RT/(1-\alpha)nF$ for the anodic peak. An example of this plot for the SnHCF film in 0.5 M phosphate buffer is shown in Fig. 5. Using such a plot and the following equation:

$$\log k_s = \alpha \log(1-\alpha) + (1-\alpha) \log \alpha - \log \frac{RT}{nF\nu} - \alpha nF(1-\alpha) \frac{\Delta E_p}{2.3RT} \quad (4)$$

the values of α and k_s were found to be 0.6 and $2.1 \pm 0.2 \text{ s}^{-1}$, respectively. Notice that the surface coverage, Γ , evaluated from the relation $\Gamma = Q_H/nFA$ was about $5.0 \times 10^{-8} \text{ mol cm}^{-2}$ at a scan rate of 20 mV s^{-1} . Further experiments showed that the values obtained for α and k_s remained almost constant for Γ values in the range 10^{-7} – $10^{-8} \text{ mol cm}^{-2}$. The peak separation will be close to zero when the electron transfer rate is fast relative to the scan rate and will increase when the electron transfer rate is slow.

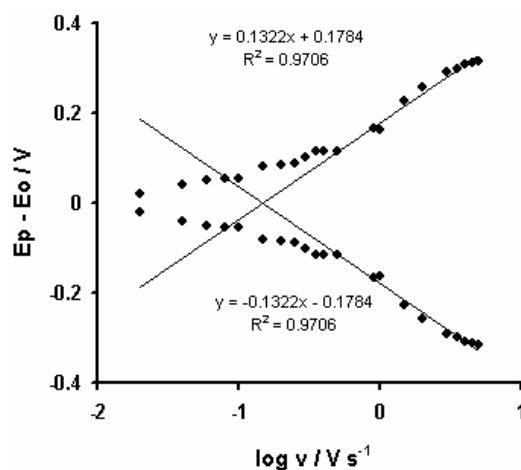


Fig. 5. Plot of $E_p - E_0$ vs. $\log \nu$ for cyclic voltammograms recorded for the SnHCF electrode in 0.5 M phosphate buffer solution at scan rates between 0.01 – 1 V s^{-1} for the anodic and cathodic peaks.

Diffusion coefficient of K^+ and Na^+ in the film

The height of the cyclic voltammogram peaks obtained at scan rates $> 350 \text{ mV s}^{-1}$ is an important criterion, which can be related to the facility of cation diffusion in a modified film.³⁴ The peak current of cyclic voltammograms obtained at scan rates higher than 350 mV s^{-1} , in the presence of potassium cations was proporti-

onal to the square root of the scan rate, $v^{1/2}$, indicating its diffusion nature. According to the experimental results, the diffusion coefficient of the cations in the modifier film could be calculated using the equation:⁴⁸

$$I_p = 2.99 \times 10^5 n^{3/2} \alpha^{1/2} A D^{1/2} c v^{1/2} \quad (5)$$

where D is the diffusion coefficient of the cations in the film ($\text{cm}^2 \text{s}^{-1}$), A the electrode area (0.045 cm^2), v potential scan rate (V s^{-1}) and I_p the peak current (A). Since at high scan rates, not all redox sites, including mixed valence iron, in the film are electroactive due to an insufficient amount of counter ions in the film, in Eq. (5), c represents the concentration of alkali metal cations in the film (mol cm^{-3}). The value of c , which varies with the scan rate, was calculated by means of the total moles of cations in the film, obtained from Q_H (the area under cyclic voltammograms recorded at scan rates higher than 350 mV s^{-1}) and the total volume of the film obtained from Q_L (the area under the cyclic voltammogram recorded at a scan rate of 20 mV s^{-1}). Using a plot of I_p vs. $cv^{1/2}$, the diffusion coefficient for Na^+ and K^+ was calculated to be $(2.45 \pm 0.23) \times 10^{-10}$ and $(4.83 \pm 0.34) \times 10^{-10} \text{ cm}^2 \text{ s}^{-1}$, respectively. A typical example of these plots is shown in Fig. 6 for the cyclic voltammogram peaks recorded in the presence of K^+ .

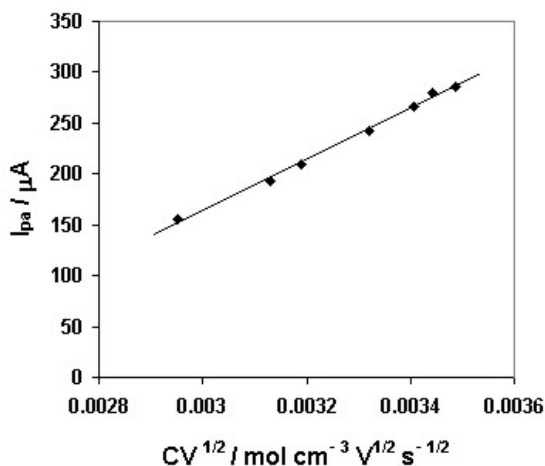


Fig.6. Plot of I_{pa} vs. $cv^{1/2}$ for cyclic voltammograms recorded for the SnHCF electrode ($A = 0.0314 \text{ cm}^2$) in 0.5 M phosphate buffer solution with Na^+ cations at scan rates between 0.3 and 5 V s^{-1} for anodic peak currents.

CONCLUSIONS

The preparation of a SnHCF modified electrode using tin chloride and hexacyanoferrate was reported. The preparation of the modified electrode is easy, fast, and reproducible. This modified electrode showed good stability toward potential recycling. Both the pH of the solution and the alkali metal cations and anions of the supporting electrolyte have a considerable effect on the electrochemical behavior of the film. K^+ and Na^+ ions can freely enter the SnHCF crystal lattice, while hydrated Li^+ are probably trapped in the SnHCF lattice. The prepared modified electrode is stable for several weeks in air, as well as in 0.5 M phosphate buffer solution.

ИЗВОД

ПРИПРЕМА И КАРАКТЕРИЗАЦИЈА ЕЛЕКТРОДЕ НА БАЗИ КАРБОНСКЕ ПАСТЕ
МОДИФИКОВАНЕ ЈОНИМА КАЛАЈА И ХЕКСАЦИЈАНОФЕРАТА

REZA E. SABZI, ALL HASANZADEH, KHOSROW GHASEMLU и PARVANEH HERAVI

Department of Chemistry, Faculty of Science, Urmia University, Urmia, Iran

Електроде на бази карбонске пасте су хемијски модификоване калај(II) или калај(IV) хлоридом и хексацијаноферат(II) или хексацијаноферат(III) јоном. Њихово електрохемијско понашање је испитивано цикличном волтаметријом. Показано је да Sn(IV) и хексацијаноферат(II) дају најбоље резултате. Циклични волтамограм такве SnHCF електроде је окарактерисан једним паром пикова: анодним на 0,195 V и катодним на 0,154 V (према ЗКЕ) при брзини линеарне промене потенцијала 20 mV s^{-1} и у 0.5 M фосфатном пуферу као основном електролиту. Током циклизирања потенцијала електрода се показала као веома стабилна. Испитиван је ефекат pH основног електролита и присутних катјона алкалних метала на електрохемијске карактеристике SnHCF електроде. Утврђено је да катјони имају значајан ефекат. Одређени су коефицијенти дифузије хидратисаних јона K^+ and Na^+ у филму, коефицијент прелаза и константа брзине прелаза електрона.

(Примљено 9. јуна 2006, ревидирано 27. марта 2007)

REFERENCES

1. I. K. Tonle, E. Ngameni, A. Walcarius, *Electrochim. Acta* **49** (2004) 3435
2. S. L. Vilakazi, T. Nyokong, *J. Electroanal. Chem.* **512** (2001) 56
3. C. H. Luangdilok, D. J. Arnet, A. B. Bocarsly, R. Wood, *Langmuir* **8** (1992) 650.
4. M. Jiang, X. Zhou, Z. Zhao, *J. Electroanal. Chem.* **287** (1990) 389
5. M. S. Lin, W. C. Shih, *Anal. Chim. Acta* **381** (1999) 183
6. Z. Gao, G. Wang, P. Li, *Electrochim. Acta* **36** (1991) 147
7. J. Joseph, H. Gomathi, G. P. Rao, *J. Electroanal. Chem.* **304** (1991) 263
8. S. M. Golabi, F. Noor-Mohammadi, *J. Solid State Electrochem.* **2** (1998) 30
9. M. H. Pournaghi-Azar, R. Sabzi, *J. Solid State Electrochem.* **6** (2002) 553
10. L. M. Siperko, T. Kuwana, *Electrochim. Acta* **32** (1987) 765
11. O. Makowski, J. Strorka, P. J. Kulesza, M. A. Malik, Z. Galus, *J. Electroanal. Chem.* **532** (2002) 157
12. S. M. Chen, C. M. Chan, *J. Electroanal. Chem.* **543** (2003) 161
13. P. Wu, Y. Shi, C. Cai, *J. Solid State Electrochem.* **10** (2006) 270
14. A. Eftekhari, *J. Electrochem. Soc.* **151** (2004) E297
15. S. Dong, Z. Jin, *Electrochim. Acta* **34** (1989) 963
16. T. R. I. Cataldi, G. E. D. Benedetto, A. Bianchini, *Electroanal.* **10** (1998) 1163
17. L. C. Chen, Y. H. Huang, K. C. Ho, *J. Solid State Electrochem.* **7** (2002) 6
18. K. Itaya, T. Ataka, S. Toshima, *J. Am. Chem. Soc.* **104** (1982) 4767
19. A. L. Crumbliss, P. S. Lugg, N. Morosoff, *Inorg. Chem.* **23** (1984) 4701
20. C. A. Lundgren, R. W. Murray, *Inorg. Chem.* **27** (1988) 933
21. S. Q. Liu, H. Y. Chen, *J. Electroanal. Chem.* **528** (2002) 190
22. P. Wang, X. Jing, W. Zhang, G. Zhu, *J. Solid State Electrochem.* **5** (2001) 369
23. A. Eftekhari, *Talanta* **55** (2001) 395
24. S. Dong, Z. Jin, *J. Electroanal. Chem.* **256** (1988) 193
25. S. Sinha, B. D. Humphrey, A. B. Bocarsly, *Inorg. Chem.* **23** (1984) 203
26. B. D. Humphrey, S. Sinha, A. B. Bocarsly, *J. Phys. Chem.* **91** (1987) 586

27. M. H. Pournaghi-Azar, H. Razmi-Nerbin, *J. Electroanal. Chem.* **456** (1998) 83
28. J. J. Xu, C. Wang, H. Y. Chen, *Anal. Sci.* **16** (2000) 231
29. S. M. Chen, C. J. Liao, *Electrochim. Acta* **50** (2004) 115
30. M. Jiang, Z. Zhao, *J. Electroanal. Chem.* **292** (1990) 281
31. M. H. Pournaghi-Azar, H. Dastangoo, *J. Electroanal. Chem.* **523** (2002) 26
32. S. Liu, H. Li, M. Jiang, P. Li, *J. Electroanal. Chem.* **426** (1997) 27
33. S. M. Chen, M. F. Lu, K. C. Lin, *J. Electroanal. Chem.* **579** (2005) 163
34. P. Wu, C. Cai, *J. Solid State Electrochem.* **8** (2004) 538
35. S. Moon, J. D. Moon, *Bull. Korean Chem. Soc.* **15** (1994) 1042
36. A. Eftekhari, *Anal. Lett.* **34** (2001) 541
37. M. Jiang, X. Zhou, Z. Zhao, *J. Electroanal. Chem.* **292** (1990) 289
38. D. Shaojun, L. Fengbin, *J. Electroanal. Chem.* **210** (1986) 31
39. Y. Wang, G. Zhu, E. Wang, *J. Electroanal. Chem.* **430** (1997) 127
40. C. Liu, S. Dong, *Electroanal.* **9** (1997) 838
41. J. Joseph, H. Gomathi, G. P. Rao, *J. Electroanal. Chem.* **431** (1997) 231
42. S. Q. Liu, Y. Chen, H. Y. Chen, *J. Electroanal. Chem.* **502** (2001) 197
43. S. Q. Liu, Y. Chen, H. Y. Chen, *Electroanal.* **14** (2002) 116
44. G. Tabrizvand, R. E. Sabzi, K. Farhadi, *J. Solid State Electrochem.* **11** (2007) 103
45. V. D. Neff, *J. Electrochem. Soc.* **125** (1978) 886
46. D. Eliss, M. Eckhoff, V. D. Neff, *J. Phys. Chem.* **85** (1981) 1225
47. E. Laviron, *J. Electroanal. Chem.* **101** (1979) 19
48. S. Dong, Z. Jin, *Electrochim. Acta* **34** (1989) 963.

Voltammetric study of the interaction between oxacillin sodium and cysteine in the presence and absence of Mn(II) ions in neutral buffer solution

ENDER BİÇER* and EMİNE COŞKUN

Ondokuz Mayıs University, Faculty of Arts and Sciences, Department of Chemistry, 55139 Kurupelit–Samsun, Turkey

(Received 14 July 2006, revised 2 April 2007)

Abstract: In this study, the voltammetric behaviour of the interaction of oxacillin sodium (OXA) and OXA–cysteine (RSH) was studied by square-wave voltammetry, cyclic voltammetry in Britton–Robinson (B–R) buffer (pH 7.0). OXA gave two peaks at -0.248 and -1.224 V. For the interaction, the peak of mercurous cysteine thiolate ($\text{Hg}_2(\text{SR})_2$) was selected. It was found that the peak currents corresponding to $\text{Hg}_2(\text{SR})_2$ significantly decreased, while the peak potential shifted to more positive potentials upon the addition of OXA. The observed phenomena are due to the interaction of OXA with RSH on the surface of the mercury electrode. When OXA was added to the electrochemical cell along with Mn(II), new peaks at -0.146 and -0.608 V were observed. These peaks were due to the catalytic activity of OXA on the reduction of Mn(II) and could be attributed to the formation of Mn(II) complexes with different metal/ligand ratios. On the other hand, in the presence of RSH, the peak at -0.608 V vanished and a reduction peak was observed at -0.662 V. The catalytic reduction peak potential of Mn(II) at -0.662 V indicated that RSH slightly prevented the catalysis process of OXA due to their mutual interaction.

Keywords: voltammetry, oxacillin, cysteine, interaction.

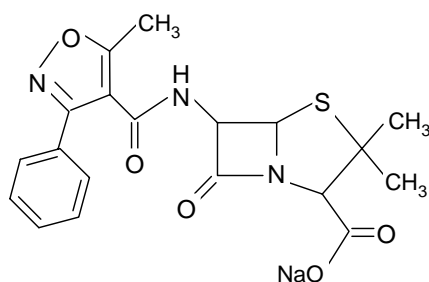
INTRODUCTION

Oxacillin sodium, OXA, (Scheme 1) is a semi-synthetic penicillin belonging to the general class of drugs called antibiotics. OXA prevents bacteria from making their cell walls and hence the cells die. It is used to treat gram-positive infections and bacteria that are resistant to penicillin.¹

The β -lactam ring of penicillins shows susceptibility towards attack by nucleophilic reagents in water, such as amines, alcohols and thiols, in competition with that by hydroxide ions.² The reaction of penicillin with proteins has been extensively reported in the literature.^{3–5} The most rapid reaction with low-molecular-weight compounds occurs when thiol groups are present.⁶ Penicillin–pro-

* Corresponding author. E-mail: ebicer@omu.edu.tr
doi: 10.2298/JSC0710003B

tein adducts produce penicillin allergy in sensitive individuals.⁷ In addition, penicillin is thought to inactivate irreversibly carboxypeptidase by forming a penicilloyl–enzyme intermediate.⁸ Mn(II) ions function as cofactors for some enzymes (enolase, isocitrate dehydrogenases, mitochondrial superoxide dismutase, etc.).⁸ Enzymes, which are all proteins, are catalysts that enhance the rates of biological reactions.⁸ Thus, the interaction between penicillin derivative drugs and amino acids in the presence and absence of cofactor metal ions is very important.



Scheme 1. The molecular structure of OXA.

Although studies on the binding mechanism of oxacillin were performed,^{9–13} no voltammetric study on the interaction of OXA with RSH could be traced in the literature. Therefore, the aim of this study was to examine the voltammetric behaviour of OXA and its interaction with RSH in the presence and absence of Mn(II) ions.

EXPERIMENTAL

Chemicals

Oxacillin, cysteine and $\text{MnSO}_4 \cdot \text{H}_2\text{O}$ were purchased from Fluka, Merck and Sigma, respectively. All chemicals were of analytical grade. The stock solutions were prepared in triply distilled and deionized water and used immediately.

Apparatus

Voltammetric measurements were obtained with an EG&G PAR 384B Polarographic Analyzer. An EG&G PARC 303A SMDE stand was used in the hanging mercury drop electrode (HMDE) mode. The three-electrode system was completed by means of an $\text{Ag} | \text{AgCl} | \text{KCl}_{\text{sat}}$ reference electrode and a platinum auxiliary electrode. The current–potential curves were recorded on a Houston Instrument DMP-40 plotter connected to the polarograph. The instrumental settings were: drop size, medium; equilibrium time, 5 s; scan rate, 200 mV s^{-1} (500 mV s^{-1} for CV).

Procedure

A 10 ml volume of B–R buffer (pH 7.0) solution was added to the voltammetric cell and the solution was purged with nitrogen gas for 5 min. The blank voltammogram was recorded. Then, the required aliquot of the stock solution of OXA was added to the cell by means of a micropipette and the sample voltammograms were recorded. For the interaction of OXA with RSH, OXA solution was added to B–R buffer (pH 7.0) containing $1.0 \times 10^{-5} \text{ M}$ RSH. The interaction between OXA and RSH was monitored by the changes of the peak potential and peak current of $\text{Hg}_2(\text{SR})_2$. In the presence of $1.0 \times 10^{-4} \text{ M}$ Mn(II) ions, the voltammetric behaviour of both OXA and RSH was studied. Finally, the interaction of oxacillin with RSH in the presence of $1.0 \times 10^{-4} \text{ M}$ Mn(II) was monitored by the voltammetric techniques.

RESULTS AND DISCUSSION

Voltammetric behaviour of OXA

The voltammetric behaviour of OXA in B–R buffer (pH 7.0) is shown in Fig. 1. On the less negative potential side, a small reduction peak is observed at -0.248 V (Fig. 1, 1U). On the more negative potential side, a broad reduction peak (main peak) occurs at -1.224 V (Fig. 1, 2U). The peak current i_{p1} , of the small peak increased with increasing frequency, f , (from 10 to 100 Hz) and the linear equation of i_{p1} vs. f relationship was i_{p1} (nA) = $1.251 \times f$ (Hz) + 11.758 ($r = 0.995$). According to this result, the peak at -0.248 V can be inferred as the adsorption of OXA molecules on the surface of the mercury electrode. For the characterization of main peak, cyclic voltammetry was also used.

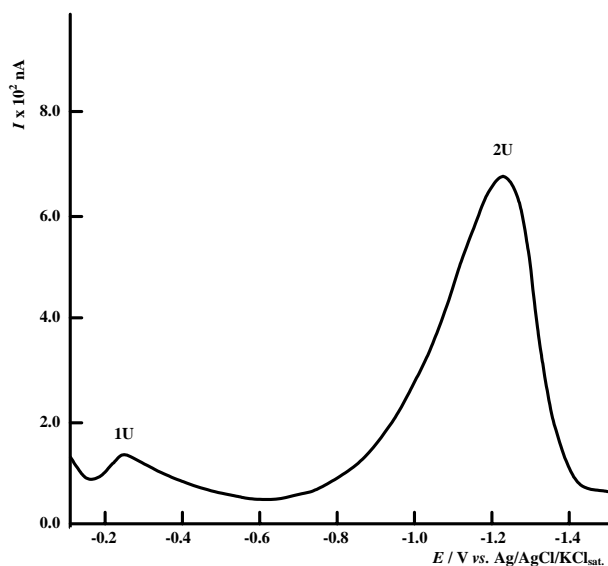


Fig. 1. Square-wave voltammogram of 5×10^{-5} M OXA in B–R buffer (pH 7.0) (Experimental conditions: scan rate, 200 mV s^{-1} ; drop size, medium and equilibrium time, 5 s). 1U, Adsorption peak; 2U, reduction of heterocyclic isoxazol ring of OXA.

The cyclic voltammogram of OXA in the potential range of -0.60 to -1.6 V is given in Fig. 2. As can be seen, the main reduction peak of OXA (Fig. 2, 2U) has an anodic counterpart. The currents (i_{p2}) of the main reduction peak for OXA are proportional to scan rates (ν) in the range of 50 to 500 mV s^{-1} ; the linear equation of the $\log i_{p2}$ vs. $\log \nu$ relationship was $\log i_{p2} = 0.8495 \log \nu + 0.0812$ ($r = 0.994$). From the value of the slope, 0.8495, of the $\log i_{p2}$ vs. $\log \nu$ relationship of the main peak, it can be deduced that the main reduction peak of OXA is diffusion-controlled with an adsorption contribution. According to the potential difference $\Delta E_p = E_{pa} - E_{pc}$ for the main peak of OXA, αn is calculated to be 0.72 (where α and n denote the transfer coefficient and the number of electron transferred, respectively). The electrochemical redox reaction of OXA at a mercury electrode in B–R buffer (pH 7.0) solution is a quasi-reversible process with an anodic counterpart and $\alpha n = 0.72$, as shown in Fig. 2 (2U).

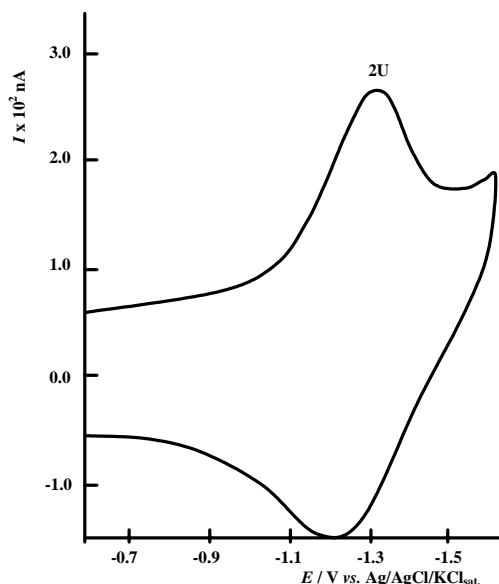


Fig. 2. Cyclic voltammogram of 1×10^{-4} M OXA in B-R buffer (pH 7.0) (Experimental conditions: scan rate, 500 mV s^{-1} ; drop size, medium and equilibrium time, 5 s). 2U, Reduction of heterocyclic isoxazol ring of OXA.

It is well known that ampicillin and amoxycillin are electrochemically inactive at a dropping mercury electrode (DME) in aqueous solution.¹⁴ The molecular structure of OXA is different from these owing to the presence of the electroactive isoxazol derivative group. In the literature, it was reported that the reduction of the heterocyclic isoxazol ring occurs at approximately -1.0 V .¹⁵ Based on this fact, the main peak at -1.224 V can probably be attributed to the cathodic reduction of the heterocyclic isoxazol ring of OXA. However, the exact mechanism of the electrode reaction of OXA will be the subject of a further study.

Interaction of OXA with RSH

The square-wave voltammograms of RSH in the absence and presence of OXA are shown in Fig. 3. Under these experimental conditions, $1.0 \times 10^{-5} \text{ M}$ RSH had a well-developed cathodic peak at -0.536 V (Fig. 3, 2U) which corresponds to $\text{Hg}_2(\text{SR})_2$ and after the addition of OXA to the RSH solution, the peak current of $\text{Hg}_2(\text{SR})_2$ decreased, its peak potential shifted to more positive potentials (-0.354 V) and a new small, more positive peak appeared at -0.160 V (Fig. 3, 1U). The main reduction peak of OXA also appeared at a more positive potential (-1.114 V (Fig. 3, 3U)) in the presence of RSH. The peak currents of the peaks at -0.160 and -1.114 V increased with increasing concentration of OXA. According to the obtained voltammetric data, it can be stated that these peaks originate from the electrode reaction of OXA in the presence of RSH.

A typical labelled antigen-antibody binding curve for $\text{Hg}_2(\text{SR})_2$ is shown in Fig. 4. A similar curve was observed by Heineman *et al.*¹⁶ for 4-mercuric acetate estriol with estriol antibody. In addition, similar curves were also obtained for the

interaction of RSH with some monosaccharides.¹⁷ Immunochemical reactions are among the most selective reactions known.¹⁸ They are based on shape recognition of the antigen by the antibody binding site.¹⁸ A voltammetric immunoassay relies on the monitoring of the binding *via* the decrease in the current response for the redox reaction of the labelled antigen in the presence of antibody.¹⁸ A similar principle applies to the labelled antibody current which decreases in the presence of antigen.¹⁸ In this first report on a voltammetric immunoassay, Heine-*et al.*¹⁶ labelled estriol with mercuric acetate (as the electroactive moiety) and monitored the reaction of this labelled antigen with estriol antibody.

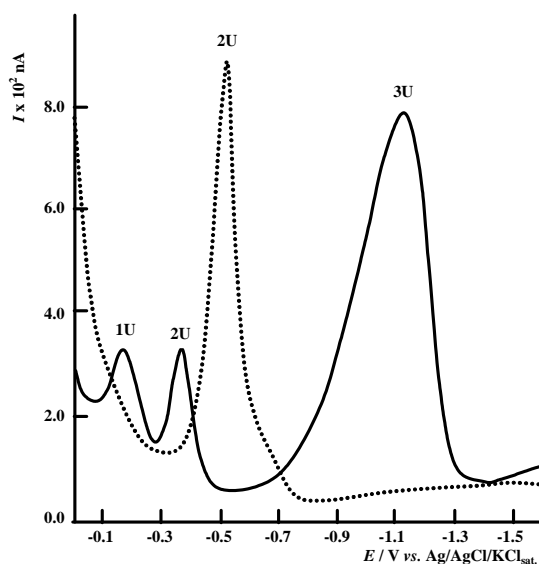


Fig. 3. Square-wave voltammograms of 1×10^{-5} M RSH in the presence of 0 M (.....) and 5×10^{-5} M OXA (—) in B-R buffer pH 7.0 (Experimental conditions as in Fig. 1). 1U, Adsorption peak of OXA; 2U, reduction of $\text{Hg}_2(\text{SR})_2$; 3U, reduction of heterocyclic isoxazol ring of OXA.

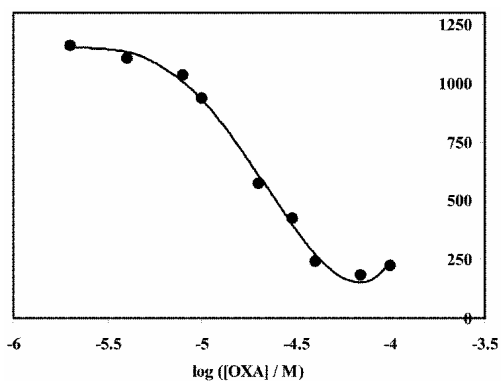


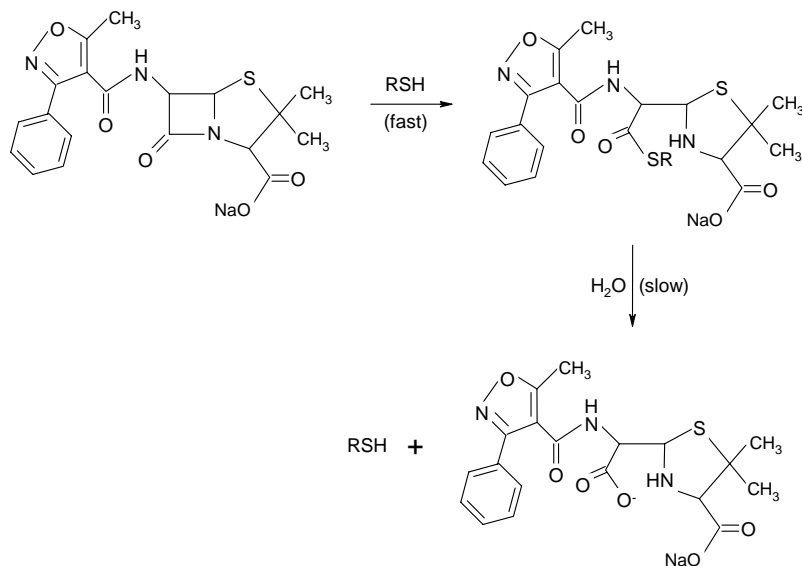
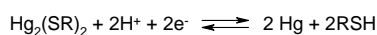
Fig. 4. Plot of peak current of $\text{Hg}_2(\text{SR})_2$ vs. $\log [\text{OXA}]$.

Shifts of the peak potential of $\text{Hg}_2(\text{SR})_2$ to more positive values was also observed for the interaction of thiols and folates on the surface of mercury.^{19,20} The effect of a chemical reaction following a reversible electron transfer is the facilitation of the redox process, *i.e.*, a shift of electroreduction towards positive po-

tentials.¹⁹ The faster is the chemical reaction, the more positive is the potential of the cathodic peaks.²⁰ With very fast follow-up reactions, the peak can shift (at a constant scan rate) by as much as 120 mV.¹⁹ On the other hand, an added adsorbable substance usually acts as an inhibitor of a reversible electrode reaction and shifts the reduction processes to negative potentials.²¹ However, the positive shift of the reduction potential of $\text{Hg}_2(\text{SR})_2$ in the presence of OXA is 182 mV. Hence, the interaction of OXA with RSH can be inferred from the follow-up chemical reaction between them. As a result, the anodic shifts of the reduction potential and the decrease in the current of $\text{Hg}_2(\text{SR})_2$ may be due to the binding of RSH with OXA on the mercury electrode.

Llinás *et al.*^{2,22} studied the thiol-catalysed hydrolysis of cephalosporins² and benzylpenicillin.²² They reported that thiols catalyse the hydrolysis through the formation of a thioester intermediate and the catalytically reactive form of the thiol is the thiolate anion.^{2,22} Thiolysis of penicillins occurs with the rate-limiting breakdown of the tetrahedral intermediate facilitated by proton transfer from the solvent water to the departing amine.²² In a similar manner to the reaction of thiols with cephaloridine in water,² the reaction between RSH and OXA can be as given in Scheme 2.

Scheme 2 represents a fast follow up reaction. In addition, the fixed current of $\text{Hg}_2(\text{SR})_2$ in the presence of excess OXA is probably due to the reproduction of RSH according to Scheme 2.



Scheme 2. Proposed mechanism for interaction of OXA with RSH.

Interaction of OXA with Mn(II) ions

The square-wave voltammogram of 1.0×10^{-4} M Mn(II) ions in B-R buffer (pH 7.0) in the absence of OXA has a peak at a potential of -1.650 V (Fig. 5, 5U). This cathodic peak was attributed to the irreversible reduction of Mn(II) ions to Mn(0), because no anodic counterpart was observed on the cyclic voltammogram of Mn(II) ions in B-R buffer (pH 7.0). The addition of OXA (Fig. 5) to the electrolyte containing Mn(II) ions strongly modified the square-wave voltammogram and two new peaks appeared at the potentials of -0.152 and -0.630 V (1U and 3U). These peaks are at more positive potentials than the peak produced by Mn(II) ions in the absence of OXA. With increasing OXA concentration, the peak currents of the new peaks increased and their peak potentials shifted to slightly positive values (-0.146 and -0.608 V) while the peak current of free Mn(II) ions was decreased (Fig. 5). These peaks can be attributed to the formation of Mn(II) complexes with different metal/ligand ratios on the mercury surface. OXA has catalytic activity on the reduction of Mn(II). It may be concluded that the voltammetric process is the reduction of Mn(II) catalysed by the formation of a complex between Mn(II) and OXA adsorbed on the electrode surface (Scheme 3). Similar results were obtained with cephalexin and Ni(II).²³ However, the peaks at -0.146 and -0.608 V can be attributed to the formation of Mn(II) complexes with different metal/ligand ratios.

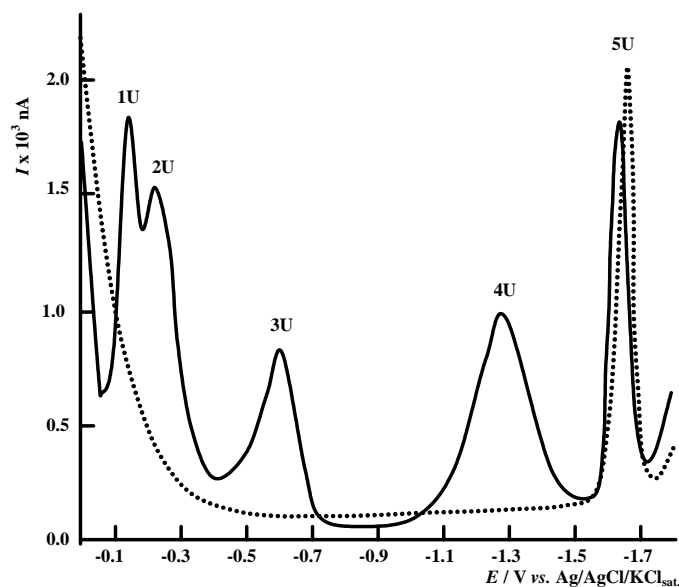
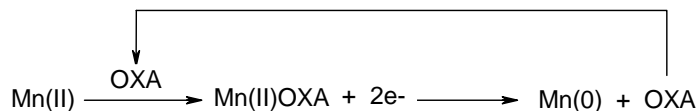


Fig. 5. Square-wave voltammograms of 1.0×10^{-4} M Mn(II) (.....) and 1.0×10^{-4} M Mn(II) + 8.0×10^{-4} M OXA (—) in B-R buffer pH 7.0 (Experimental conditions as in Fig. 1). 1U and 3U, catalytic peaks of Mn(II) in the presence of OXA; 2U, adsorption peak of OXA; 4U, reduction of heterocyclic isoxazol ring of OXA; 5U, the reduction of free Mn(II).



Scheme 3. The proposed pathway for the catalytic reduction of Mn(II).

Interaction of RSH with Mn(II) ions

The square-wave voltammogram of 1.0×10^{-4} M Mn(II) in the presence of RSH is shown in Fig. 6, from which it can be seen that with increasing RSH concentration, the peak current of free Mn(II) decreased, while reduction peaks of mercuric and mercurous cysteine thiolates ($\text{Hg}(\text{SR})_2$) and $\text{Hg}_2(\text{SR})_2$) were observed at -0.132 and -0.598 V (Fig. 6, 1U and 2U). In addition, a new small peak was observed at -0.704 V (Fig. 6, 3U) and its peak current increased with increasing RSH concentration. This additional peak can be attributed to the reduction of the adsorbed chelate. The appearance of the chelate peak depends on the molar ratio, $[\text{RSH}]/[\text{Mn(II)}]$. The chelate peak was observed at molar ratios $\geq 1:2$.

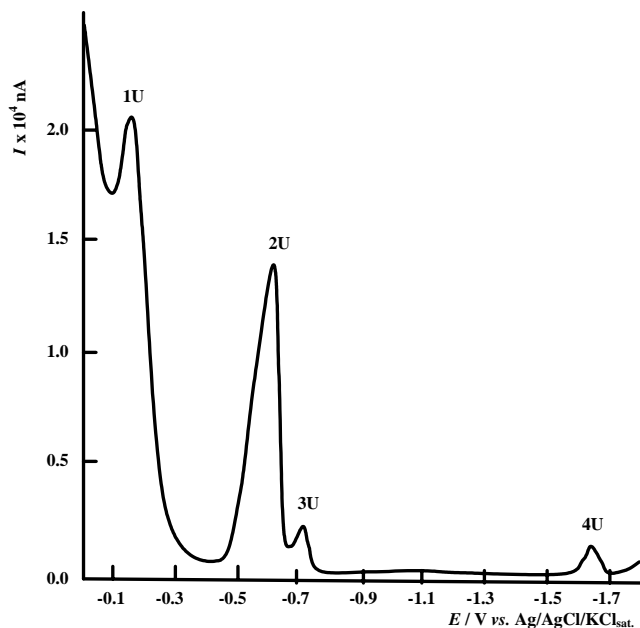


Fig. 6. Square-wave voltammogram of 4.0×10^{-4} M RSH in the presence of 1.0×10^{-4} M Mn(II) in B-R buffer pH 7.0 (Experimental conditions as in Fig. 1). 1U, Reduction of $\text{Hg}(\text{SR})_2$; 2U, reduction of $\text{Hg}_2(\text{SR})_2$; 3U, catalytic peak of Mn(II) in the presence of RSH; 4U, the reduction of free Mn(II).

Interaction between OXA and RSH in the presence of Mn(II) ions

With addition of RSH solution to the cell containing 1.0×10^{-4} M Mn(II) and 8.0×10^{-4} M OXA, the peak at -0.608 V (Fig. 5, 3U) vanished and a reduction peak was observed at more negative potential (-0.662 V) (Fig. 7, 4U). The current of this reduction peak increased and its peak potential shifted towards more negative values with increasing RSH concentration. On the other hand, a new

peak was also seen at -0.490 V (Fig. 7, 3U). This peak (-0.490 V) belongs to the reduction of $\text{Hg}_2(\text{SR})_2$. As its reduction was observed at more positive potentials in the presence of OXA (see above).

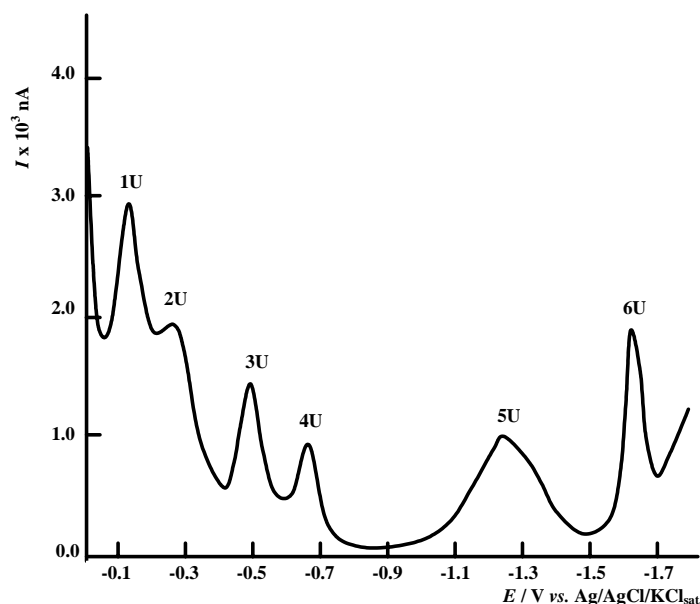


Fig. 7. Square-wave voltammogram of 1.0×10^{-4} M Mn(II) and 8.0×10^{-4} M OXA mixture in the presence of 1.0×10^{-4} M RSH in B-R buffer pH 7.0 (Experimental conditions as in Fig. 1). 1U, Reduction of $\text{Hg}(\text{SR})_2$; 2U, adsorption peak of OXA; 3U, reduction of $\text{Hg}_2(\text{SR})_2$ in the presence of OXA; 4U, catalytic peak of Mn(II) in the presence of RSH and OXA; 5U, reduction of heterocyclic isoxazol ring of OXA; 6U, the reduction of free Mn(II).

According to the data, it can be said that RSH interacts with OXA in the presence or absence of Mn(II) ions. Moreover, OXA catalyzes the reduction of Mn(II). However, this catalysis process is thermodynamically difficult in the presence of RSH because of the fact that the catalytic reduction peak potential of Mn(II) is observed at more negative potentials. Perhaps, Mn(II) forms a mixed ligand complex with adsorbed species of OXA and RSH on the surface of the mercury electrode.

Complex formation between Mn(II) and OXA or RSH and also the interaction of OXA with RSH may give valuable information concerning what occurs when administrating OXA drug. On the other hand, the voltammetric techniques could be used to determine these interactions. Consequently, the observed interactions *in vitro* may perhaps be employed as a model for the metabolic processes of OXA in the living matter.

ИЗВОД

ВОЛТАМЕТРИЈСКО ИСПИТИВАЊЕ ИНТЕРАКЦИЈА ИЗМЕЂУ НАТРИЈУМ-ОКСАЦИЛИНА И ЦИСТЕИНА У ПРИСУСТВУ И ОДСУСТВУ $Mn(II)$ ЈОНА У НЕУТРАЛНОМ ПУФЕРСКОМ РАСТВОРУ

ENDER BIÇER и EMİNE COŞKUN

Ondokuz Mayıs University, Faculty of Arts and Sciences, Department of Chemistry, 55139 Kurupelit-Samsun, Turkey

У раду је испитивано волтаметријско понашање натријум-оксацилина (ОХА) и интеракције ОХА и цистеина (RSH) у Бритон–Робинсоновом (Britton–Robinson, B–R) пуферу pH 7.0 коришћењем волтаметрије са правоугаоним таласом и цикличне волтаметрије. ОХА је показала два волтаметријска пика: на -0.248 и -1.224 V. За испитивање интеракција изабран је пик цистеинтиолата живе ($Hg_2(SR)_2$). Запажено је да струјни пикови који потичу од $Hg_2(SR)_2$ након додатка ОХА значајно опадају и да се потенцијал пика помера ка позитивнијим вредностима. То потиче од интеракција ОХА са RSH на површини живине електроде. Када се у електрохемијску ћелију додају и ОХА и $Mn(II)$ јони, појављују се нови пикови на -0.146 и -0.608 V. Они потичу од каталитичке активности ОХА за редукцију $Mn(II)$ јона и могу се приписати формирању $Mn(II)$ комплекса са различитим односима металног јона и лиганда. С друге стране, у присуству RSH пик на -0.608 V нестаје, а запажа се редукциони пик на -0.662 V. Потенцијал пика каталитичке редукције $Mn(II)$ на -0.662 V указује да RSH у извесној мери умањује каталитичку активност услед њихове међусобне интеракције.

(Примљено 14. јула 2006, ревидирано 2. априла 2007)

REFERENCES

1. http://www.cancer.org/docroot/CDG/content/CDG_oxacillin_sodium.asp
2. A. Llinás, B. Vilanova, M. I. Page, *J. Phys. Org. Chem.* **17** (2004) 521
3. B. M. Beadle, R. A. Nicholas, B. K. Shoichet, *Protein Sci.* **10** (2001) 1254
4. K. Graves–Woodward, R. F. Pratt, *Biochem. J.* **332** (1998) 755
5. S. Barbosa, P. Taboada, V. Mosquera, *Chem. Phys.* **310** (2005) 51
6. K. F. Nakken, L. Eldjarn, A. Pihl, *Biochem. Pharmacol.* **3** (1960) 89
7. B. B. Levine, *J. Exp. Med.* **112** (1960) 1131
8. E. L. Smith, R. L. Hill, I. R. Lehman, R. J. Lefkowitz, P. Handler, A. White, *Principles of Biochemistry: General Aspects*, International Student Edition, Seventh Edition, McGraw–Hill Book Company, London, 1985, p.p. 474, 397, 355, 325, 179
9. S. Y. Bi, L. Ding, D. Q. Song, Y. Tian, H. Q. Zhang, *Acta Chim. Sinica* **63** (2005) 2169
10. A. M. Bressler, T. Williams, E. E. Culler, W. M. Zhu, D. Lonsway, J. B. Patel, F. S. Nolte, *J. Clin. Microbiol.* **43** (2005) 4541
11. M. A. Zeitlinger, R. Sauermann, F. Traunmuller, A. Georgopoulos, M. Muller, C. Joukhadar, *J. Antimicrob. Chemother.* **54** (2004) 876
12. D. Mihai, G. Mocanu, A. Carpov, *J. Bioact. Compat. Polym.* **15** (2000) 245
13. A. Dasgupta, A. Sperelakis, A. Mason, R. Dean, *Pharmacotherapy* **17** (1997) 375
14. S. J. Lyle, S. S. Yassin, *Anal. Chim. Acta* **274** (1993) 225
15. M. Al–Omar, A. Al–Majed, E. A. Gadkariem, F. Belal, *J. Pharm. Biomed. Anal.* **37** (2005) 199
16. W. R. Heineman, C. W. Anderson, H. B. Halsall, *Science* **204** (1979) 865
17. S. Çakır, E. Biçer, O. Çakır, *Glycoconjugate J.* **16** (1999) 579
18. J. Wang, *Electroanalytical Techniques in Clinical Chemistry and Laboratory Medicine*, 1988, VCH Publishers, Inc., New York, p. 42

19. M. Heyrovský, B. Prokopová, *Collect. Czech. Chem. Commun.* **62** (1997) 172
20. B. Prokopová, M. Heyrovský, *Bioelectrochem. Bioenerg.* **41** (1996) 209
21. J. Heyrovský, J. Kůta, *Principles of Polarography*, Academic Press, New York, 1966, p. 299
22. A. Llinás, J. Donoso, B. Vilanova, J. Frau, F. Muñoz, M. I. Page, *J. Chem. Soc., Perkin Trans.* **2** (2000) 1521
23. J. H. Méndez, A. S. Pérez, M. D. Zamerreño, L. V. Laso, *Anal. Chim. Acta* **160** (1984) 335.

Pressure drop during evaporation of 1,1,1,2-tetrafluoroethane (R-134a) in a plate heat exchanger

EMILA DJORDJEVIĆ^{1*#}, STEPHAN KABELAC² and SLOBODAN ŠERBANOVIĆ^{1#}

¹Faculty of Technology and Metallurgy, University of Belgrade, Karnegijeva 4, 11120 Belgrade, Serbia and ²Helmut Schmidt University of Federal Armed Forces, Holstenhofweg 85, D-22043 Hamburg, Germany

(Received 22 February 2007)

Abstract: Experimental results for the pressure drop during the evaporation of the refrigerant 1,1,1,2-tetrafluoroethane (R-134a) in a vertical plate heat exchanger are presented in this paper. The influences of mass flux, heat flux and vapor quality on the two-phase pressure drop are specially analyzed and compared with previously published experimental data and literature correlations. All results are given in graphical form as the dependency of the frictional pressure drop on the mean vapor quality.

Keywords: plate heat exchanger, evaporation, 1,1,1,2-tetrafluoroethane, pressure drop.

INTRODUCTION

The advantages of plate and frame (or gasketed) plate heat exchangers over shell and tube type heat exchangers may be summarized as:

- a) better thermal performance,
- b) lower space requirements,
- c) easy accessibility to all areas and
- d) lower capital and operating costs.

These are the reasons for the expanded application of plate heat exchangers (PHE) in recent years.

The use of plate heat exchangers in food, pharmaceutical and utility industries is known since the 1960s¹ but the application in the process industry had to wait for a further 20 years. Today, in refineries and petrochemical plants, PHE are applied to many hydrocarbon processes, including catalytic reforming, desulphurization, isomerization, aromatic recoveries, sour water treatment, gas separation, *etc.*²

Plate heat exchangers were also found to be useful for two-phase applications as evaporators or condensers in refrigeration and air conditioning systems, and in district heating systems with steam condensation.

On the other hand, one limitation of their application is the demand for higher allowable pressure drops. Since heat transfer and the pressure drop in PHEs

* Corresponding author. E-mail: emila@tmf.bg.ac.yu

Serbian Chemical Society member.

doi: 10.2298/JSC0710015D

are closely connected to each other and dependant on the plate geometry, they should be studied together; the characteristics of the pressure drop have to be known in order to predict thermal behavior.

A detailed literature survey of the current state of investigations concerning the evaporation heat transfer coefficient and two-phase pressure drop in PHEs was given in a previous study.³

A comparison of the heat transfer coefficients (or j factors) of a typical plate heat exchanger with a mild corrugation angle and shell-and-tube (S&T) heat exchanger showed that with the same allowable pressure drop, a PHE can give 1.5–2.5 times higher heat transfer rates.² On the contrary, a similar comparison of frictional factors, shown in Fig. 1, suggests that for the same Re number, this parameter can reach ten times higher values in a plate heat exchanger than in a shell-and-tube heat exchanger.

It was also confirmed² that the pressure drop in a PHE is very sensitive to the corrugation angle, much more than to the heat transfer characteristics. It can be seen in Fig. 2 that a change in the corrugation angle from 40 to 55° more than doubles the friction factor but increases the j factor by 50 %.

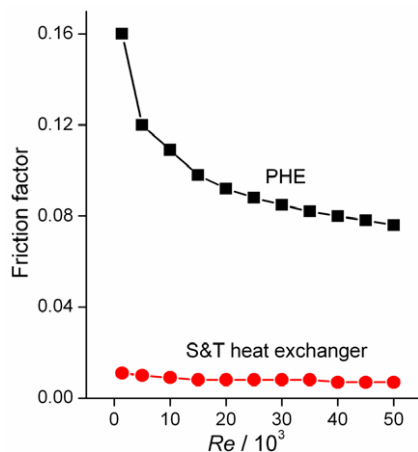


Fig. 1. Comparison of the frictional factors for PHE and S&T heat exchangers.

Fig. 2. Influence of plate corrugation angle on the j factor and the frictional factor.

In the study presented here, the focus was directed to the experimental investigation of the pressure drop during the evaporation process of R-134a in a plate heat exchanger and its dependency of mass flux, heat flux and vapor quality.

EXPERIMENTAL

A detailed description of the experimental setup used for investigation of the evaporation of the refrigerant R-134a in a vertical plate heat exchanger was given in the previous paper.³ However, it should be noted here that it consists of two main loops, a refrigerant loop and a water–glycol loop, and a data acquisition unit.

The refrigerant includes several main elements: an evaporator, a separation vessel, an expansion valve, an inner heat exchanger, a compressor, two oil separators, a condenser, a refrigerant collector with level indicator, two sight glasses and two volume flowmeters, one at the evaporator inlet and the other just before the expansion valve. A vertical plate and frame heat exchanger are used as the evaporator and the condenser, respectively.

The water–glycol loop is constructed from two sub-cycles – each connected with one of the plate heat exchangers – the evaporator or the condenser. One of the characteristics of the water–glycol loop, in the evaporator sub-cycle, is a four-way valve, which enables the change of the water–glycol flow direction from concurrent to countercurrent and, consequently, the investigation of the influence of flow direction on the heat transfer and pressure drop.

The data acquisition system consists of the following elements: a recorder, a power supply and a personal computer. The experiment was monitored and controlled and a preliminary balance check was performed by a routine written in the LabVIEW program. The main screen is shown in Fig. 3, which includes a simplified schematic representation of the refrigerant loop with all the temperature, pressure and flow rate measuring points connected to the acquisition system. A detailed description of the measuring instrumentation and equipment, including the measuring accuracy, was given in the previous paper.³

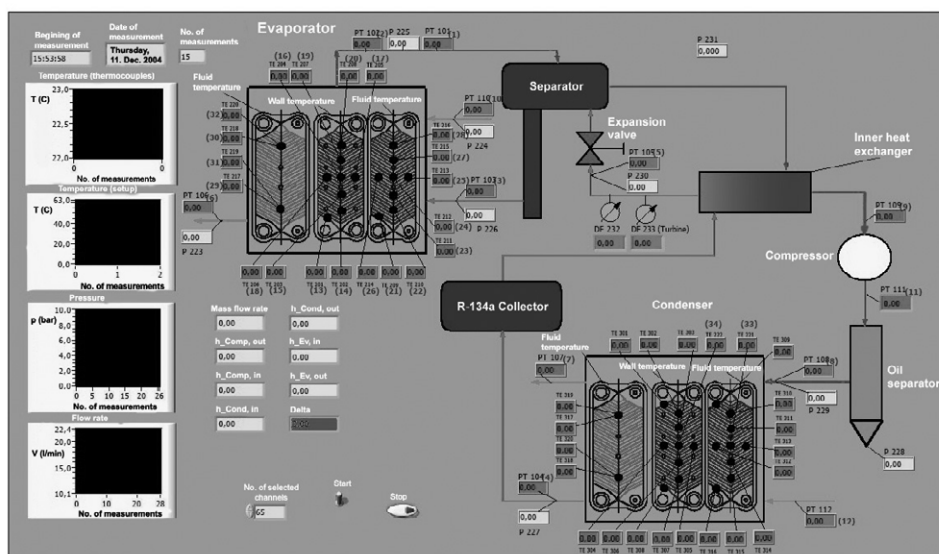


Fig. 3. Refrigerant cycle.

All the measurements were performed in a stationary state regime and the time dependency of the measured process parameters could be followed in the diagrams on the left side of the screen. Results of the preliminary balance check were also shown on the main screen. A second and more accurate balance check was performed after the experiment as a part of a data reduction procedure. Only then could the further calculation of the heat transfer coefficient and pressure drop be undertaken.

Details of the calculations of the heat transfer coefficient were described in our previous work.³

For the vertically upward refrigerant flow, the frictional pressure drop can be calculated from the Equation:

$$\Delta p_f = \Delta p_{exp} - \Delta p_{man} - \Delta p_{acc} - \Delta p_{ele} \quad (1)$$

The acceleration and elevation pressure drops were estimated by the homogenous model for two-phase flow:⁴

$$\Delta p_{acc} = m_{flux,r}^2 \Delta v_{lg} \Delta x \quad (2)$$

$$\Delta p_{ele} = \frac{gL_p}{v_m} \quad (3)$$

The mean specific volume of a homogeneously mixed, vapor-liquid flow v_m can be determined as:

$$v_m = xv_g + (1-x)v_l = v_l + x\Delta v_{lg} \quad (4)$$

where Δv_{lg} is the difference between the specific volumes of the vapor and liquid:

$$\Delta v_{lg} = v_g - v_l \quad (5)$$

The pressure drops in the inlet and outlet manifolds and ports can be calculated from the empirical correlation:⁵

$$\Delta p_{man} \approx 1.5 \left(\frac{u_m^2}{2v_m} \right)_{i,o} \quad (6)$$

while the mean flow velocity u_m can be expressed as:

$$u_m = m_{flux,r} v_m \quad (7)$$

Finally from the definition of the friction factor, its value can be obtained as:

$$f_{fp} = - \frac{\Delta p_f D_h}{2m_{flux,r}^2 v_m L_p} \quad (8)$$

Mass flux of the refrigerant and the hydraulic diameter were calculated from the equations:

$$m_{flux,r} = \frac{m_{r,ch}}{2aB_p} \quad (9)$$

$$D_h \approx 4a \quad (10)$$

An uncertainty analysis was conducted using a formula proposed by Kline and McClinton⁶ and the evaluation results are presented in the previous work.³

RESULTS AND DISCUSSION

In the present investigation of R-134a evaporation in a vertical plate heat exchanger, series of experiments were conducted under different test conditions. The evaporation temperature was varied from -8.85 to 11.08 °C (saturation pressure from 0.21 to 0.43 MPa), the values of the refrigerant mass flux were between 40 and 90 $\text{kg m}^{-2} \text{s}^{-1}$) and the imposed heat flux was gradually increased from 9 to 15 kW m^{-2} . Thermophysical properties of R-134a are taken from the REFPROP database.⁷ The calculated values of pressure drop are presented as a dependency on the mean vapor quality x_m in the plate heat exchanger. The mean vapor quality was defined and calculated as the arithmetic mean value between the inlet and the outlet vapor qualities.

Comparison of the current data with previous measurements involving evaporation of the refrigerant R-134a⁸ showed satisfactory agreement, although the experiments were conducted using a plate heat exchanger of smaller size, diffe-

rent geometry, with a smaller number of single plates and at the room temperature (25–31 °C). The results presented in this study were obtained using a plate heat exchanger with a larger number of plates in order to approach real exploitation conditions, and at the lower temperatures. The characteristics and dimensions of the plates are summarized in Table I.

TABLE I. Plate dimensions

Length, L_p / mm	872
Width, B_p / mm	486
Amplitude, a / mm	1.6
Wave length, λ / mm	12
Plate thickness, δ_p / mm	0.6
Thermal conductivity, λ_p / W m ⁻¹ K ⁻¹	15
Corrugation angle, ψ / °	63.26

The influences of the mass flux of the refrigerant, imposed heat flux and vapor quality in the two-phase pressure drop are now closely analyzed. Selected data shown in Fig. 4 represent the dependency of the frictional pressure drop on the vapor quality for three different mass fluxes. It can be seen that the pressure drop rises with increasing vapor quality, but less significantly than in the case of the heat transfer coefficient.³ Higher mass fluxes also induces higher pressure drops, as can be seen in Fig. 4. This is the consequence of the fact that a higher mass flux also means a higher velocity of the two-phase flow and thus a higher pressure drop.

The effects of heat flux on the frictional pressure drop are presented in Fig. 5. Two heat fluxes are compared under the same conditions of mass flux and system pressure. It seems that the pressure drop is only slightly affected by increasing heat flux, less than in the previous case of the influence of mass flux. A similar behavior was noticed previously when the influences on the heat transfer coefficients were analyzed.³

In addition to the experimental results for the friction pressure drop Δp_f , the values calculated from correlations based on the heterogeneous pressure drop model and the Lockhard–Martinelli approach, as described in the literature,⁹ are also presented in Fig. 5:

$$\Delta p_{lit} = \Delta p_{1ph} \left(1 + \frac{5}{X_{tt}} + \frac{1}{X_{tt}^2} \right) \quad (11)$$

where X_{tt} is the Martinelli parameter:

$$X_{tt} = \left(\frac{1-x}{x} \right)^{0.9} \left(\frac{\mu_{r,l}}{\mu_{r,g}} \right)^{0.1} \left(\frac{\rho_{r,g}}{\rho_{r,l}} \right)^{0.5} \quad (12)$$

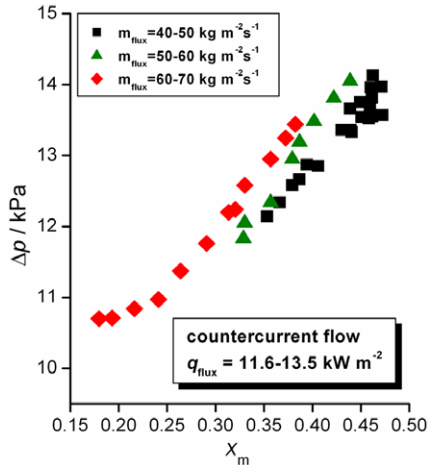


Fig. 4. Influence of mass flux on the pressure drop.

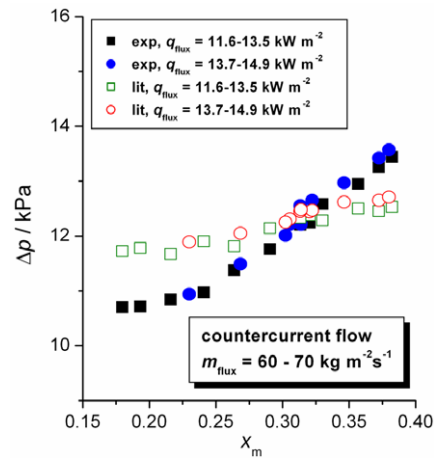


Fig. 5. Influence of heat flux on the pressure drop.

The agreement between the experimental and literature values is very good with a maximum deviation of approximately 10 % for all presented cases, as can be seen in Fig. 6.

The results of the experiments obtained under various test conditions are compared in Fig. 7 with previous measurements reported in the literature for the same refrigerant.⁸ Although differences in plate geometry and working conditions exist, the amplitude, the wave length and the corrugation angle are similar, which gave a reasonable basis for comparison. It can be concluded from Fig. 7 that the agreement between the two series of measurements is fair.

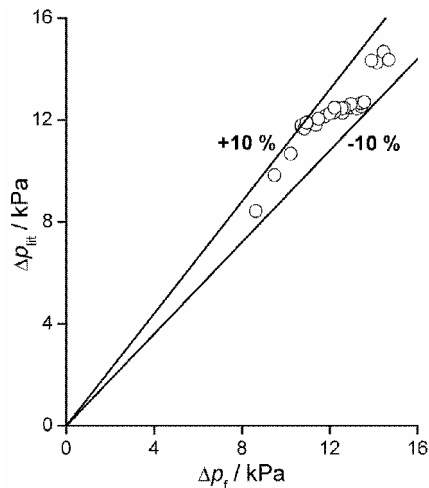


Fig. 6. Comparison of the current data with literature correlations.

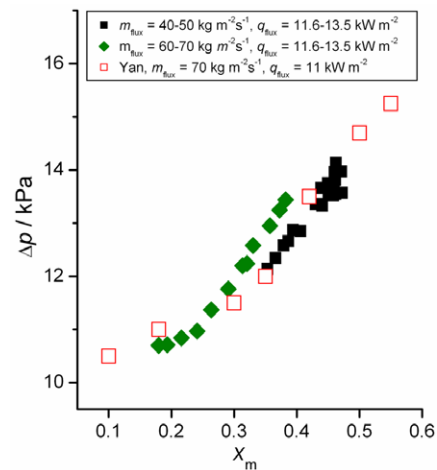


Fig. 7. Comparison with previous experimental data.⁸

CONCLUSIONS

The results presented in this paper show that both the mass flux and heat flux influence, to some extent, the frictional pressure drop during the evaporation process. The pressure drop is also a function of vapor quality, although the effect is not as significant as in the previously reported case of the heat transfer coefficient.³ Comparison with previously reported measurements for the same refrigerant under different test conditions and with a different plate geometry⁸ shows a good agreement, which opens the possibility for future successful and accurate prediction of pressure drop in new processes involving this refrigerant.

NOMENCLATURE

A – Amplitude of plate corrugation, m
 B – Width, m
 D_h – Hydraulic diameter, m
 f_{fp} – Friction factor
 g – Gravitational acceleration, $m\ s^{-2}$
 L – Length, m
 mch – Mass flow rate through one of the channels, $kg\ s^{-1}$
 m_{flux} – Mass flux, $kg\ m^{-2}s^{-1}$
 q – Heat flux, $W\ m^{-2}$
 u_m – Mean flow velocity, $m\ s^{-1}$
 v_g – Vapor specific volume, $m^3\ kg^{-1}$
 v_l – Liquid specific volume, $m^3\ kg^{-1}$
 v_m – Specific volume of mixed vapor and liquid flow, $m^3\ kg^{-1}$
 x_m – Mean vapor quality
 X_{tt} – Martinelli parameter

Greek letters

δ_p – Thickness of the plate, m
 Δp_{acc} – Acceleration pressure drop, Pa
 Δp_{ele} – Elevation pressure drop, Pa
 Δp_{exp} – Experimental pressure drop, Pa
 Δp_f – Friction pressure drop, Pa
 Δp_{ma} – Pressure drop in ports and manifolds, Pa
 Δx – Change of vapor quality between inlet and outlet
 λ – Wavelength of plate corrugation, m
 λ_p – Thermal conductivity of plate material, W/mK
 μ – Viscosity, $Pa\ s$
 ρ – Density, $kg\ m^{-3}$
 ψ – Angle of plate corrugation, deg

Subscripts

ch – Channel
g – Gas
i – Inlet
l – Liquid
o – Outlet
p – Plate
r – Refrigerant

Acknowledgement: The experimental results presented in this study were obtained courtesy of the Laboratory of the Institute of Thermodynamics at Helmut Schmidt University of the Federal Armed Forces in Hamburg, Germany. This work was also supported by a grant from the Ministry of science of Serbia and the Faculty of technology and metallurgy, University of Belgrade.

ИЗВОД

ПАД ПРИТИСКА ПРИ ИСПАРАВАЊУ 1,1,1,2-ТЕТРАФЛУОРЕТАНА (R-134a) У ПЛОЧАСТОМ РАЗМЕЊИВАЧУ ТОПЛОТЕ

ЕМИЛА ЂОРЂЕВИЋ¹, СТЕРНАН КАБЕЛАС² и СЛОБОДАН ШЕРБАНОВИЋ¹

¹ Tehnološki fakultet, Univerzitet u Beogradu, Karnegi jeva 4, 11120 Beograd i ² Helmut Schmidt University of Federal Armed Forces, Holstenhofweg 85, D-22043 Hamburg, Germany

У овом раду су представљени експериментални резултати за пад притиска током проеса испаравања расхладног флуида R-134a у вертикалном плочастом размењивачу топлоте. Посебно су анализирани утицаји масеног и топлотног флукса на пад притиска у двофазном току и упоређени са раније објављиваним експерименталним подацима и корелацијама из литературе. Сви резултати су представљени у графичком облику, као зависност фриксионог пада притиска од средњег степена сувоће.

(Примљено 22. фебруара 2007)

REFERENCES

1. M. D. Sloan, *Chem. Eng.* **105** (1998) 78
2. J. H. Wang, *3rd International Conference on Compact Heat Exchangers and Enhancement Technology for the Process Industries*, Davos, Switzerland, Proceedings, 2001, p. 503
3. E. Djordjević, S. Kabelac, S. Šerbanović, *J. Serb. Chem. Soc.* **72** (2007) 833
4. J. G. Collier, *Convective Boiling and Condensation*, McGraw–Hill, New York, 1982
5. R. K. Shah, W. W. Focke, in *Heat Transfer Equipment Design*, R. K. Shah, E. C. Subbarao, R. A. Mashelkar, Eds., Hemisphere, Washington DC, 1988, p. 227
6. S. J. Kline, F. A. McClintock, *Mechan. Eng.* **75** (1953) 3
7. M. O. McLinden, S. A. Klein, E. W. Lemmon, A. P. Peskin, *NIST Thermodynamic and Transport Properties of Refrigerant Mixtures – REFPROP*, Version 6.0, NIST, Boulder, 1998
8. Y. Y. Yan, T. F. Lin, *ASME J. Heat Transfer* **121** (1999) 118
9. H. Baehr, K. Stephan, *Heat and Mass transfer*, Springer Corp., Berlin, 1998.

The use of image analysis for the study of interfacial bonding in solid composite propellant

JASMINA DOSTANIĆ*, GORDANA UŠĆUMLIĆ[#], TATJANA VOLKOV–HUSOVIĆ,
RADMILA JANČIĆ–HEINEMANN and DUŠAN MIJIN[#]

Faculty of Technology and Metallurgy, University of Belgrade, Karnegijeva 4, 11000 Belgrade, Serbia

(Received 6 July 2006)

Abstract: In the framework of this research, the program Image Pro Plus was applied for determining the polymer–oxidizer interactions in HTPB-based composite propellants. In order to improve the interactions, different bonding agents were used, and their efficiency was analyzed. The determination of the quantity, area and radius of non-bonded oxidizer crystals is presented. The position of formed cracks in the specimen and their area have a great influence on the mechanical properties of composite propellant. The preparation of the composite propellant in order to enable the photographing of their structure by means of stereoscopic and metallographic microscopes with the digital camera is also described as well.

Key words: composite propellant, interactions, grain distribution, dewetting, image analysis, mechanical properties.

INTRODUCTION

Image Pro Plus is a software package used for image acquisition, enhancement and analysis. Image data can be enhanced using a large variety of color and contrast filters. Image Pro Plus enables users to trace and count objects manually or automatically. The attributes of objects, such as length, area, diameter and angle, can be measured and the image can be calibrated to the desired unit of measure.¹

Within the framework of this research, the program Image Pro Plus was employed for the determination the interactions between the components of solid composite materials.

Modern composite propellants are heterogeneous powders (mixture), which use a crystallized or finely ground mineral salt as an oxidizer (often ammonium perchlorate), which constitutes between 60 and 90 % of the mass of the propellant. The fuel itself is aluminum. The propellant is held together by a polymeric binder (usually polyurethane or polybutadiene). The final products are rubber like substances, with the consistency of a hard rubber eraser.

* Corresponding author. E-mail: jdostanic@tmf.bg.ac.yu

[#] Serbian Chemical Society member.

doi: 10.2298/JSC0710023D

Composite propellants require certain interactions between the polymer and filler (oxidizer and metal component) in order to prevent separation around a particle of filler. If dewetting occurs between the binder and filler, the flame front propagates below the burning surface to produce a more rapid combustion of the propellant.² This would have two undesired consequences: an increase of the pressure in the rocket engine and creation of cracks, which may cause detonation during the combustion process.

Poor interactions between binders and fillers are found mostly with oxidizers and not with the metal fuels. The metals are not a problem, because metals have a more irregular surface and a greater ease for chemical bonding with the filler.² On the other hand, oxidizers have surfaces which are very smooth and, in some cases, the oxidizers do not chemically bond with the filler.

Attempts to improve the binder–filler interactions in composite propellants have included the addition of a bonding agent. A bonding agent produces an interaction between the oxidizer crystal and the binder by forming either primary or secondary bonds with the oxidizer and a primary bond with the binder.³

In addition, the role of bonding agents is to facilitate the formation of propellants through decreasing the viscosity of the emulsion and to improve the physical and mechanical properties of the propellant by preventing adhesion of the binder to the solids, thereby decreasing its tensile strength. Thus, bonding agents play a double role, serving as a wetting agent for the solids and increasing the cohesion between the binder and the solids.

The bonding agents used in this research were functionally substituted isocyanurates, which are universal bonding agents, and can be used for all binder–filler systems (Fig. 1).

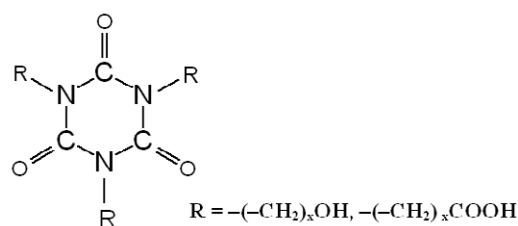


Fig. 1. The studied 1,3,5-trisubstituted isocyanurates.

Selection of R was based on the binder and the reactivity of R therewith. The R functional group of the bonding agent must be reactive or compatible with and is preferably the same as the functional group on the binder.⁴

Interactions between two ingredients are improved with an even distribution of ammonium perchlorate (AP) particles. If the bonds between polymer and filler are not very strong, dewetting will occur. By determining the area and diameter of non-bonded AP particles, the efficiency of bonding agents in providing binder–filler interactions can be assessed.

So far, no polymeric binder material has been found which prevents moisture from diffusing into the interior of the propellant grain. Although moisture at ordinary temperatures does not undergo chemical reaction to any significant degree with the components of the propellant, it nevertheless, strongly affects the mechanical properties. This deterioration of the properties is caused by the accumulation of moisture on the surface of the oxidizer crystals, thus creating a low modulus (liquid) layer which envelops the particle. In essence, this means that the "bond" between the oxidizer and binder is destroyed and dewetting will commence at low stress levels with commensurate loss of mechanical properties.⁵ The area of the cross section of cracks and their position in the specimens are good indicators of mechanical properties.

The topic of this study was to establish the conditions of the preparation of composite propellants containing ammonium perchlorate (AP), hydroxyl terminated polybutadiene (HTPB) and 1,3,5-trisubstituted isocyanurate as bonding agents. The bonding phenomenon was investigated by the stereoscopic and metallographic microscopes with a digital camera. The morphological characteristics of the images obtained were analyzed using Image Pro Plus software package.

EXPERIMENTAL

Synthesis of 1,3,5-trisubstituted isocyanurates

Tri(2-carboxyethyl) isocyanurate was obtained by reacting cyanuric acid with a molar excess of acrylonitrile in the presence of a strongly alkaline catalyst (trimethylphenylammonium hydroxide) and in a reaction medium containing a suitable solvent (dimethylformamide) for the reactants and the intermediate product tri(2-cyanoethyl) isocyanurate which is formed. The tri(2-cyanoethyl) isocyanurate was hydrolyzed to the corresponding tri(2-carboxyethyl) isocyanurate by heating them to boiling with an aqueous mineral acid according to a modified literature procedure.^{6,7}

Tri(2-hydroxyethyl) isocyanurate was prepared by the reaction of cyanuric acid and 2-chloroethanol in alkaline medium, according to literature data.⁸

The synthesized 1,3,5-trisubstituted isocyanurates were identified by their melting points and FTIR, ¹H-NMR and UV spectroscopic data.

Ammonium perchlorate and hydroxyl-terminated poly(butadiene) were obtained from Fluka and Arco Chemical.

Preparation of the composite propellants

Specimens containing ammonium perchlorate (AP), hydroxyl-terminated polybutadiene (HTPB) and different trisubstituted isocyanurates as bonding agents, in a weight ratio of 7:2:1 were prepared.

Specimen No. 1 contained tri(2-carboxyethyl) isocyanurate, while specimen No. 2 contained tri(2-hydroxyethyl) isocyanurate as bonding agents. These bonding agents are abbreviated as BA I and BA II, respectively.

Propellant paste was made in the laboratory in a 10 g scale. Active coal was added to the bonding agent, and the mixture was homogenized in a stamp mortar. Sufficiently dried ammonium perchlorate (AP) was added, the mixture was placed in a beaker and HTPB was added. The paste was mixed with the help of a spatula inside the beaker for about one minute. This phase was followed by homogenization designed to improve the wetting of the solids by the binder and to decrease the viscosity to the point where casting could be performed under good conditions. In the next phase the propellant sample mixture was shaped in order to obtain a sample pellet, after which the pellet was maintained at 60 °C for 48 h.^{7,9}

Analysis of composite samples

The first obtained specimen was hard, but it crumbled during cutting (Fig. 2). The uncured mixture was typically dough-like. Trapped air, creating voids in the grains, could cause problems.

The obtained second specimen was jelly-like and stuck to the employed tools, which was complicated the preparation for image analysis (Fig. 3).

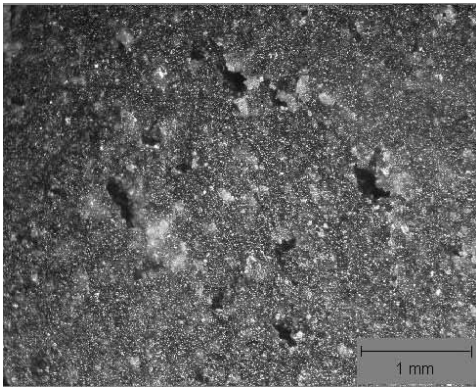


Fig. 2. Micrograph of the composite specimen No. 1.

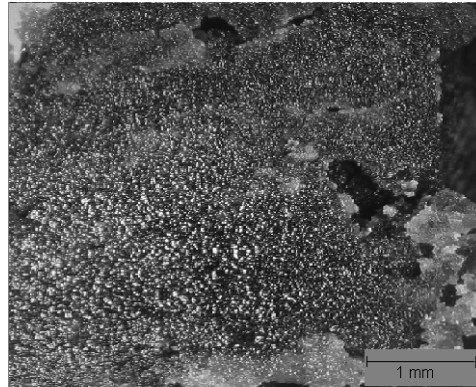


Fig. 3. Micrograph of the composite specimen No. 2.

RESULTS AND DISCUSSION

The obtained composites were photographed using the stereoscopic and metallographic microscope with the digital camera, and images obtained were analyzed using program Image Pro Plus.

AP Distribution

When small amounts of active coal were introduced into the composite propellant, all ingredients became colored, except AP which maintained its natural color. Using Image Pro Plus, the observed change in color was utilized to determine the percentage of AP particles and their distribution. In order to determine distribution of AP, the specimens were divided into several segments.

The distribution of AP in specimen No. 1 and 2 is presented in Table I.

TABLE I. Distribution of AP in specimen No. 1 and 2

Segment	Area, mm ²		AP Area, mm ²		AP Ratio, %	
	1	2	1	2	1	2
I	2.5781	3.6655	1.4600	2.1413	56.6321	61.7900
II	2.1512	3.3445	1.4647	2.1635	68.0883	64.6881
III	1.8443	3.2145	1.1124	1.6504	60.3122	51.3434
IV	2.8190	3.1422	1.9036	2.1621	67.5247	64.6912
V	2.4058	–	1.4057	–	58.4292	–
VI	1.8689	–	1.1977	–	64.0877	–

The obtained results show that AP particles were nearly equally distributed and their ratio ranged from 58 to 69 % in specimen No. 1 and from 51 to 65 % in specimen No. 2. Although this distribution has a great influence on the interactions between polymer and oxidizer, the process of dewetting has a dominant influence on binder–AP interactions.

Binder–AP interactions

If the bonds between the binder matrix and the oxidizer are not very strong, dewetting occurs and halos are formed in the vicinity of the oxidizer.

In order to assess the influence of bonding agent on the binder–AP interactions, two specimens containing different bonding agents were used. By determining the quantity, area, radius and roundness of non-bonded AP particles, significant information about binder–filler interactions can be gained. The determined parameters for the specimen containing BA I (specimen No. 1) are given in Table II.

TABLE II. Statistics for specimen No. 1

	Area, μm^2	Diameter (max), μm	Diameter (min), μm	Holes	Roundness
Min	20.576	5.1230	5.1230	0	1
Max	22530.0	250.07	126.45	0	147.28
Range	583.07	28.202	13.917	0	3.8367
Sum	60640.00	2933.00	1447.4	0	399.02
Samples	104.00	104	104	104	104

The grain size distribution and area distribution is significant, because AP particles are agglomerated into clusters. According to the different area, non-bonded APs are classified into three classes, Table III.

TABLE III. Area classification for specimen No. 1

Class	Objects	Objects, %	Area (mean), μm^2	Diameter (mean), μm	Roundness (mean)
1	102	98.077	271.852	18.476	1.160
2	1	0.9615	10380.6	124.02	2.737
3	1	0.9615	22530.0	196.74	2.595

From the obtained results it can be noticed that the specimen contains a large percentage of non-bonded AP particles. The discrete AP particles (102 objects) had nearly orbicular configurations (roundness around 1), while the clusters (2 objects) had irregular conformations. Clusters formation has a negative influence on binder–filler interactions.

The formation of halos in specimen No.1 can be interpreted as the failure of the adhesive bond between the binder matrix and oxidizer. Before dewetting, tiny voids were created next to the AP particles, but distinctly located in the matrix, away from the AP surface.¹⁰ After further straining, these voids coalesce and merge into vacuoles, exposing the oxidizer surface, Fig. 4. The dewetted particles exhibit a typical eye-texture.

The determined parameters for the specimen containing BA II (specimen No. 2) are given in Table IV.

TABLE IV. Statistics for specimen No. 2

	Area, μm^2	Diameter (max), μm	Diameter (min), μm	Holes	Roundness
Min	62.011	8.712	8.163	0	1.000
Max	193.43	16.012	13.744	0	1.046
Range	117.60	12.070	10.845	0	1.010
Sum	2116.7	217.25	195.22	0	18.178
Samples	18	18	18	18	18

Only a small percentage of non-bonded AP particles was observed and it can be concluded that very strong bonds between the polymer binder and oxidizer prevent dewetting, Fig. 5.

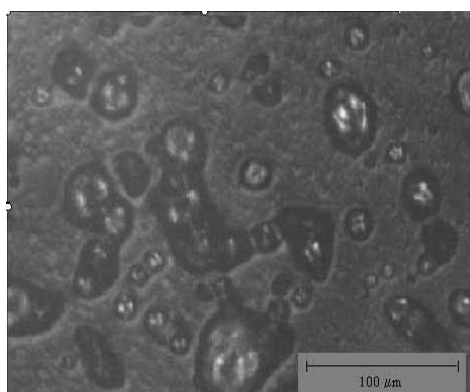


Fig. 4. Cavity formation around non-bonded AP crystals in specimen No. 1.

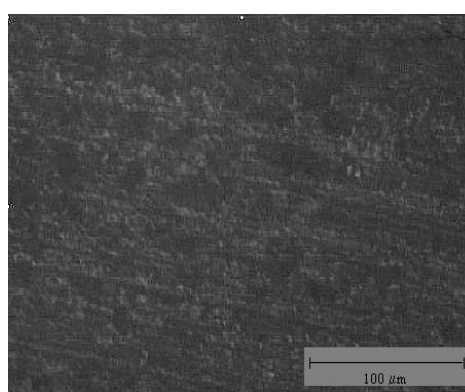


Fig. 5. AP Crystal bonded to the polymer matrix in specimen No. 2.

The minority of non-bonded particles can be classified into three groups, Table V.

Table V. Area classification for specimen No. 2

Class	Objects	Objects, %	Area (mean), μm^2	Diameter (mean), μm	Roundness (mean)
1	2	11.111	65.482	8.583	1
2	4	22.222	83.877	9.717	1
3	12	66.667	137.520	12.561	1.015

For each class, minor differences between the radius and area of the particles are observed, and it can be inferred that the AP particles had the same area and grain size. Particle agglomeration was not observed. Further evidence that the AP particles were non-agglomerated is that the roundness had a value around 1 for every class.

Crack cross section

During the synthesis of HTPB based propellants with tri(2-carboxyethyl) isocyanurate as the bonding agent, trapped air can be a problem, creating voids in the grains. Likewise, voids and bubbles can result from gases evolved during curing as a result of moisture absorption. This results in crack formation. The area of the cross section of the cracks was 0.2679 cm^2 , which was 1.96 % of the overall surface area of the sample. All the cracks occurred in the interior of the sample and they occupied a considerable part of the sample area, Fig. 6.

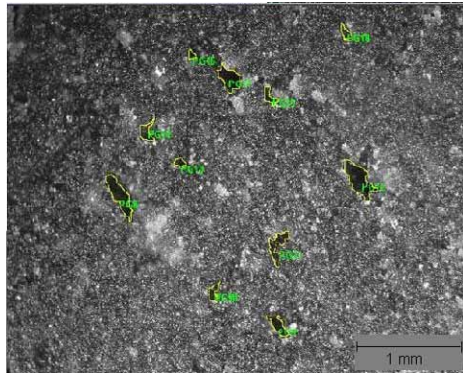


Fig. 6. Micrograph of crack formation.

Crack formation can lead to bad mechanical properties, but during the preparation of the specimens, this drawback can be eliminated.

In the HTPB based propellant with tri(2-hydroxyethyl) isocyanurate as bonding agent, no crack formation was found, hence the specimen had better mechanical properties compared to the specimen No. 1.

These results are in accordance with previous investigations⁷ of the interactions between ammonium perchlorate, different bonding agents and hydroxyl-terminated poly(butadiene), studied by means of the FTIR spectroscopic method. It was shown that the interfacial bonding force arises from hydrogen bonding in the case of tri(2-hydroxyethyl) isocyanurate. This effect was not observed when tri(2-carboxyethyl) isocyanurate was used as the bonding agent.

CONCLUSION

Based on the analysis of the experimental results, the following conclusions can be deduced:

- In HTPB based propellants with tri(2-carboxyethyl) isocyanurate as the bonding agent, the AP particles were nearly equally dispersed in the polymer binder, but there was a large percentage of non-bonded AP particles, which were generated during dewetting. The non-bonded AP particles were agglomerated, probably because of deficient homogenization during the preparation of the specimens. During synthesis, trapped air was a problem, creating voids in the grains. This resulted in crack formation, which covered 1.93 % of the overall surface area of the sample.

- In HTPB based propellants with tri(2-hydroxyethyl) isocyanurate as the bonding agent, the AP particles were nearly equally distributed in the polymer binder. Only a small percentage of non-bonded AP particles was observed, from which it can be concluded that very strong bonds between polymer binder and oxidizer prevented dewetting. The mechanical properties were better compared to the first specimen, because no crack formation was found. The drawback of this specimen was its stickiness, which complicated the preparation for image analysis.
- The effects of the bonding agents in improving the interactions between polymer and AP were significant when tri(2-hydroxyethyl) isocyanurate was employed.
- The effects of tri(2-carboxyethyl) isocyanurate as bonding agent were negligible in improving the interactions between polymer and filler.
- Tri(2-carboxyethyl) isocyanurate as bonding agent does not have a great influence on improving the AP–polymer interactions.

Acknowledgments: This work was financially support by the Ministry of Science of the Republic of Serbia, Contract No. TR 6717.

ИЗВОД

КОРИШЋЕЊЕ АНАЛИЗЕ СЛИКЕ ЗА ОДРЕЂИВАЊЕ ИНТЕРАКЦИЈА У ЧВРСТИМ КОМПОЗИТНИМ ГОРИВИМА

ЈАСМИНА ДОСТАНИЋ, ГОРДАНА УШЋУМЛИЋ, ТАТЈАНА ВОЛКОВ–ХУСОВИЋ,
РАДМИЛА ЈАНЧИЋ–ХАЈНЕМАН и ДУШАН МИЈИЊ

Technol of ko-metalur{ki fakul tet, Uni verzi tet u Beogradu, Karnegi jeva 4, 11000 Beograd

У оквиру истраживања програм Image Pro Plus је примењен за одређивање интеракција између полимера и оксиданса у композитним горивима на бази НТРВ. У циљу побољшања ових интеракција, коришћени су различити везујући агенси и анализирана је њихова ефикасност. У раду је такође вршено одређивање количине, удела, површине и пречника честица, које нису везане за полимер. Површина формираних пукотина и њихова расподела у узорку имају велики утицај на механичка својства композита. Припрема узорака композитних горива за снимање њихове морфолошке структуре помоћу стереомикроскопа и метаграфског микроскопа са дигиталном камером је такође описана.

(Примљено 6. јула 2006)

REFERENCES

1. Image Pro Plus, *The Proven Solution for image Analysis*, Media Cybernetics, 1993
2. J. P. Consaga, US 4.944.815 (1990) (US Navy)
3. G. P. Sutton, *Rocket propulsion elements*, John Wiley & Sons, New York, 1996
4. J. P. Consaga, US 4.214.928, (1980) (US Navy)
5. A. E. Oberth, R. S. Bruenner, US 4000 023 (1976)
6. A. Sadle, US. 3.485.833 (1969)
7. G. S. Ušćumlić, M. M. Zreigh, D. Z. Mijin, *J. Serb. Chem. Soc.* **71** (2006) 445
8. A. A. Suyigh, H. Ubrich, *J. Chem. Soc* (1961) 3148
9. K. Hori, *PhD Thesis*, The Institute of Space and Astronautical Science, Tokyo, Japan, 1987
10. A. E. Oberth, R. S. Bruenner, *Trans. Soc. Rheol.* **9** (1965) 165.

A simple *in situ* visual and tristimulus colorimetric method for the determination of diphosgene in air

VLADIMÍR PITSCHMANN^{1*}, ZBYNĚK KOBLIHA²,
EMIL HALÁMEK² and IVANA TUŠAROVÁ¹

¹Oritest spol. s r.o., Staropramenná 17, 150 00 Praha 5 and ²NBC Defense Institute, University of Defense, Kounicova 65, 612 00 Brno, Czech Republic

(Received 3 August 2006)

Abstract: A simple visual and tristimulus colorimetric method (three-dimensional system CIE- $L^*a^*b^*$) for the determination of trace amounts of diphosgene in air has been developed. The method is based on the suction of diphosgene vapors through a modified cotton fabric filter fixed in a special adapter. Prior to analysis, the filter is saturated with a chromogenic reagent based on 4-(*p*-nitrobenzyl)pyridine. The optimal composition of the reagent is 2 g of 4-(*p*-nitrobenzyl)pyridine and 4 g of *N*-phenylbenzylamine in 100 ml of a 50:50 ethanol–glycerol mixture. The intensity of the formed red coloration of the filter is evaluated visually or by a tristimulus colorimeter (LMG 173, Lange, Germany). The detection limit is 0.01 mg m⁻³. Acetyl chloride and benzoyl chloride react in 150 and 50 times higher concentrations, respectively. The method is suitable for mobile field analysis.

Keywords: tristimulus colorimetry, diphosgene, air analysis, 4-(*p*-nitrobenzyl)pyridine, *N*-phenylbenzylamine.

INTRODUCTION

Diphosgene (trichloromethyl chloroformate) was developed especially as a choking war agent and a more stable alternative to gaseous phosgene. Liquid diphosgene, as well as solid triphosgene (hexachlorodimethyl carbonate), has found laboratory use as a substitute for phosgene and recently there has also been a growing interest in the industrial utilization of both compounds as highly reactive halogenation and acylation reagents.

In spite of the different physical properties and structures of phosgene, diphosgene and triphosgene,¹ their chemical behavior is genetically similar. Thus, *e.g.*, both diphosgene and triphosgene decompose thermally to give phosgene and therefore the same methods and technical means are often employed for their chemical analysis. Naturally, papers in the literature most often deal with the analysis of the industrially most important phosgene. Prevalent methods of phosgene

* Corresponding author. E-mail: pitschmann@oritest.cz
doi: 10.2298/JSC0710031P

determination are based on its color reactions with some chromogenic reagents. One of the oldest color reactions of phosgene consists in the halogenation of *p*-dimethylaminobenzaldehyde followed by condensation with aromatic amines, which is utilized particularly for the preparation of indicator papers and detection tubes. A classical reagent of this type is a mixture of *p*-dimethylaminobenzaldehyde with diphenylamine which gives a yellow coloration.² A similar reaction of phosgene with *p*-dimethylaminobenzaldehyde in the presence of *N,N*-dimethylaniline affords a green to deep blue color due to products of the diphenylmethane or triphenylmethane type,^{3,4} an oxidized form of crystal violet. This reaction has been repeatedly modified.^{4–10}

A great variety of analytical techniques are based on the reaction of phosgene with 4-(*p*-nitrobenzyl)pyridine, affording a yellow to orange product.¹⁰ This reaction has been improved by the addition of *N*-phenylbenzylamine, which gives an intense red coloration. This modification can also be used for simple detection devices^{10,11} and for spectrophotometric determination.¹² The reaction has been employed also for the automatic determination of phosgene in air.^{13,14}

This paper relates to a simple and sensitive method for the determination of diphosgene in air using tristimulus colorimetry. This method is currently employed in the industry for controlling the surface quality of a variety of colored materials and has recently also found application in analytical chemistry, *e.g.*, in the determination of iron, cobalt and nickel,¹⁵ mercury,¹⁶ arsenic,¹⁷ alkylbenzenesulfonates,¹⁸ phosphates¹⁹ and residual chlorine.²⁰ The devised method consists in the reaction of diphosgene with a chromogenic reagent based on 4-(*p*-nitrobenzyl)pyridine and *N*-phenylbenzylamine, with the formation of a red coloration. The reaction occurs on a special filter made of modified cotton fixed in a special adapter. The chromogenic reagent is applied on the filter and air is sucked through it. The intensity of the formed color spot is then evaluated by a tristimulus colorimeter or visually.

EXPERIMENTAL

Chemicals and equipment

Diphosgene of 98 % purity (VOZ Zemianske Kostolany, Slovak Republic) served as a standard. The chromogenic reagent was prepared with 4-(*p*-nitrobenzyl)pyridine, *N*-phenylbenzylamine, glycerol (all Sigma–Aldrich, of at least *p.a.* grade) and absolute ethanol (Riedel de Haen). The chromogenic reagent was prepared by dissolving 2.0 g of 4-(*p*-nitrobenzyl)pyridine, 4.0 g of *N*-phenylbenzylamine and 50 ml of glycerol in ethanol, after which the solution was made up to 100 ml.

The coloration intensity of the spot was evaluated with a portable tristimulus colorimeter (spectrophotometer LMG 173, Lange, Germany). Diphosgene vapors were generated in a thermostated test chamber of 617 dm³ volume (Lamon, Czech Republic). Samples were taken using a hand-operated suction apparatus Universal-86 (Kavalier Votice, Czech Republic), stroke volume 100±5 cm³, suction under pressure 23.33±0.66 kPa. The diphosgene concentration in the chamber was controlled using a XDS-10C vacuum pump (BOC Edwards, UK) with an attached flowmeter and a Helios-α UV-VIS spectrophotometer (Thermo Electron, UK).

Filter preparation

The filter consisted of a fabric made of cotton threads of 0.31–0.33 mm thickness. The fabric was impregnated with a solution containing 0.3 g of $\text{Na}_2\text{B}_4\text{O}_7 \cdot 10 \text{H}_2\text{O}$, 0.45 g of H_3BO_3 , 0.1 g of NaCl, 2.5 g of silica gel (particle size less than 5 μm) and 3.0 g of dextran in 100 ml of water. The impregnated fabric was first dried in air and finally in a desiccator over solid sodium hydroxide. After drying, it was cut into circles of 45 mm diameter.

Sample preparation and checking diphosgene concentration

Various concentrations of diphosgene were prepared in the test chamber by evaporation of its toluene solution. The actual diphosgene vapor concentration was determined spectrophotometrically. The diphosgene vapors were pumped for 30 minutes by vacuum pump at a rate $1 \text{ dm}^3 \text{ min}^{-1}$ and were absorbed in a bubbler containing 10 ml of 0.1 % 4-(*p*-nitrobenzyl)pyridine in toluene. The absorbency of the solution was measured spectrophotometrically at 422 nm. The air temperature in the test chamber was held at $24 \pm 2 \text{ }^\circ\text{C}$ and the relative humidity at $50 \pm 10 \%$.

Determination by the devised method

Diphosgene concentration was determined using the apparatus depicted in Fig. 1. The filter was fixed in the adapter connected by a tube with a hand-operated suction device. The chromogenic reagent (50 μl) was applied on the center of the filter and then contaminated air was sucked through it (20 strokes, *i.e.*, $2000 \pm 100 \text{ cm}^3$). After the sampling, the intensity of the color spot of about 20 mm diameter was evaluated visually, as well as by tristimulus colorimeter (Fig. 2).



Fig. 1. Filter with adapter.



Fig. 2. Measurement of filter coloration by tristimulus colorimeter.

Tristimulus colorimetry

Tristimulus colorimetry is a type of reflectance colorimetry (spectrophotometry) based on the CIE- $L^*a^*b^*$ color system.²¹ In this system, L^* represents the neutral axis of lightness, a^* denotes the chromatic green-red axis ($+a^*$ red, $-a^*$ green) and b^* the chromatic blue-yellow axis ($+b^*$ yellow, $-b^*$ blue). In practice, also the color difference, ΔE , is used, which is defined by the Equation:

$$\Delta E = [(\Delta L^*)^2 + (\Delta a^*)^2 + (\Delta b^*)^2]^{1/2}$$

where ΔL^* , Δa^* and Δb^* are the differences between the individual values L^* , a^* and b^* for the standard and for the color in question. All these parameters can be used as analytical signals, which enable the quantification of the course of a color reaction.

RESULTS AND DISCUSSION

Stability of coloration

Passage of diphosgene-contaminated air through the filter practically instantaneously induced a red coloration, which could be characterized by a reflection curve (Fig. 3). After the sampling, this coloration was relatively stable for a lon-

ger period of time. The development of the red component of the coloration (parameter a^*) in the course of 10 minutes is depicted in Fig. 4. During this time the value of parameter a^* increased by 9.7 %.

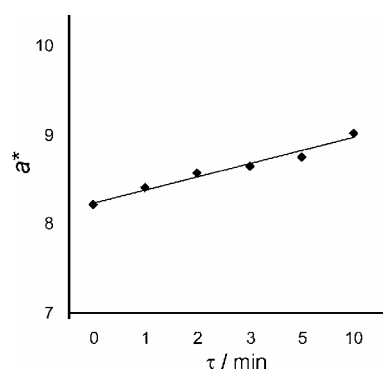
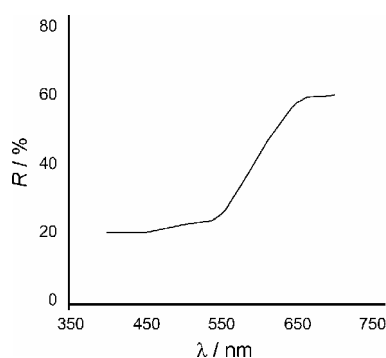


Fig. 3. Reflection curve. Dependence of light reflection (reflection factor R) on wavelength (λ).

Fig. 4. Time dependence of coloration.

The coloration intensity of the spot on the filter increased with the volume of the analyzed sample. Increasing the sample volume resulted in a darkening of the filter and an increasing value of the yellow (b^*), and particularly of the red (a^*), color component. The individual color differences ΔL^* , Δa^* , Δb^* and the total color differences ΔE are given in Table I.

TABLE I. Dependence of coloration on sample volume (diphosgene concentration 0.4 mg m^{-3})

Parameter	Sample volume, dm^3			
	1	2	3	5
ΔL^*	0.49	-4.20	-5.78	-9.79
Δa^*	2.39	11.72	14.80	21.92
Δb^*	9.88	13.16	13.46	14.57
ΔE	10.18	18.12	20.82	28.08

Calibration graph

The calibration graph for the determination of diphosgene is given in Fig. 5. The limit of detection of diphosgene by the tristimulus colorimeter was 0.01 mg m^{-3} . A reproducibility test showed that, at this concentration, the relative standard deviation of the response (Δa^*) amounted to 15 %. For visual evaluation, it is advisable to compare the intensity of the color spot with a reference standard representing a color scale $0\text{--}1.0 \text{ mg m}^{-3}$ with a 0.1 mg m^{-3} resolution. For the visual method, the detection limit of diphosgene was 0.05 mg m^{-3} .

Interference

A higher concentration of acidic vapors and gases which lower the intensity of the formed coloration interfere with the determination of diphosgene in air.

The presence of oxidizing and reducing substances may induce undesirable color changes. No interference was observed with 10 mg m^{-3} HCl, 15 mg m^{-3} Cl₂, 250 mg m^{-3} NO₂, 150 mg m^{-3} SO₂ or 50 mg m^{-3} NH₃.

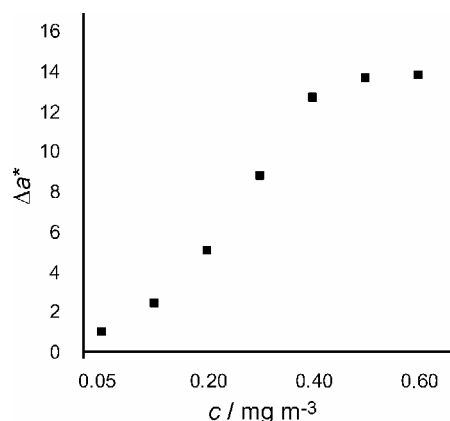


Fig. 5. Calibration graph.

Concerning organic compounds, no interference was observed *e.g.*, with benzyl chloride, trichloroethylene and chloroform at a concentration of 100 mg m^{-3} . Coloration similar to that of diphosgene (phosgene, triphosgene) was also produced by other compounds with an analogous propensity to acylation, however, it appears only at higher concentrations. Table II contains data on the interference by acetyl chloride and benzoyl chloride.

TABLE II. Interference of benzoyl chloride and acetyl chloride (the interference factor β is the ratio of the detection limit of the interfering compound to the detection limit of diphosgene)²²

Compound	Detection limit, mg m^{-3}	Interference factor β	Concentration, mg m^{-3} , at $\Delta a^* = 5$
Diphosgene	0.01	—	0.2
Benzoyl chloride	0.5	50	2.5
Acetyl chloride	1.5	150	5

Application to field analysis

The devised visual and tristimulus colorimetric method of diphosgene determination can be applied to many types of field analysis. If stored in hermetically sealed containers, the filter is usable for several years. Solutions of the chromogenic reagents are usable for at least 12 months.

The method is comparable with existing colorimetric methods for the determination of phosgene (Table III). Using the tristimulus method, it is possible to evidence trace amounts of diphosgene in air. The method can be applied also at night or at reduced visibility and the obtained data can be stored. Moreover, the devised method is universal, *i.e.*, it enables use of other liquid chromogenic reagents for the determination of a number of various toxic substances in air.

TABLE III. Comparison of the devised method with some active-sampling colorimetric methods of phosgene determination in air

Method	Detection limit, mg m ⁻³	Sampling conditions
Paper (Dixon, Hands)	1	0.12 dm ³ of air, 40 s
Detection tube Dräger	0.08	2 dm ³ of air, 240 s
Tape analyzer (Nakano)	0.02	0.4 dm ³ min ⁻¹ , 60 s
Devised method	0.01	2 dm ³ of air, 30 s

ИЗВОД

ЈЕДНОСТАВНА *IN SITU* ВИЗУЕЛНА И ТРИСТИМУЛУС КОЛОРИМЕТРИЈСКА МЕТОДА ЗА ОДРЕЂИВАЊЕ ДИФОЗГЕНА У ВАЗДУХУVLADIMÍR PITSCHMANN¹, ZBYNĚK KOBLIHA², EMIL HALÁMEK² и IVANA TUŠAROVÁ¹¹*Oritest spol. s r.o., Staropramenná 17, 150 00 Praha 5* и ²*NBC Defense Institute, University of Defense, Kounicova 65, 612 00 Brno, Czech Republic*

Развијена је једноставна визуелна и тристимулус метода (тродимензионални систем СЕ– $L^*a^*b^*$) за одређивање дифозгена у ваздуху у траговима. Метода се заснива на усисавању паре дифозгена кроз прилагођени филтер од памучне тканине који је фиксиран у специјалном адаптеру. Пре анализе, филтер је засићен хромогеним реагенсом базираном на 4-(*p*-нитробензил)пиридину. Оптимални састав реагенса је 2 г 4-(*p*-нитробензил)пиридина и 4 г *N*-фенилбензиламина у 100 ml 50:50 смеше етанол–глицерол. Интезитет насталог црвеног обојења филтера одређиван је визуелно или помоћу тристимулус колориметра (LMG 173, Lange, Немачка). Граница детекције износи 0,01 mg m⁻³. Ацетил хлорид и бензоил хлорид реагују у 150 и 50 пута већој концентрацији, респективно. Метода је погодна за анализе на терену.

(Примљено 3. августа 2006)

REFERENCES

1. Field Manual FM 3-11.9. *Potential Military Chemical/Biological Agents and Compounds*. Eximdyne, Wentzville, USA, 2005
2. A. Suchier, *Z. Anal. Chem.* **79** (1929) 183
3. H. Moureu, P. Chovin, L. Truffert, *Compt. Rend.* **228** (1949) 1954
4. A. L. Linch, S. S. Lord, K. A. Kubitz, M. R. Brunner, *Am. Ind. Hyg. Assoc. J.* **26** (1965) 465
5. M. Hayashi, M. Okazaki, Z. Shinohava, *J. Soc. Org. Synth. Chem.* **12** (1954) 292
6. H. F. Liddel, *Analyst* **82** (1957) 375
7. A. Spěvák, V. Kratochvíl, *Chem. Prům.* **15** (1965) 682
8. J. Studinger, *Chem. Ind.* (1937) 225
9. H. Gillman, O. R. Sweeney, *J. Am. Chem. Soc.* **52** (1930) 1604
10. B. Witten, A. Prostak, *Anal. Chem.* **29** (1957) 885
11. B. C. Dixon, G. C. Hands, *Analyst* **84** (1959) 463
12. M. H. Noweir, E. A. Pfitzer, *Am. Ind. Hyg. Assoc. J.* **32** (1971) 163
13. E. A. Peregud, D. O. Gorelik, *Instrumentalnyi metody kontrolya zagryazneniya atmosfery*, Khimiya, Leningrad, 1981, p. 75
14. N. Nakano, A. Yamamoto, Y. Kobayashi, K. Nagashima, *Talanta* **42** (1995) 641
15. F. Yokota, S. Abe, *Anal. Commun.* **34** (1997) 111
16. F. Yokota, S. Abe, *Bunseki Kagaku* **46** (1997) 689
17. M. Rahman, K. Fujinaga, Y. Seike, M. Okomura, *Anal. Sci.* **20** (2004) 165

18. M. Zenki, T. Yoshiba, M. Ohiwane, M. Nakanuta, *Bunseku Kagaku* **50** (2001) 345
19. I. Kasahara, A. Fujinawa, N. Hata, S. Taguchi, *J. Ion Exchange* **14** (Supplement) (2003) 317
20. Y. Suzuki, M. Endo, J. Jin, K. Iwase, M. Iwatsuki, *Anal. Sci.* **22** (2006) 411
21. G. Wysecki, W. S. Stiles, *Color Science*, Wiley, 1982
22. E. Halánek, Z. Koblíha, *Talanta* **48** (1999) 163.